AD-A116 383 TEXAS UNIV AT AUSTIN DEPT OF ELECTRICAL ENGINEERING F/G 9/1
AN ISOLATOR IN IMAGE GUIDE.(U)
MAY 82 N CAMILLERI, T ITOH N00014-79-C-0553
UNCLASSIFIED UT-MW-N-82-1 NL

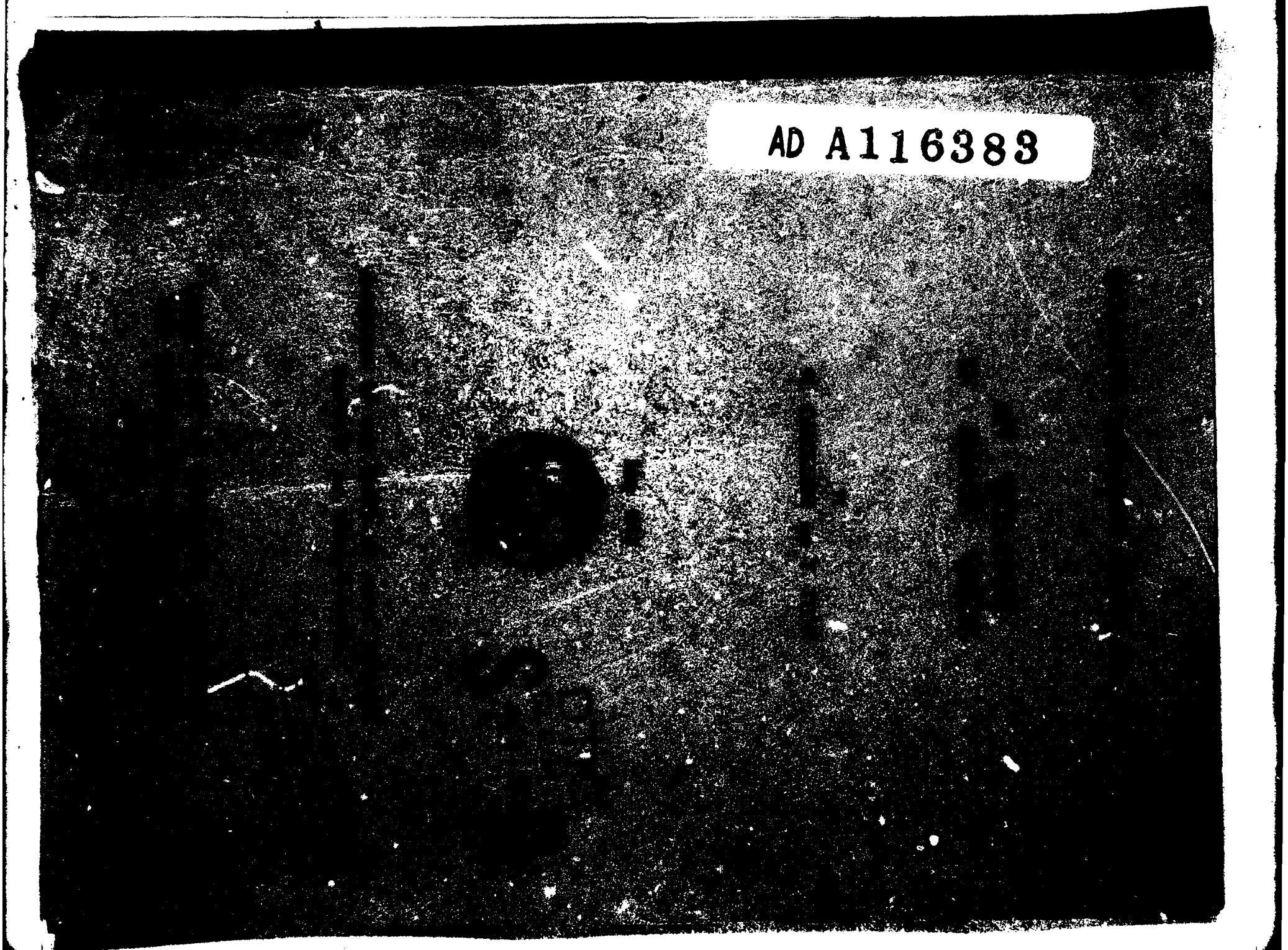

Unclassified

SECURITY CLASSIFICATION OF THIS PAGE *(When Data Entered)*

REPORT DOCUMENTATION PAGE		READ INSTRUCTIONS BEFORE COMPLETING FORM
1. REPORT NUMBER UT-MW-N-82-1	2. GOVT ACCESSION NO. AD-A116 383	3. RECIPIENT'S CATALOG NUMBER
4. TITLE *(and Subtitle)* An Isolator in Image Guide		5. TYPE OF REPORT & PERIOD COVERED Technical Report
		6. PERFORMING ORG. REPORT NUMBER
7. AUTHOR(s) N. Camilleri and T. Itoh		8. CONTRACT OR GRANT NUMBER(s) N00014-79-C-0553
9. PERFORMING ORGANIZATION NAME AND ADDRESS University of Texas at Austin P.O. Box 7728 Austin, TX 78712		10. PROGRAM ELEMENT, PROJECT, TASK AREA & WORK UNIT NUMBERS
11. CONTROLLING OFFICE NAME AND ADDRESS Office of Naval Research Arlington, VA 22217		12. REPORT DATE 11 May 82 13. NUMBER OF PAGES 125
14. MONITORING AGENCY NAME & ADDRESS*(if different from Controlling Office)*		15. SECURITY CLASS. *(of this report)* Unclassified 15a. DECLASSIFICATION/DOWNGRADING SCHEDULE
16. DISTRIBUTION STATEMENT *(of this Report)* Unlimited		
17. DISTRIBUTION STATEMENT *(of the abstract entered in Block 20, if different from Report)*		
18. SUPPLEMENTARY NOTES		
19. KEY WORDS *(Continue on reverse side if necessary and identify by block number)* isolators, image guides, Galerkin's Method, leaky wave filters		

20. ABSTRACT *(Continue on reverse side if necessary and identify by block number)*

An image guide consisting of a layer of dielectric and a layer of ferrite with periodic metal strips between these layers is analyzed. Non-reciprocity of the phase constants caused by the gyrotropic nature of the ferrite makes it possible to create non-reciprocal leakage phenomena by means of the metal strips. These phenomena can be used to develop a distributed isolator. Numerical results and data from the experimental investigation performed are presented.

DD FORM 1 JAN 73 1473 EDITION OF 1 NOV 65 IS OBSOLETE
S/N 0102-014-6601 |

UNCLASSIFIED
SECURITY CLASSIFICATION OF THIS PAGE *(When Data Entered)*

MICROWAVE LABORATORY REPORT NO. 82-1

AN ISOLATOR IN IMAGE GUIDE

by

N. Camilleri

and

T. Itoh

May 1982

Sponsored by the Office of Naval Research

Contract No. N00014-79-C-0553

Microwave Laboratory
Department of Electrical Engineering
The University of Texas at Austin
Austin, Texas 78712

AN ISOLATOR IN IMAGE GUIDE

ABSTRACT

An image guide consisting of a layer of dielectric and a layer of ferrite with periodic metal strips between these layers is analyzed. Non-reciprocity of the phase constants caused by the gyrotropic nature of the ferrite makes it possible to create non-reciprocal leakage phenomena by means of the metal strips. These phenomena can be used to develop a distributed isolator. Numerical results and data from the experimental investigation performed are presented.

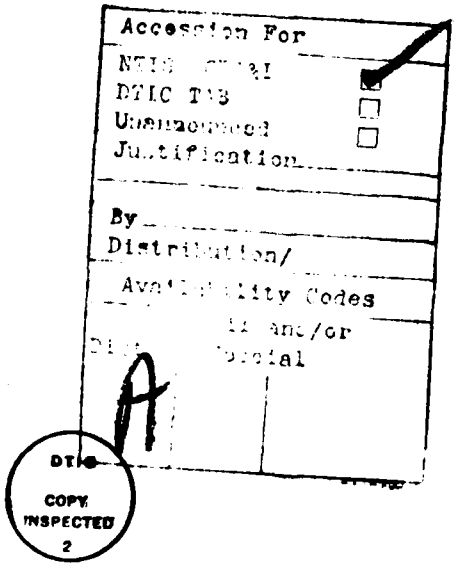

TABLE OF CONTENTS

Table of Contents (Cont'd)

Table of Contents (Cont'd)

INTRODUCTION

In the last decade, the microwave engineers have been trying to extend integrated circuits at microwave frequencies to millimeter-wave frequencies. The approach to millimeter-wave I.C.'s tends more to optical waveguides than to coaxial lines as is the case for microwave I.C.'s. The most promising means to make millimeter-wave I.C.'s is the image guide system. Various components have been built. However, to date little has been done to create a non-reciprocal device compatible with image guide systems. The structure proposed here is one that is compatible with image guides and is reasonable in size at millimeter-wave frequencies.

The isolators available at millimeter-wave frequencies are the Faraday rotation type, the resonance type using hexagonal ferrites, and those made from a junction circulator. None of these are very compatible with image guide systems although the resonance type could possibly be. Also, hexagonal ferrites are not commercially available.

Several structures have been proposed to make a non-reciprocal device compatible with image guides. These are mainly field displacement devices and structures[7,8,9,20] that have physical resonances at different frequencies in the opposite directions[18]. The present structure is an extension of a previously suggested one where a periodic grating was created in the dielectric

guide attached to a ferrite guide[1]. The structure analyzed in this article consists mainly of a ferrite guide next to a dielectric guide with periodic metal strips between the guides and oriented in the E-plane.

In this article, Chapters 1 and 2 review ferrite theory at microwave frequencies and with a simple explanation of how the non-reciprocal ferrite devices presently in use work. Chapter 3 deals with the derivation of the theory for analyzing the propagation constant in the proposed structure. Chapter 4 presents the numerical procedure and the computer program. Chapter 5 deals with the experimental investigations and the comparison between the experimental and the theoretical results.

CHAPTER 1

GENERAL FERRITE THEORY, PARAMETERS AND MATERIALS

The purpose of this chapter is to give some insight of what ferrite is, what makes it different from other materials and what parameters distinguish different types of ferrite materials. This chapter also deals in some detail with the derivation of the so called permeability tensor of ferrites. This tensor permeability is the most direct tool which could give an engineer insight into how ferrite material is going to behave. The tensor permeability is what makes ferrites different from other dielectric materials and it would be used back and forth in analysis of systems containing ferrite materials, so it would be a good idea to look at the tensor and see how it originates and how to control it to obtain the desired characteristics.

1.1 Types of Magnetism

a. Diamagnetism and Paramagentism

For any material the magnetic moment of an atom is equal to the sum of the moments of its electrons. In a large number of cases, this moment is zero due to the symmetry of the atom which contains as many electrons rotating in one sense as in the other sense. Just as in electromagnetism, where a flux gives rise to an induced current tending to oppose any change, a substance which is acted on by a magnetic field tends to respond by the creation of internal charges. If the moments of the atoms are zero, then the induction is smaller than the applied field and the magnetic susceptibility must be negative. Such a substance is said to be diamagnetic. The magnetic susceptibility is very small of the order of 10^{-5} (e.g., water has $\chi = -0.91 \times 10^{-5}$).

If the magnetic moment of the atom is not zero, the body is said to be paramagnetic. Substances where atoms have an odd number of electrons are paramagnetic. This is the case of atoms which have an incomplete internal shell as well as for free ions. Metals are often paramagnetic because of the presence of conduction electrons, as are also some bodies which have an even number of electrons.

The susceptibility is now positive but it is still very small (of the order of 10^{-5} to 10^{-4}).

b. Ferromagnetism

A substance is said to be ferromagnetic when it possesses a spontaneous magnetic moment in the absence of any applied magnetic field. The spontaneous magnetic moment per unit volume is called the saturation intensity M_s.

An explanation of this phenomenon was first given by Weiss[29] who postulated the existence of a force tending to align all the magnetic moments of the atoms in the material in one direction. Thus, a ferromagnetic substance is a paramagnetic substance in which there exists a field, called the molecular or exchange field by Weiss. This field aligns the magnetic moments of all the paramagnetic atoms into one direction.

Heisenberg[22] later showed that the molecular field was a coupling of electrical origin which existed only if the distances between the atoms in the material lay between certain well-defined limits. The energy of this coupling is called the exchange energy. It can be shown that for two neighboring atoms, whose spin moments equal S and at an angle ϕ to each other, the exchange energy is given by

$$W = J S^2 \phi^2 \qquad (1.1)$$

where J is a coefficient called the exchange integral.

However, the exchange energy which tends to align the moment is more or less counterbalanced by the thermal energy which, by random agitation of the atoms, tends to destroy the alignment.

This energy is proportional to the product of Boltzmann's constant and the absolute temperature. At low temperatures the exchange energy is predominant and a large number of the moments are aligned. The saturation intensity M_s is, thus, relatively important. As the temperature rises, the increase in the thermal energy gradually destroys the alignment and the saturation intensity decreases. When the two energies are equal, the saturation intensity becomes statistically zero. The temperature at which this occurs is called the Curie point or Curie temperature.

Above the Curie point, the substance is no longer ferromagnetic and becomes paramagnetic. Below it, the moment M_s varies as shown in Fig. (1.1).

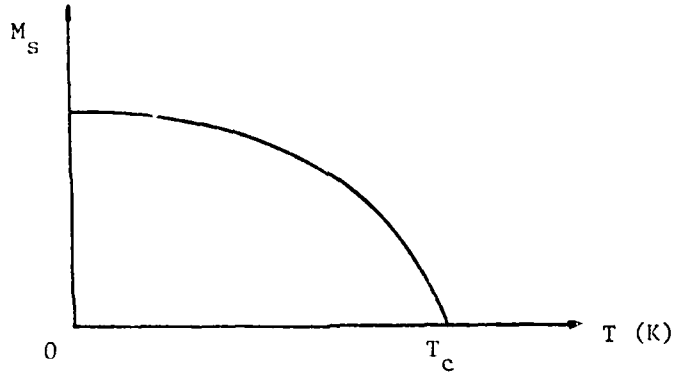

Fig. (1.1) The variation of saturation magnetization with temperature

The value of the molecular field can be deduced from a knowledge of the Curie temperature T_c. In the case of iron it turns out to be of the order of 5 million oersteds.

The exchange energy is important only if the distances between atoms lie between very narrow limits. There exist relatively few ferromagnetic materials. In fact, only iron, cobalt and nickel exhibit this property at normal temperatures.

It should be noted that a ferromagnetic material is not necessarily magnetized to saturation. The reason is that in the absence of an external magnetic field, the substance is divided into small domains, called Weiss[16] domains in which the moments are aligned spontaneously and which are, therefore, saturated. But the direction of magnetization varies from one domain to another so that the overall magnetization can be quite small or even zero. Fig. (1.2) shows schematically the distribution of Weiss domains in a ferromagnetic material and the direction of magnetization for each.

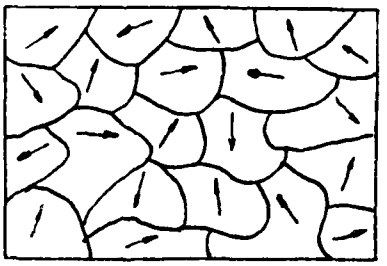

Fig. (1.2) Weiss domain in Ferromagnetic materials

This microscopic domain structure has been verified photographically. It is assumed that each domain is separated from its neighbors by a thin region, called a Bloch[13] wall, in which the magnetization changes direction.

In the presence of an external field, two phenomena can happen; an increase in the size of the domains in which the magnetization lies in the direction of the applied field, or a rotation of the magnetization directions in the various domains tending to align them with the field. The first of these two effects seems to exist for relatively weak fields and the second for fields approaching saturation. When the latter condition is reached, as in Fig. (1.3), all the domains are aligned with the applied field.

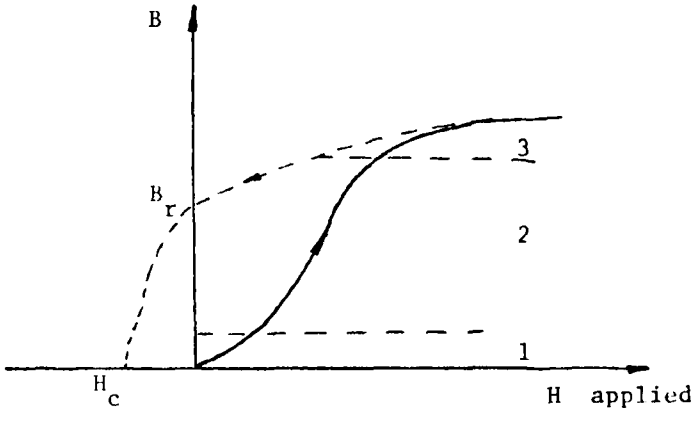

Fig. (1.3)

(1) Reversible zone
(2) Increase in the size of certain domains
(3) Rotation of the magnetization of the domains

If the applied field is reduced or removed after a specimen of ferromagnetic metal has been magnetized to saturation, the domains do not revert to their original positions. A certain amount of magnetization or remanent induction B_r, is left. If it is

large, we have a permanent magnet; if it is small, the material is said to be soft. The corrective field is the field which must be applied to reduce the remanent induction to zero.

c. Antiferromagnetism

In a ferromagnetic body, magnetized to saturation, all the moments of the atoms are oriented parallel to the applied field when the temperature is much below the Curie point. It can happen, however, that the moments form an antiparallel arrangement, as shown in Fig. (1.4). In this case the magnetization remains weak, the susceptibility being then of the same order of magnitude as that of a paramagnetic substance; the material is than said to be antiferromagnetic.

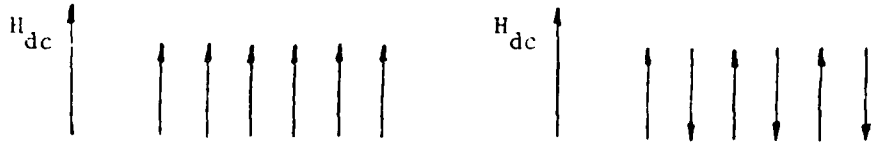

J>0: Ferromagnetic J<0: Antiferromagnetic

Fig. (1.4)

It can be shown theoretically that ferromagnetism corresponds to a positive exchange integral and antiferromagnetism to a negative exchange integral.

d. Ferrimagnetism

Knowing the molecular composition of a material, one can determine the number of magnetons available to the part in the magnetization; (one magneton usually defined as the Bohr[13] magneton is the smallest magnetic moment possible, which occurs due to one electron spin). It is then easy to deduce the saturation intensity of the material when all the magnetons are aligned parallel to each other. It is now found that for certain compounds such as iron oxide, FeO, Fe_2O, for example, the saturation intensity obtained experimentally is considered less than the predicted value. If the calculation is done in reverse, it is found that only 4.2 magnetons per molecule of Fe_3O_4 have contributed to the magnetization, as against the 14 magnetons available. To explain this, Neel[16] presumed that the trivalent Fe^{3+} ions of Fe_2O_3 were antiferromagnetic (moment aligned antiparallel), whereas, the divalent Fe^{2+} ions of FeO were ferromagnetic (moment parallel); analogous ideas had been proposed by Guilland on the subject of the components of manganese and bismuth. This type of magnetism, which applies to the ferrites which we are about to discuss, has been given the name ferrimagnetism.

In a ferrimagnetic molecule, then, there are atoms between which the exchange integrals are positive and atoms between which they are negative. The overall moment of the molecule is the difference between the sums of the moments of opposite senses.

1.2 Material Composition, Saturation and Curie Temperature Relationships

As the temperature of ferrite is raised, the magnetic structure is weakened and eventually falls into complete disarray (the Curie point). When non-magnetic ions are substituted, the structure is already weakened and the Curie point reduced Fig. (1.5)[28]. Rare earth substitutions for yttrium in YIG do not weaken the interaction, and the saturation magnetization can be varied without affecting the Curie temperature.

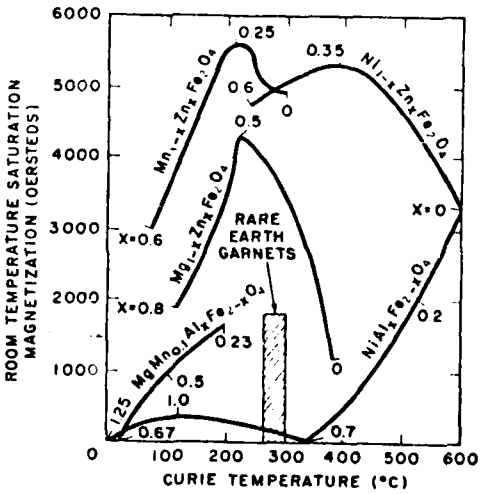

Fig. (1.5) Saturation Magnetization and Curie temperature for various ferrite systems

For ferrite devices, the Curie point determines both the maximum operating temperature and a critical temperature range where small temperature variations will have large effects on device characteristics.

1.3 Precession and Gyromagnetic Resonance

Consider a particle rotating about itself (in this case a spinning electron) which we shall assume to have the shape of a small sphere Fig. (1.6). The axis of rotation is along a direction Ot_1, which makes an angle θ with the Oz axis of a set of reference axes with origin 0 at the center of the electron. Since the electron has mass, there exists along the Ot a kinetic moment which is designated by the vector $\bar{p}$.

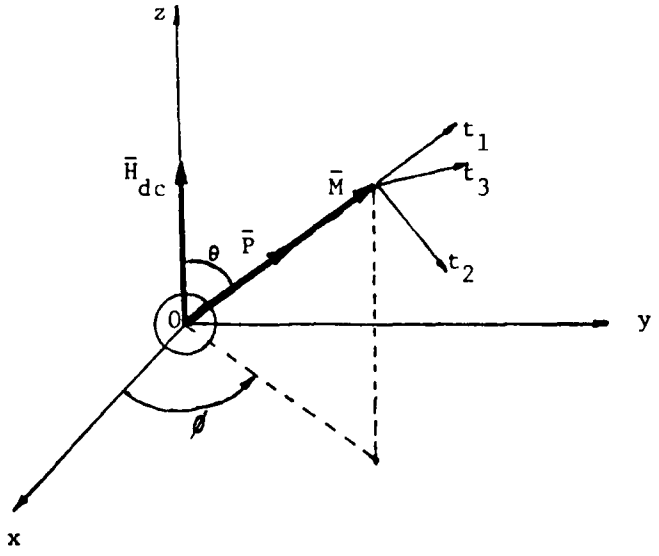

Fig. (1.6)

It can be shown that the kinetic moment is the product of the action quantum h and the spin quantum number s, which has only two possible values ± 1/2. Since $h = 105.4 \times 10^{-36}$ J/s, the only two possible values of the kinetic moments are $p_e = hs = \pm 52.7 \times 10^{-36}$ J/s. We know, however, that the electron also possesses a magnetic moment M which, in this particular case, is the Bohn magneton $M_b = 9.27 \times 10^{-21}$ Mx - cm.

Any particle having mass and spin will give simultaneously a kinetic moment and a magnetic moment. By definition, the ratio $\gamma = \bar{M}/\bar{P}$ is called the gyromagnetic ratio of the particle. In the particular case of the electron:

$$|\gamma| = \frac{M_b}{P_e} = 17.6 \times 10^6 \tag{1.2}$$

If no external force is applied to the particle, it rotates about the axis Ot, where direction remains fixed. Let us suppose that a d.c. magnetic field $\bar{H}$ is applied along the Oz axis. This magnetic field exerts on the moment $\bar{M}$ a couple:

$$\bar{c} = \bar{M} \times \bar{H}, \tag{1.3}$$

and the time derivative of the kinetic moment is:

$$\frac{d\bar{p}}{dt} = \bar{M} \times \bar{H} \tag{1.4}$$

But from $\gamma = \bar{M}/\bar{P}$ we also get

$$\frac{d\bar{p}}{dt} = \frac{1}{\gamma} \frac{d\bar{M}}{dt}. \tag{1.5}$$

Combining the above equations we get

$$\frac{1}{\gamma}\frac{d\bar{M}}{dt} = \bar{M} \times \bar{H} \tag{1.6}$$

which is the differential equation of motion for the moment $\bar{M}$.

With M, the tip of the vector $\bar{M}$, as origin, let us take a set of coordinate axis Mt_1, Mt_2, Mt_3: Mt_2 is in the place of $\bar{M}$ and Oz, and Mt_3 is perpendicular to this plane. The projections of $d\bar{M}/dt$ on these three axes are given by kinematics. They are

$$\begin{aligned} &\text{on } Ot_1 && \frac{dM}{dt} \\ &\text{on } Ot_2 && \frac{Md\theta}{dt} \\ &\text{on } Ot_3 && M \sin\theta \frac{d\phi}{dt}\ , \end{aligned} \tag{1.7}$$

ϕ being the angle between the projection of M on xOy and the Ox axis.

Further, the projections of the vector product on the three axes are: on Ot_1 & Ot_2 = 0; and on $Ot_3 = MH_{dc} \sin\theta$. Finally, the equations of motion of $\bar{M}$ are written $\frac{1}{\gamma}\frac{dM}{dt} = 0$, $\frac{1}{\gamma} M \sin\theta \frac{d\phi}{dt} = MH_{dc} \sin\theta$. This last relationship gives:

$$\frac{d\phi}{dt} = \gamma H_{dc}. \tag{1.3}$$

Since, in addition, $\frac{dM}{dt} = 0$ and $M\frac{d\theta}{dt} = 0$, then the locus of the tip of the $\bar{M}$ vector is a circle lying in a plane perpendicular to Oz. The circle is described with an angular velocity:

$$\omega = \frac{d\phi}{dt} \quad . \tag{1.9}$$

The M vector, therefore describes a cone around the Oz axis with semi apex angle 0. We recognize here the phenomenon of precession in a gyroscope. The frequency of rotation is given by: $\omega = 2\pi f$, so that $f = \frac{\gamma}{2\pi} H_{dc}$. In the case of an electron,

$$f = 2.8H_{dc} \tag{1.10}$$

where f is in GHz and H is kilo oersteds.

The precession thus produced is accompanied by a dissipation of energy which appears almost entirely as heat, the remainder being transformed into an electromagnetic radiation of frequency f. This dissipation of energy brings about a decay of the motion, the angle θ becomes progressively smaller and precession ceases when $\bar{M}$ is aligned with $\bar{H}_{dc}$. The time between the application of $\bar{H}_{dc}$ and the end of the precessional motion is called the relaxation time.

Let us now consider an electron under the influence of a d.c. magnetic field $\bar{H}_{dc}$ for a time long enough for the moment $\bar{M}$ to be aligned with $\bar{H}$ and for all precession motion to have ceased, Fig. (1.7).

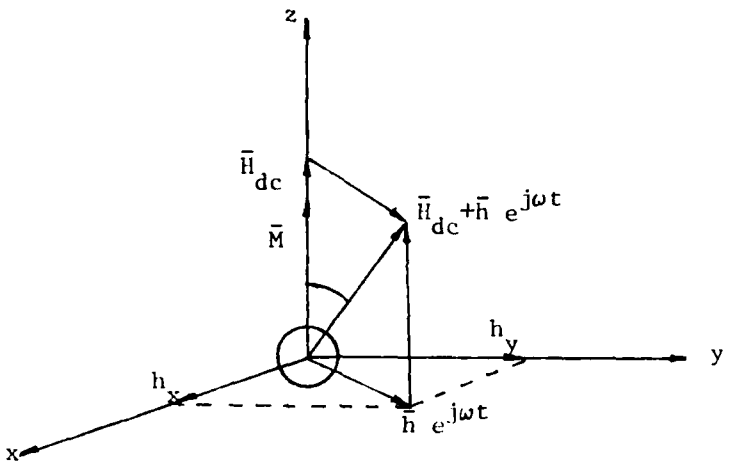

Fig. (1.7)

Let us apply to the electron a second magnetic field $\bar{h}$, lying in the x0y plane. The resultant field will be a vector $\bar{H}_{dc} + \bar{h}$ making an angle θ with the direction Oz of the moment $\bar{M}$, and we find ourselves in the situation of the preceding paragraph and the spin moment will again acquire a precessional motion around the direction of $(\bar{M} + \bar{h})$.

Let us now suppose that the field $\bar{h}$ is a high frequency, circularly polarized field. It is known that such a field is characterized by a vector $\bar{h}$ which rotates in the plane of magnetic polarization (here, the plane x0y) at the given frequency. In these conditions, the vector $(\bar{H}_{dc} + \bar{h})$ describes a cone around Oz, carrying with it the moment $\bar{M}$ which acquires a precessional motion around it. Two cases can then arise:

a. The sense of rotation of $\bar{h}$ is such that the cone is described by $(\bar{H}_{dc} + \bar{h})$ in the same sense as that of the precession; in this case, if the frequency of $\bar{h}$ is the same as that of the precession, there will be synchronization of the two phenomena and we have resonance. The amplitude of the precession (aperture of the cone) increases until the energy supplied by the high frequency field exactly balances the losses, and the motion is maintained in equilibrium at the expense of the high frequency field which, therefore, suffers a significant absorption. This phenomenon is known as gyromagnetic resonance.

   If $\bar{h}$ is small compared with $\bar{H}$, it appears when the value of the latter is such that the frequency given by $f = 2.8\bar{H}_{dc}$ is equal to the frequency of the field $\bar{h}$. The d.c. field at resonance, $\bar{H}o$, is therefore

$$\bar{H}o = \frac{f}{2.8} .$$

b. The sense of rotation of $\bar{h}$ is such that the cone is described by $(\bar{H}_{dc} + \bar{h})$ in the opposite sense to that of the precession.

In this case, synchronization is impossible and there cannot be any gyromagnetic resonance.

One important fact will be observed: resonance occurs for only one sense of polarization. Now, for a circularly polarized high frequency wave, the sense of rotation depends on the direction of propagation. Resonance, therefore, occurs in one direction of propagation only; in the opposite direction, no significant absorption occurs. This is a formal contradiction of the reciprocity theorem. Gyromagnetic resonance is, therefore, a nonreciprocal phenomenon.

The absorption curve of ferrite material vs. H_{dc} will be as shown in Fig. (1.8). One may notice that changing the direction of H_{dc} or the microwave field has just the same effect.

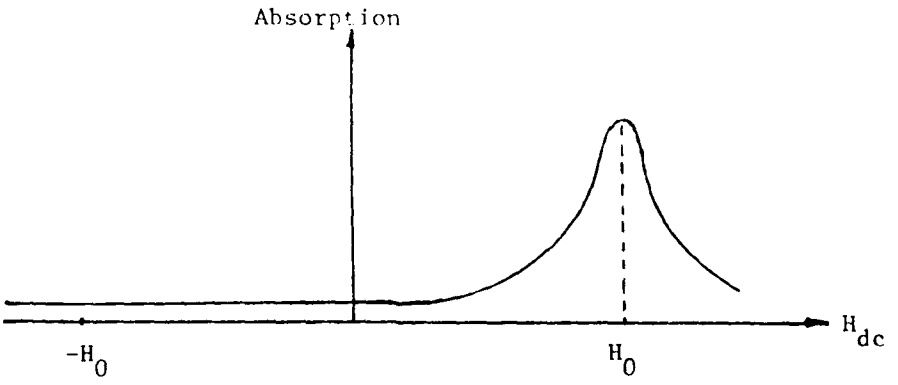

Fig. (1.8)

1.4 The Permeability Tensor and Line Width

In the simplest microwave case, the total effective magnetic field in the equation of motion ($\frac{d\bar{M}}{dt} = \gamma \bar{M} \times \bar{H}$) consists of the d.c. magnetic field H_{dc} and the r.f. magnetic field $\bar{h}$.

$$\bar{H} = \bar{H}_{dc} + \bar{h} \ . \tag{1.11}$$

The total magnetization consists of the d.c. magnetization $\bar{M}_{d.c.}$ and the r.f. magnetization $\bar{m}$

$$\bar{M} = \bar{M}_{d.c.} + \bar{m} \ . \tag{1.12}$$

In component form, the above equations are:

$$\bar{H}_{dc} = \begin{bmatrix} 0 \\ 0 \\ H_{dc} \end{bmatrix} , \quad \bar{h} = \begin{bmatrix} h_x \\ h_y \\ h_z \end{bmatrix} , \quad \bar{M}_{dc} = \begin{bmatrix} 0 \\ 0 \\ M_{dc} \end{bmatrix} , \quad \bar{m} = \begin{bmatrix} m_x \\ m_y \\ m_z \end{bmatrix}$$

The equation of motion now gives

$$\begin{aligned} \frac{dm_x}{dt} &= m_y \gamma (H_{dc} + h_z) - h_z \gamma (M_{dc} + m_z) \\ \frac{dm_y}{dt} &= -m_x \gamma (H_{dc} + h_z) + h_x \gamma (M_{dc} + m_z) \\ \frac{dm_z}{dt} &= m_x \gamma h_y - m_y \gamma h_x \ . \end{aligned} \tag{1.13}$$

In the small signal approximation higher order terms of m and h are set equal to zero. The small signal approximation is, therefore:

$$\frac{dm_x}{dt} = m_y \gamma H_{dc} - h_y \gamma M_{dc}$$

$$\frac{dm_y}{dt} = -m_x \gamma H_{dc} + h_x \gamma M_{dc} \qquad (1.14)$$

$$\frac{dm_z}{dt} \simeq 0$$

Rewriting and differentiating the last equations, we have:

$$\ddot{m}_x + \omega_o^2 m_x = \omega_m \omega_o h_x - \omega_m \dot{h}_y$$

$$\ddot{m}_y + \omega_o^2 m_y = \omega_m \dot{h}_x + \omega_m \omega_o h_y \qquad (1.15)$$

$$m_z \simeq 0 \quad ,$$

where $\omega_m = \gamma M_{dc}$, $\omega_o = \gamma H_{dc}$, and $\cdot$ indicates time derivative.

If the time dependence of the r.f. quantities is of the form $\exp(j\omega t)$, a susceptibility tensor $[\chi]$ can be defined which relates the r.f. magnetization to the r.f. magnetic field.

$$\bar{m} = [\chi]\, \bar{h}$$

$$\text{Where } [\chi] = \begin{bmatrix} \chi_{xx} & \chi_{xy} & 0 \\ \chi_{yx} & \chi_{yy} & 0 \\ 0 & 0 & 0 \end{bmatrix} \qquad (1.16)$$

$$\text{and } \chi_{xx} = \chi_{yy} = \frac{\omega_m \omega_o}{\omega_o^2 - \omega^2} \tag{1.17}$$

$$\chi_{yx} = \chi_{xy} = \frac{j\omega_m \omega}{\omega_o^2 - \omega^2} \tag{1.18}$$

The components of the susceptibility tensor have a singularity at $\omega = \omega_o$. This is defined as the resonance condition.

A tensor permeability can also be defined by relating the r.f. flux density $\bar{b}$ to the r.f. magnetic field $\bar{h}$,

$$\bar{b} = \mu_o \bar{h} + \bar{m} \tag{1.19}$$

or

$$b = \mu_o [\mu_r] \bar{h}$$

where $[\mu_r] = [1] + [\chi]$.

In component form, the tensor permeability is given by

$$[\mu_r] = \begin{bmatrix} \mu & jk & 0 \\ jk & \mu & 0 \\ 0 & 0 & 1 \end{bmatrix} \tag{1.20}$$

where $\mu = 1 + \chi_{xx}$

$$jk = -\chi_{xy}$$

This is the well known Polder[21] tensor permeability. The permeability tensor is usually employed in conjunction with Maxwell's equations to solve microwave ferrite boundary problems.

Damping may be introduced into the equations of μ and k by adding an imaginary frequency term $j\alpha\omega$ to ω_o in these equations. We shall next discuss where the $j\alpha\omega$ term comes from and what is the value of α.

To stabilize the motion of the magnetization vector at resonance, a damping term must be introduced into the equation of motion. One form of phenomenological damping term is due to Landau - Lifshitz[17] given by:

$$\frac{d\bar{M}}{dt} = \gamma(\bar{M} \times \bar{H}) - \frac{\gamma\alpha}{|M|}[M \times (\bar{M} \times \bar{H})] \qquad (1.21)$$

where α is a dimensionless parameter that determines the damping. Solving for $\gamma(\bar{M} \times \bar{H})$ in the above equation gives

$$\gamma(\bar{M} \times \bar{H}) = \frac{d\bar{M}}{dt} + \frac{\gamma\alpha}{|M|}[M \times (\bar{M} \times \bar{H})] \qquad (1.22)$$

and introducing this into the last part of the previous equation gives:

$$\frac{d\bar{M}}{dt} = \gamma(\bar{M} \times \bar{H}) - \frac{\alpha}{|M|}(\bar{M} \times \frac{d\bar{M}}{dt}) - \frac{\gamma\alpha^2}{|M|^2}\bar{M} \times [\bar{M} \times (\bar{M} \times \bar{H})]. \qquad (1.23)$$

For most ferrites the last term is negligible since α is small. Therefore, the equation could be written as,

$$\frac{d\bar{M}}{dt} = \gamma(\bar{M} \times \bar{H}) - \frac{\alpha}{|M|}(\bar{M} \times \frac{d\bar{M}}{dt}). \qquad (1.24)$$

This damping term is shown in Fig. (1.9). The components of the tensor susceptibility obtained from the small signal solution to

the above equation containing the damping terms are:

$$\chi_{xx} = \chi_{yy} = \frac{\omega_m (\omega_o + j\omega\alpha)}{(\omega_o + j\omega\alpha)^2 - \omega^2} \tag{1.25}$$

$$\chi_{yx} = -\chi_{xy} = \frac{j\ \omega_m\ \omega}{(\omega_o + j\omega\alpha)^2 - \omega^2} \tag{1.26}$$

Hence, the only difference between these equations and the equations when we did not consider damping is that an imaginary frequency term $j\omega\alpha$ has been added to the resonant frequency ω_o. Hence, the damping term can always be introduced by replacing ω_o by $\omega_o + j\omega\alpha$ in the loss free components. The real and imaginary parts of the susceptibility tensor are plotted in Fig. (1.10) as a function of ω_m/ω, ω_o/ω and α.

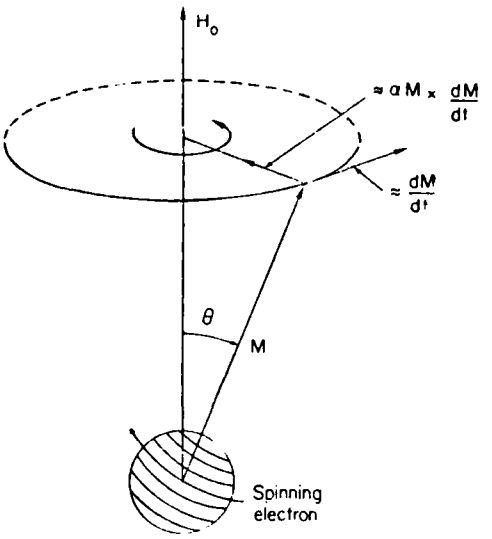

Fig. (1.9)

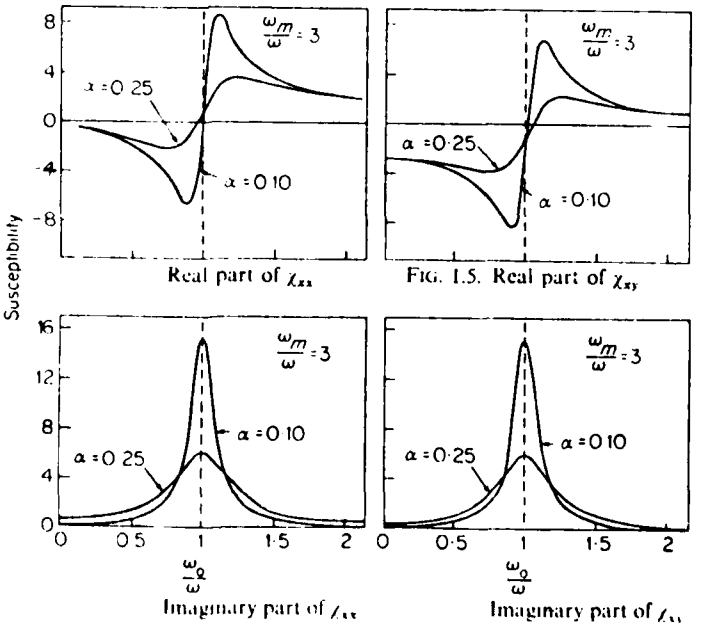

Fig. (1.10)

The damping factor α can be related to the linewidth of ferrites in the following way. The linewidth is usually defined as the difference between the magnetic field values at a constant frequency where χ''_{xx}, the imaginary parts of the diagonal component of the susceptibility tensor, attains the value of half its value at resonance as shown in Fig. (1.11).

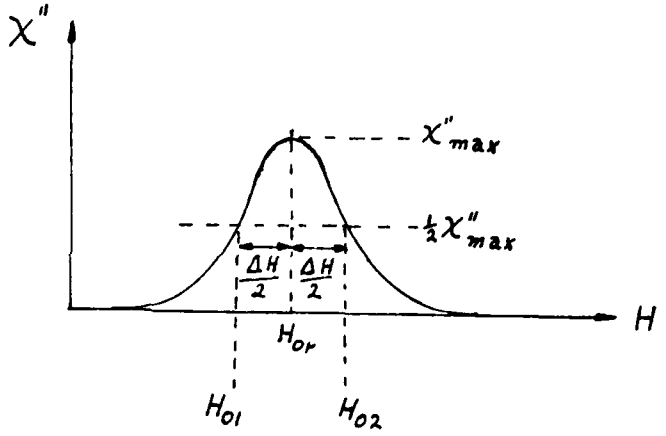

Fig. (1.11) Linewidth of Ferrites

Equating the imaginary part of χ_{xx} to half the maximum value of χ''_{xx}, we get

$$\frac{\omega_m \omega\alpha (\omega_{01}^2 - \omega^2)}{(\omega_{01}^2 - \omega^2)^2 + 4\omega_{01}^2\omega^2\alpha^2} = 1/2 \frac{(\omega_m)}{2\omega\alpha} . \qquad (1.27)$$

Rearranging gives a quadratic in ω_{01}^2

$$\omega_{01}^4 - 2\omega^2\omega_{01}^2 + \omega^4(1 - 4\alpha^2) = 0, \qquad (1.28)$$

whose solution is

$$\omega_{01,2} = \omega(1 \pm 2\alpha)^{1/2} \simeq \omega \pm \omega\alpha. \tag{1.29}$$

Hence,

$$\omega\alpha = \frac{\omega_{02} - \omega_{01}}{2} . \tag{1.30}$$

The linewidth is usually defined by

$$\Delta\bar{H} - \frac{\omega_{02} - \omega_{01}}{\gamma} \tag{1.31}$$

$$\therefore \quad \alpha\omega = \frac{\gamma\Delta\bar{H}}{2} . \tag{1.32}$$

For engineering purposes the imaginary frequency $j\alpha\omega$ is usually written in terms of ΔH from the last equation.

1.5 The Permeability Tensor Below Saturation

Below saturation there exists no additional formulation of the tensor, since not all the electron spins are aligned to the applied magnetic field, and we do not have any measure of alignment to formulate a theory which would give us a good result.

The only remaining solution is to measure the tensor and then fit empirical equations to the experimental results. One such work has been done by J. J. Green and F. Sandy[10]. In their 1974 paper they discuss the experimental results of a number of different types of ferrites and then fit the appropriate general empirical formulas which are given by

$$\tilde{\mu} = \begin{bmatrix} \mu & -jk & 0 \\ jk & \mu & 0 \\ 0 & 0 & \mu_z \end{bmatrix} \qquad (1.33)$$

where $k = -\omega_o/\omega$

$$\mu_0 = 2/3\ [1 - (\omega_m/\omega)^2]^{1/2} + 1/3$$

$$\mu = \mu_0 + (1 - \mu_0)\ (\omega_0/\omega_m)^{3/2}$$

$$\mu_z = \mu_0\ (1 - \omega_0/\omega_m)^{5/2}$$

1.6 Measurement of the Permeability Tensor

The permeability tensor obtained by measurement is perhaps the best way to characterize a ferrite material. Actually when ferrites are produced the only way to obtain important parameters such as saturation magnetization and linewidth is by making measurements.

There exist various types of measurement techniques, the main two being the cavity perturbation and the ferrite filled waveguide method. The former method is usually preferred since it gives better results and the sample size required is very small. The cavity perturbation technique could be classified into two methods, namely the non-degenerate cavity method and the degenerate cavity method due to J. O. Artman[5]. Using non-degenerate cavities provides information only about the diagonal element of the tensor.

However, at times this is sufficient, especially close to resonance and for small damping where the diagonal and off-diagonal elements are closely related by equation

$$k = 1 - \mu \tag{1.34}$$

Degenerate cavity methods give information about the diagonal and off-diagonal element of the tensor but the overall inaccuracies involved in having a good degenerate cavity make it difficult to obtain reasonable results with this method.

The perburbation theory for various types of cavities and sample shapes have been derived; a good account of this is given by Lax and Button[16]. A general idea of the derivation of perturbation relations is given next.

In the cavity methods the way to determine the susceptibility tensor is to measure the shift in resonant frequency and the change in Q of the cavity loaded by a small sample of ferrite material.

In the case of the unperturbated cavity resonating at a frequency ω_0 Maxwell's equations are

$$\nabla \times \bar{E}_0 = -j\omega_0 \mu_0 \bar{h}_0 \tag{1.35}$$

$$\nabla \times \bar{h}_0 = j\omega_0 \varepsilon_0 \bar{E}_0 \tag{1.36}$$

If the cavity is now perturbed by a sample having a volume Δv, the cavity will resonate at a new resonant frequency ω.

Maxwell's equations applicable to the perturbed cavity are

$$\Delta \times \bar{E} = -j\omega\mu_0\bar{h}\ (1 + [\chi]) \tag{1.37}$$

$$\Delta \times \bar{h} = j\omega\varepsilon_0\bar{E}\ (1 + [\chi_\ell]). \tag{1.38}$$

$[\chi]$ and $[\chi_\ell]$ are in general tensors, although in a ferrite $[\chi_\ell]$ is a scalar χ_ℓ.

In the above equations the electric and magnetic susceptibility terms are zero everywhere outside the region $\Delta\nu$ occupied by the ferrite material. After some algebraic manipulations, and taking into account the boundary conditions at the surface of the cavity, we obtain

$$\frac{\omega - \omega_0}{\omega_0} = \frac{-j\int_{\Delta\nu} [\varepsilon_0([\chi_\ell].\bar{E}).\bar{E}_0^* + \mu_0([\chi].\bar{h}).\bar{h}_0^*]d\nu}{\int_\nu [(\varepsilon_0\bar{E}_0^* .\bar{E}) + (\mu_0\bar{h}_0^* .\bar{h})\ d\nu} \tag{1.39}$$

This equation is exact and could be evaluated if the field components of the perturbed cavity were known. However, according to first order perturbation theory, we can set $\bar{E} \simeq \bar{E}_0$, and $\bar{h} \simeq \bar{h}_0$ throughout the cavity.

If the sample is located at a point in the cavity where $E_0 = 0$, then we have

$$\frac{\omega - \omega_0}{\omega_0} = \frac{-j\int_{\Delta\nu} ([\chi_\ell].\bar{h}_0^*).\bar{h}_0]d\nu}{2\int_\nu (\bar{h}_0 \cdot \bar{h}_0^*)\ d\nu} \tag{1.40}$$

In the above equation we have used the fact that the stored electric and magnetic energies averaged out over time are nearly equal. We have also made use of the fact that

$$[\chi]\ \bar{h} = [\chi_\ell]\ \bar{h}_0$$

This equation, therefore, gives the external susceptibility tensor of the material. Since the susceptibility is complex in general, the frequency ω is complex also. For small change this can be written as

$$\omega = \omega_0 + \omega_0 + j\Delta\ (\frac{\omega_0}{2Q_u}) \tag{1.41}$$

where Q_u is the unloaded Q of the cavity. Hence,

$$\frac{\Delta\omega_0}{\omega_0} = \frac{-\int_{\Delta\nu} ([\chi_\ell]' \cdot \bar{h}_0) \cdot \bar{h}_0^*\ d\nu}{2\int_\nu (\bar{h}_0 \cdot \bar{h}_0^*)\ d\nu} \tag{1.42}$$

$$\Delta(\ \frac{1}{2Q_u}\ ) = \frac{\int_{\Delta\nu} ([\chi_\ell]'' \cdot \bar{h}_0^*\ d\nu}{2\int_\nu (\bar{h}_0 \cdot \bar{h}_0^*)\ d\nu} \tag{1.43}$$

The real and imaginary parts of the susceptibility tensor are, therefore, obtained by measuring the shift in resonant frequency and the change in unloaded Q of the cavity. A detailed description of how to perform such measurements is given by Sucher and Fox[24].

1.7 Commercially Available Ferrites

Properties of typical commercially available ferrite materials are shown in Figs. (1.12) and (1.13)[28,26]. The saturation magnetization varies from 250G for substituted YIG to 5000G for NiZn ferrites; Mg Mn Al ferrites have a saturation which ranges from 600 to 3000G. Actually these are the general purpose ferrites mainly used at X-band.

Materials with narrow linewidth will be mainly substituted YIG or Mg Mn Al ferrites. Addition of Ni or Co usually tends to increase the linewidth. The dielectric loss tangent tends to be lower for garnets and MG ferrites than for Mn and Ni ferrites so if a high saturation is not required, it appears to be advantateous to choose garnets or Mg Al ferrites for low magnetic and dielectric loss over a wide range saturation magnetization.

PROPERTIES OF SOME TYPICAL COMMERCIALLY AVAILABLE MICROWAVE FERRITES[a]

Composition	Saturation magnetization $4\pi M_s$ (gauss)	Curie temperature T_c (K)	Resonance line width ΔH (Oe)	Landé g-factor	Coercive force H_c (Oe)	Dielectric constant ϵ	Dielectric loss factor δ_ϵ	Density (g/cm^3)
				Garnets				
Y	1740-1800	550-575	35-60	2.00-2.01	0.7	15.0-16.3	< 0.00025-0.0005	5.05-5.1
YAl	225-1540	370-550	35-75	1.99-2.03	0.4-1.2	13.4-15.5	< 0.00025-0.0005	5.00-5.03
YGd	725-1600	525-555	55-220	2.00-2.08	0.75-1.1	15.0-16.0	< 0.00025-0.0005	5.26-5.85
YGdAl	340-1200	475-525	55-310	2.05-2.10	–	14.8-15.0	< 0.00025-0.0005	5.1-5.73
				Nickel ferrites				
Ni	1500-3000	850-865	350-800	2.3-2.42	—	9.4-12	0.0005-0.0017	5.1
NiZn	5000	650	135	2.08	0.9	12.5	0.001	—
NiCo	3000	860-865	200-350	2.2-2.21	12	13	0.0005-0.0025	—
NiCoAl	800-2440	642-826	200-1000	2.33-2.94	6.5-36	9-12.5	< 0.0005-0.0021	5.05
NiTiAl	2200	825	500	2.45	—	12.0	0.002	4.80
NiAl	350-2000	430-835	155-450	1.4-2.7	4-7	8.2-12.8	0.0003-0.001	4.7-4.8
				Magnesium ferrites				
MgMn	1650-2220	515-595	150-650	2.0-2.1	1.4-2.5	12-13	< 0.00025-0.0008	4.2-4.3
MgMnAl	680-1760	375-565	120-490	2.00-2.11	0.4-2.1	11.5-12	< 0.00025-0.0005	3.9-4.3

Fig. (1.12)

MICROWAVE MATERIALS CHARACTERISTICS

Bulletin No	Composition And Type Number	Saturation Magnetization $4\pi M_s$ (Gauss)	Landé g Factor g eff	Line Width ΔH oe @ - 3db	Dielectric Constant ϵ'	Dielectric Loss Tangent Tan$\delta = \epsilon''/\epsilon'$	Curie Temperature T_c (°C)	Spin Wave Line Width ΔH_k oe	Remanent Induction* B_r (Gauss)	Coercive Force* H_c (oe)	Initial Permeability† μ_o
	Magnesium Ferrites						(Nominal Value)	(Nominal Value)	(Nominal Value)	(Nominal Value)	(Nominal Value)
101 67	TT 1 414	750 ± 5%	1.98 ± 5%	120 ± 20%	11.3 ± 5%	< 00025	90	5.19	544	0.48	120
102 67	TT 1 1000	1000 ± 5%	1.98 ± 5%	130 ± 20	11.6 ± 5%	< 00025	100	3.98	627	0.62	93
103 67	TT 1 1199	1300 ± 5%	1.98 ± 5%	135 ± 20	11.8 ± 5%	< 00025	140	2.75	940	0.81	65
104 67	TT 1 1500	1500 ± 5%	1.98 ± 5%	180 ± 20%	12.0 ± 5%	< 00025	180	2.28	968	0.99	51
105 67	TT 1 105	1 500 ± 5%	1.98 ± 5%	225 ± 20%	12.2 ± 5%	< 00025	225	2.28	1220	1.16	55
106 67	TT 1 390	2 150 ± 5%	2.04 ± 5%	540 ± 20%	12.7 ± 5%	< 00025	320	2.50	1288	1.85	50
107 68	TT 1 2500	2 [illegible]	2.01 ± 1%	500 ± 20%	12.9 ± 5%	< 00025	275	2.04	1410	1.37	57
108 68	TT 1 2630	2 [illegible]	2.02 ± 1%	530 ± 20%	13.0 ± 5%	< 00025	245	2.88	1511	1.33	65
109 68	TT 1 2800	2800 ± 5%	2.01 ± 1%	540 ± 20%	13.1 ± 5%	< 00025	245	2.06	1477	0.63	140
110 69	TT 1 3000	3000 ± 5%	1.93 ± 1%	190 ± 20%	12.9 ± 5%	< 0005	240	3.24	2000	0.85	54
	Nickel Ferrites										
111 67	TT 2 111	500 ± 10%	1.54 ± 5%	150 ± 25%	9.0 ± 10%	< 0008	120	–	140	2.06	23
112 67	TT 2 130	1000 ± 10%	2.60 ± 5%	320 ± 25%	12.0 ± 10%	< 0010	400	–	448	3.39	5
113 67	TT 2 116	1400 ± 10%	2.40 ± 5%	260 ± 25%	12.3 ± 5%	< 0010	425	21.0	512	4.07	6
114 67	TT 2 115	1500 ± 10%	2.40 ± 5%	370 ± 25%	12.3 ± 5%	< 0010	450	19.4	437	4.13	8
115 67	TT 2 118	1800 ± 10%	2.45 ± 5%	775 ± 25%	9.0 ± 5%	< 0015	500	24.5	739	24.10	4
116 67	TT 2 120	1900 ± 10%	2.60 ± 5%	880 ± 25%	9.0 ± 10%	< 0020	545	33.0	615	26.00	4
117 67	TT 2 125	2100 ± 10%	2.10 ± 5%	460 ± 25%	12.6 ± 5%	< 0010	560	6.1	1428	4.42	26
118 67	TT 2 102	2500 ± 10%	2.25 ± 5%	490 ± 25%	12.7 ± 5%	< 0020	570	6.9	1435	4.42	23
119 67	TT 2 101	3300 ± 10%	2.19 ± 5%	350 ± 25%	12.8 ± 5%	< 0025	585	12.4	1853	5.70	17
121 69	TT 2 4000	4500 ± 10%	2.22 ± 5%	340 ± 25%	12.3 ± 10%	< 0025	470	–	1800	3.00	93
120 67	TT 2 111	5000 ± 10%	2.11 ± 5%	160 ± 25%	12.5 ± 10%	< 0010	375	–	1956	0.96	217
122 71	TT 2 4097	1800 ± 10%	2.58 ± 5%	700 ± 25%	10.0 ± 5%	< 0015	500	> 45	–	–	–

† Measured @ 1 KHz

* Measured @ 2 KHz with $H_{app} = 5 \times H_c$

Fig. (1.13)

CHAPTER 2

CONVENTIONAL NON-RECIPROCAL EFFECTS

Before describing the original work done in this research project, it is worth mentioning what has already been developed in the field of non-reciprocal devices. A brief description of most of the non-reciprocal effects discovered up to now is given in this cahpter. Finally, a brief discussion on the merit and improvement methods of each type of device will be given.

2.1 Resonance Effect

Consider a piece of ferrite in which a circularly polarized wave is propagating in a given direction. Let us suppose that the plane containing the magnetic field vector of the wave is perpendicular to a d.c. magnetic field applied to the ferrite. These are the conditions under which resonance is possible and, if the circular polarization is rotating in the positive direction, we obtain the maximum value of (μ"+) at a certain value of the d.c. applied field. For a wave propagating in the reverse direction, it is (μ"-) which is involved and we know that, under these conditions, quite a large attenuation is possible in the ferrite.

It is easy to visualize an application of this phenomenon with the arrangement shown in Fig. (2.1). In a circular guide, a wave is propagating with circular polarization in the TE_{11} mode.

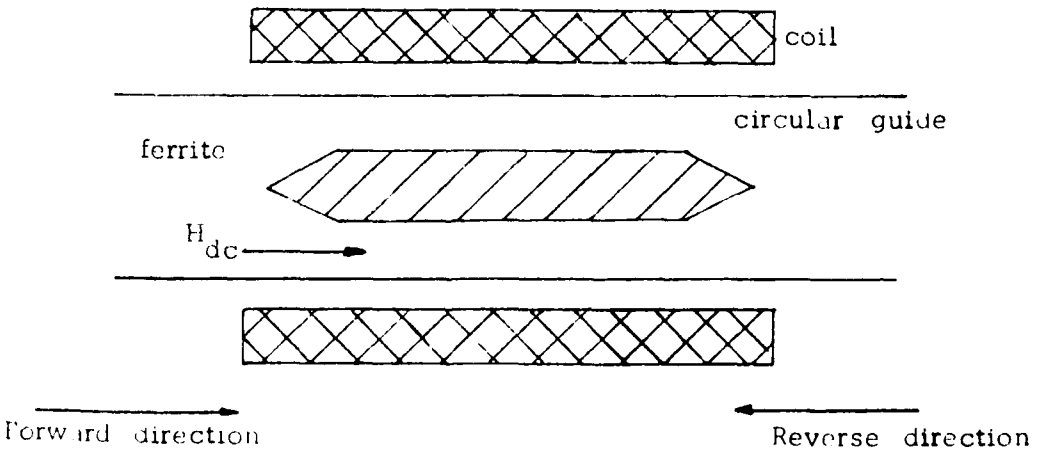

Fig. (2.1) Circular guide filled with ferrite and magnetized along the axis

A coil placed around the guide develops a d.c. field in the axis of the guide, along which lies a strip of ferrite. If the sense of rotation of the polarization is such that the ferrite exhibits its $\mu''-$ permeability in the forward direction, the attenuation in this direction is low. On the other hand, when propagation takes place in the reverse direction, it is $\mu''+$ which appears and a high attenuation occurs when H is adjusted for resonance.

The ferrite isolation has not, however, been developed in this form and in practice it is the arrangement of Fig. (2.2) which is used.

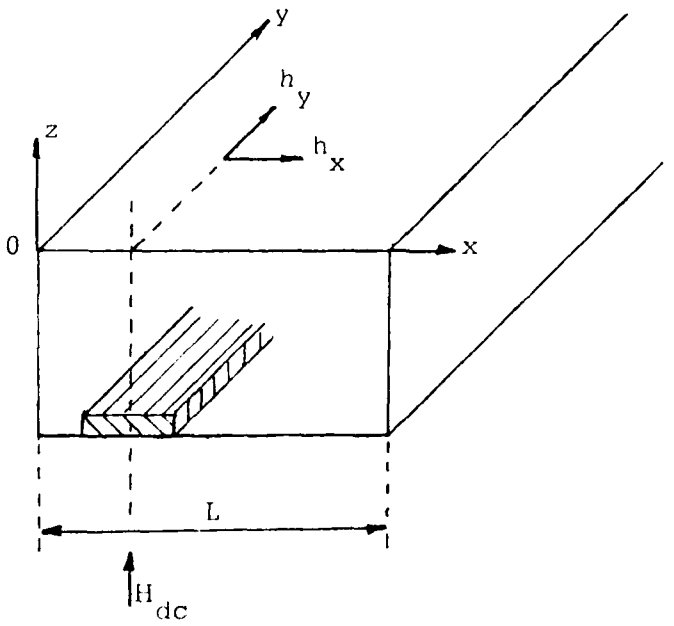

Fig. (2.2) The actual construction of the resonance isolation in rectangular waveguide

In a rectangular guide, when propagation is in the TE_{01} mode, the components of the magnetic field in the directions Ox and Oy are as follows:

$$h_x = -j\beta \sin \frac{\pi x}{L} e^{-j\beta y} \tag{2.1}$$

$$h_y = -\frac{\pi}{L} \cos \frac{\pi x}{L} e^{-j\beta y} \tag{2.2}$$

where $\beta = \frac{2\pi}{\lambda g}$.

The amplitudes of these components depend only on x, while the exponential term is representing the phase of the propagating field component. Since circular polarization is defined by two components in quadrature in space and 90° apart in phase, for all points where:

$$h_x = jh_y \tag{2.3}$$

the polarization of the magnetic field is circular.

This relationship is verified for a plane parallel to the narrow side of the waveguide at a distance x_o from the origin such that:

$$-j\beta \sin \frac{\pi xo}{L} = -j \frac{\pi}{L} \cos \frac{\pi xo}{L} \tag{2.4}$$

i.e.

$$\tan \frac{\pi xo}{L} = \frac{\lambda g}{2L} \tag{2.5}$$

But in a rectangular guide:

$$\lambda g = \frac{\lambda o}{\sqrt{[1 - (\lambda o/2L)^2]}} \tag{2.6}$$

So the formula shows that xo depends on frequency. Using this formulation, we could locate the position where we have circular polarization in a rectangular waveguide. A piece of ferrite will be placed at this position in the waveguide such that the effect same as in the circular waveguide will occur. For an applied static magnetic field, the ferrite material will go into resonance and absorb the microwave energy for one direction of propagation while nothing will happen in the opposite direction. The main problem of such a device is that the position where we have circular polarization varies with frequency. Various techniques are used to counteract this shift with frequency. The most popular methods used are placing a piece of dielectric next to the ferrite or by tapering the ferrite cross section.

2.2 The Faraday Effect

Consider again the arrangement in Fig. (2.1), but suppose now that a TE_{11} wave with rectilinear polarization is propagating along the guide from left to right.

We know that a linearly polarized wave can be resolved into two circularly polarized waves of the same amplitude and opposite sense of rotation. In the ferrite acted on by the field H_{dc}, one of the two waves will, therefore, be affected by the permeabilities $\mu+$ and the other by the permeabilities $\mu-$. The resolution of the linear polarization into two circular polarizations is

represented in Fig. (2.3(a)). It can be seen that the vector R is the sum of the two vectors P_1 and P_2 rotating in opposite directions.

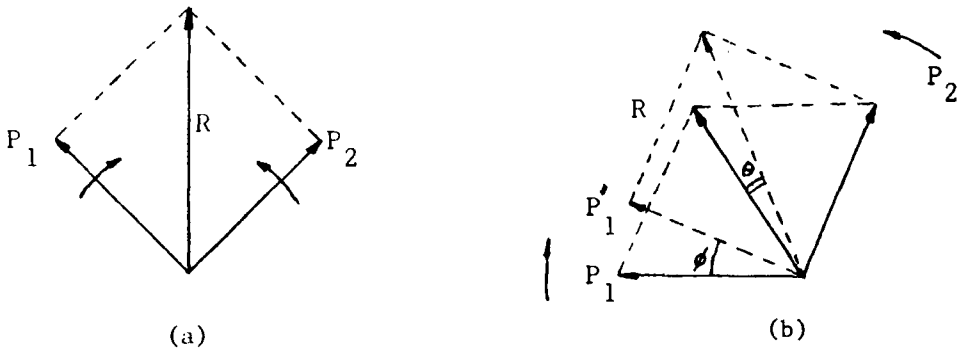

Fig. (2.3) The vector representation of the Faraday effect, considering the wave propagating down the guide as two circularly polarized waves in opposite directions

P_1 and P_2 being synchronous, R remains always vertical. If, in the course of propagation, one of the two components slowly changes phase with respect to the other, R will rotate as shown in Fig. (2.3(b)). The component P_1, instead of being at P_1', symmetrical about the vertical with P_2, lags by an angle ϕ so that the position of R is now as indicated on the diagram and makes an angle θ with the vertical.

Now this is exactly what happens in the guide. Since $\mu'+$ and $\mu'-$ are different, the propagation constants,

$$\beta^+ = \frac{2\pi}{\lambda g^+} \quad \text{and} \quad \beta^- = \frac{2\pi}{\lambda g^-} \tag{2.7}$$

are different.

The relative lag of one component behind the other is:

$$\phi = [\beta^{+} - \beta]\ \ell \tag{2.8}$$

so that, the rotation of the direction of R is:

$$\theta = \frac{[\beta^{+} - \beta^{-}]}{2}\ \ell \tag{2.9}$$

This rotation of the plane of polarization of the wave, which is also found in optics is the Faraday effect. Faraday rotation depends on the relative values of μ'^{+} and μ'^{-} and, to make use of it, it is necessary to work in a region where they differ appreciably. However, μ''^{+} and μ''^{-} must be small so that the system will not introduce any appreciable attenuation in the propagation.

The essential feature of the Faraday effect is its nonreprocity. Let us assume that, in the case of Fig. (2.1), for propagation from left to right, the Faraday rotation takes place from left to right as seen by an observer looking in the direction of propagation of the wave. In the reverse direction of propagation, the position would be the same if H_{dc} were also reversed; but H_{dc} has maintained its direction so that the μ are permuted and Faraday rotation takes place from right to left as seen by an observer looking in the direction of the inverse wave and, therefore, from left to right as seen by the first observer. The two rotations corresponding to the forward and reverse directions are equal and add; it suffices, therefore, to make $\theta = 45°$ to produce an isolator.

The structure used is that of Fig. (2.4) which shows also the position of the electric field vectors. A rectangular guide excites a circular guide containing the ferrite. The axial magnetic field is created by a coil around the circular guide. The latter in turn excites a rectangular guide set at 45° to the input guide. It can be seen that for a Faraday rotation of 45° there is transmission from left to right. In the right-to-left direction, the rotation brings the electric field into quadrature with the field of the TE_{01} mode in the input guide. The field in quadrature cannot be propagated in the guide. It is, therefore, reflected to the right where after suffering a rotation of 45° it finds itself in quadrature with the normal field of the output guide from which it is again reflected to the left and again rotated, this time into the right direction to enable it to re-enter the input guide. To prevent this an absorbent load is placed near the input guide; this load is a resistive slab perpendicular to the input field (and so, having no effect on it) and, consequently, parallel to the field coming from the right, thus insuring maximum absorption.

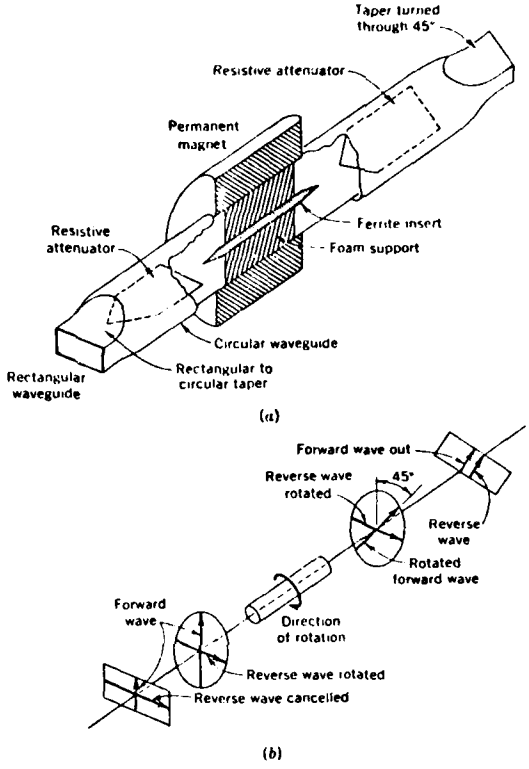

Fig. (2.4) The Faraday rotation isolator.
a. Cutaway view
b. Method of operation

It will be seen that the ferrite employed is a cylindrical rod which occupies only a small part of the cross-section of the circular guide. In fact, a small cross-section of ferrite is sufficient to affect a large part of the transmitted energy because of the high values of ε and μ; it is found that there is an optimum ratio of the diameters of the ferrite and the guide for a maximum figure of merit.

2.3 The Field Displacement Effect

The field displacement effect is due to the appearance of higher modes in the ferrite as a result of the high value of the product of its dielectric constant and its permeability. Since the permeability tensor depends on the direction of propagation of the wave, it is conceivable that one might get non-reciprocal effects.

The mechanism of field displacement can be represented by Fig. (2.5) for a rectangular guide loaded with a slab of ferrite stuck to one of the narrow sides of the guide.

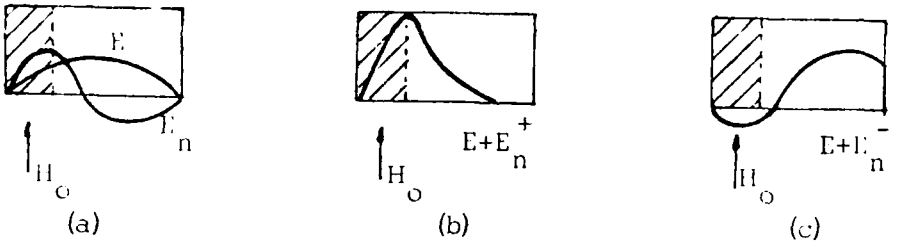

Fig. (2.5) Fields in a wave guide partially filled with ferrite.
a. The field distribution of the two modes
b. Resultant field in +ve direction
c. Resultant field in -ve direction.

In this guide, partially filled with dielectric (ferrite), there is a mode whose configuration is E: this TE_{01} mode is independent of the direction of propagation and is a function of the dimensions of the ferrite and its dielectric constant only. However, the high

value of the permeability tensor causes higher modes to appear, the effect of which is indicated by E_n, the values of E_n depending on the direction of propagation. If we denote by E_n^+ the distribution obtained for one direction and by E_n^- that obtained for the opposite direction, the resultant field is $E + E_n^+$ in the one case and $E + E_n^-$ in the other.

The resultant configurations are arranged as shown in Fig. (2.5(b)) and (2.5(c)). In the former case nearly all the energy is concentrated in the ferrite with a field maximum at the air-ferrite interface, whereas, in (c) nearly all the energy is in the air. If an absorbent strip is stuck to the ferrite, there will be a large attenuation in the direction of propagation corresponding to (b) and a low attenuation in the reverse direction.

It is very difficult to calculate field displacement systems because of the complex permeability tensors. A relatively simple case is that of a thin slab in the plane of circular polarization of the guide: in this case the permeability would be μ'^+ in the propagation direction and μ'^- in the reverse direction.

We can have either $\mu'^+ < \mu'^-$ or $\mu'^+ > \mu'^-$ depending on the value of H_o. It is essential to operate in the former range so as to have the maximum difference between the two directions of propagation, which means using magnetic fields below the resonant field. Under these conditions, however, the system is only of interest at high frequencies where the low-field waves are negligible.

2.4 The Junction Circulator

A particularly compact device which has found a great many applications over a wide frequency range is the symmetrical Y-junction circulator as shown in Fig. (2.6).

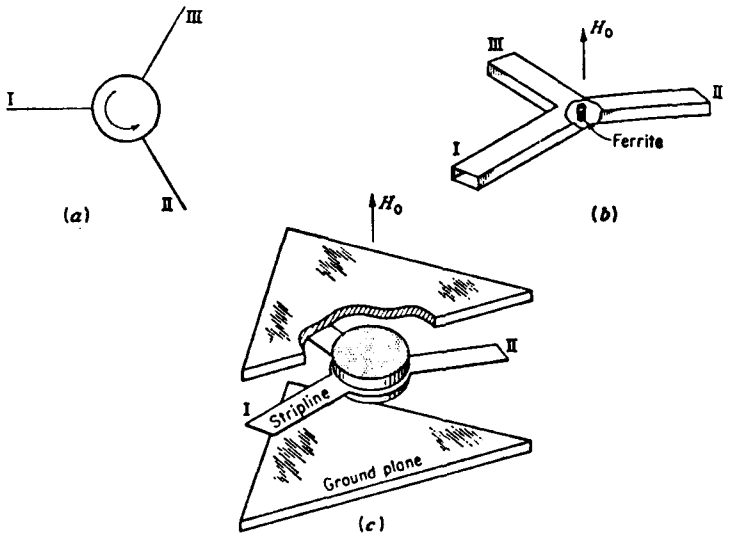

Fig. (2.6) (a) The circuit symbol for the Y-junction circulator indicates transmission as I→II→III→I, and so on,
(b) The waveguide version shows a vertically magnetized ferrite rod as the nonreciprocal element,
(c) The stripline version shows the ferrite disc which is magnetized perpendicular to the broad face.

The feature that makes this device so attractive is its simple, compact, light construction at all frequencies. Although it has been designed to operate in bands from 100 MHz through the UHF region and the microwave region to the mm-wave range, it

rarely weighs more than a pound, and the largest models are less than 6 inches in diameter. In the stripline version Fig. (2.6(c)), it is often manufactured by printed circuit techniques and is miniaturized through the use of high dielectric constant materials, which also permits it to carry higher r-f power before corona effects set in. The device will tolerate high signal power considerably in excess of 50 Kw (peak) and 500 watts (average) when operated as a circulator, switch, or modulator.

Until very recently, the Y circulator and switches have been developed empirically and explained on a phenomenological basis in terms of the scattering matrix treatment.

The circulation mechanism can be explained briefly, as follows: The wave incident at Port I of Fig. (2.7) is the fundamental mode with the r-f electric vector polarized parallel to the direction of the applied magnetic field. Thus, the ferrite disc supports two typical electromagnetic modes characteristic of such a tensor magnetic medium. Two mutually orthogonal components of the r-f magnetic field are excited in the plane perpendicular to the d-c magnetic field vector, i.e., the plane parallel to the broad face of the disc. One mode has a right-hand circularly polarized r-f magnetic vector and has increasing field intensities toward the right side of the input port. The other mode has the opposite sense of rotation. The combination of these two modes has a hyperbolic transverse electric field dependence. The plane wave incident at the input stripline port is distorted within the

ferrite so that field intensities increase toward the region between input Port I and output Port II, as shown by the contours of constant electric field intensity Fig. (2.7).

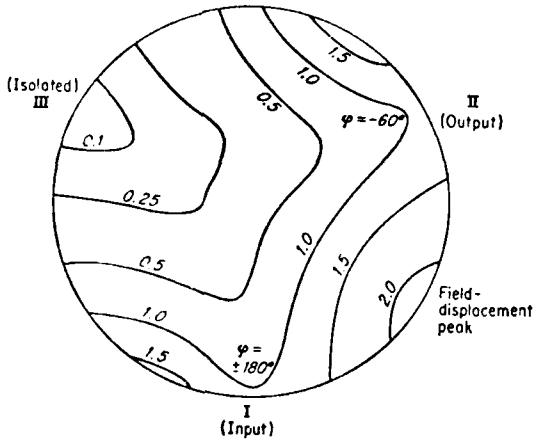

Fig. (2.7) Idealized sketch of the contours of constant r-f electric field intensity within the ferrite disc of the stripline Y-circulator illustrating the nonreciprocal field displacement principle of circulation.

This combination of the two sets of rotating modes computed by Bosma[16] produces a wave pattern which has its field-displacement peak between the input and output ports and a null at the isolated port. Both the electric and magnetic field configurations established by the superposition of these two modes result in a pattern for which Poynting vectors exist at input Port I and output Port II and are oppositely directed, whereas the vector vanishes at Port III.

2.5 Comparison of Isolator Types

In this chapter four basic types of isolators have been discussed with respect to method of operation, construction, and design consideration. It is appropriate to compare the types to bring out the advantages of each. Fig. (2.8) is convenient for this purpose.

The field displacement isolator requires a medium biasing field and, thus, a medium weight magnet. The Faraday rotation isolator requires the lowest biasing field and seems capable of providing isolation approaching those of the field displacement isolator. Its bandwidth capabilities are somewhat greater than the field displacement device but not as great as the resonance isolator. The power handling capabilities of both the field displacement and Faraday rotation isolators are limited by the loss films employed which can dissipate a relatively small amount of power.

It should be pointed out that a circulator can be used as an isolator by terminating the unused ports. This can be particularly advantageous from a power handling standpoint, since reflected power can be dissipated in a termination which is capable of being cooled, rather than in the ferrimagnetic material. The Y-junction circulator, when used as an isolator, rates an E on all counts in Fig. (2.8).

	Isolator Type			
	Faraday rotation	Field displacement	Resonance	Y-junction circulator
Isolation	G	G	E	E
Broadband capability	G	F	E	E
Biasing field	E	G	F	E
Power handling	F	F	G	E
Cost	F	F	E	E

Code used : E= Excellent, G= Good, F= Fair.

Fig. (2.8) Comparison of isolator types.

CHAPTER 3

ANALYTICAL FORMULATION

This chapter deals mainly with explaining the derivation of the analytical expression of the proposed structure. The structure (Fig. 3-1) consists of a dielectric waveguide containing a ferrite layer in which periodic metal strips are provided. This new structure is an improvement of the recently proposed device in which a notched grating was used instead of the metal strips[1]. In the analysis it has been assumed that the structure is infinitely periodic in the x-direction and that it is invariant in the y-directions. The metal strips are also assumed to be infinitely thin.

The operating principle of this device lies in the fact that the propagation constants of the guided waves in the opposite directions are different when a dc magnetic field is applied. When a periodic perturbation is provided along the waveguide, it is possible at a certain frequency interval that a guided wave propagating in one direction becomes leaky and, hence, it attenuates as it propagates; whereas, the one propagating in the opposite direction is still guided without leakage. Hence, the structure works as an isolator.

In the structure proposed previously, the periodic perturbation was produced by a grooved grating. It turns out that the

grooved grating provides only a small perturbation[2]. In the new structure the metal strips would provide an appreciable amount of perturbation, since the principal electric field is chosen to be parallel to the strips. Hence, the attenuation constant due to leakage in this new system would also be large and the entire device length can be reduced for a given degree of isolation.

In the analysis it is assumed that the problem in invariant in the y-direction. It is also assumed that the strips have no thickness and only E_y, H_x and H_z components are present. The problem is first solved for the system without metal strips using the transverse resonance technique. Then by applying Floquet's theorem, the electric fields outside the strip and the currents in the strips are represented in terms of space harmonics. The transverse equivalent circuit of each space harmonic is then derived with the effect of the metal strip. The next step is the application of Galerkin's method to the entire spectrum. In this method the current is expanded in terms of known basis functions. The resulting equation could then be used to solve for the propagation constant of the grating structure.

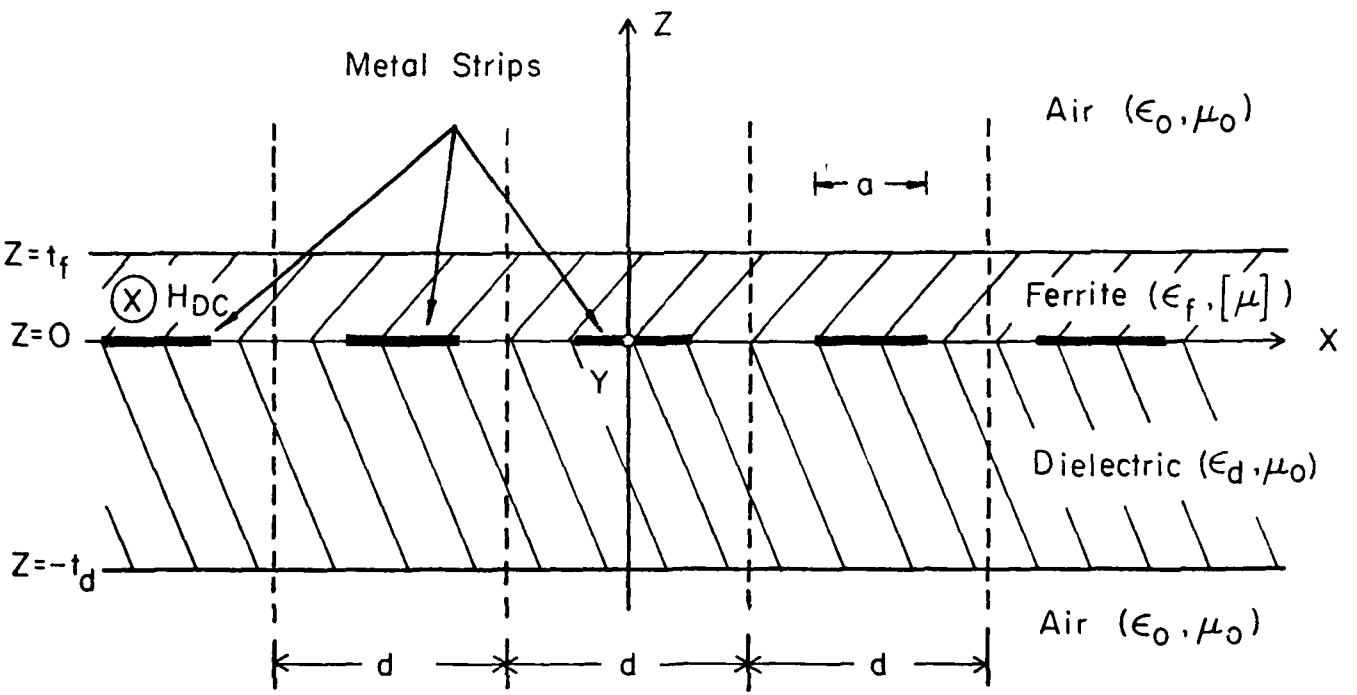

Fig. (3.1) Cross sectional sketch of the ferrite - dielectric waveguide showing the geometry and the co-ordinate system.

3.1 The Transfer Matrices and the Equivalent Transverse Resonance Circuit

The transverse resonance method[19] is a powerful way to derive a transcendental equation in terms of the propagation constant of the system in question. The sum of the impedances at one point in the transverse direction is zero (resonance) only for the correct values of propagation constant.

In the case of a multi-layered structure, formulation of the impedance in the transverse direction can be facilitated by the use of transfer matrices for each layer in question. In this way one could easily obtain the impedance at any plane in the system with respect to the impedance at a given reference plane.

The derivation of the transfer matrix for a ferrite layer is as follows. Consider the structure in Fig. 3.2.

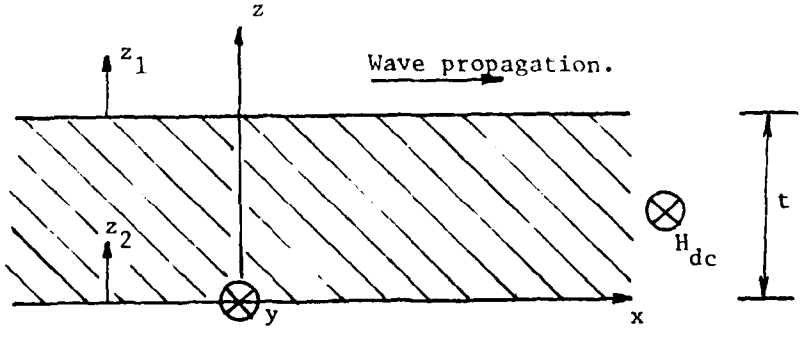

Fig. (3.2).

From Maxwell's equations

$$\nabla x\bar{E} = -j\ \omega\bar{\mu}\ \bar{H} \tag{3.1}$$

For a TE wave in the x direction we are going to have E_y, H_x and H_z components only.

Let

$$\bar{E}_y\ (Z) = [a\ e^{-j\eta z} + b\ e^{j\eta z}]\ e^{j(\omega t - \beta x)} \tag{3.2}$$

then,

$$\nabla x\bar{E} = \begin{bmatrix} \bar{a}_x & \bar{a}_y & \bar{a}_z \\ \frac{\partial}{\partial x} & \frac{\partial}{\partial y} & \frac{\partial}{\partial z} \\ 0 & E_y & 0 \end{bmatrix} = \frac{\partial E_y}{\partial z}\,\bar{a}_x \quad , \quad \frac{-\partial E_y}{\partial x}\,\bar{a}_z \tag{3.3}$$

also,

$$-j\omega\bar{\mu}\bar{H} = -j\omega\mu_o \begin{bmatrix} \mu & 0 & jk \\ 0 & 1 & 0 \\ -jk & 0 & \mu \end{bmatrix} \begin{bmatrix} H_x \\ 0 \\ H_z \end{bmatrix} \tag{3.4}$$

$$= -j\omega\mu_o\ [(\mu H_x + jKH_z)\ \bar{a}_x + (-jKH_x + \mu H_z)\ \bar{a}_z] \tag{3.5}$$

Equatin for $\bar{a}_x$ and $\bar{a}_z$ in Maxwell's equations and solving for $H_x(z)$ we get

$$H_x(z) = \frac{j}{\omega\mu_o\mu_e}\ [a(\alpha\beta + j\eta)\ e^{-j\eta z} + b(\alpha\beta - j\eta)\ e^{j\eta x}] \tag{3.6}$$

where $\mu_e = (\mu^2 - K^2)/\mu$, $\sigma = K/\mu$, $\mu = 1 + [\omega_o\omega_n/(\omega_o^2 - \omega^2)]$,

$$K = \omega\omega_n/(\omega_o^2 - \omega^2) \quad , \quad \omega_o = \gamma H \quad , \quad \omega_m = \gamma 4\pi M \quad \text{and} \quad \eta = \sqrt{\omega_o^2 \mu_o \mu_e \varepsilon_o \varepsilon_m - \beta^2} \, .$$

Here, γ is the gyromagnetic ratio and $4\pi M$ is the saturation magnetization. Also, the time and propagation factor exp $\{j(\omega t - \beta x)\}$ is to be understood and suppressed.

We will now identify E_y and H_x as V and -I, respectively. Then the values of V(o) and I(o) at Z = 0 are related to those at V(z) and I(z) at z = z by

$$\begin{bmatrix} V(o) \\ I(o) \end{bmatrix} = \begin{bmatrix} \cos \eta z - \frac{\sigma\beta}{\eta} \sin \eta z & j \frac{\omega\mu_o\mu_e}{\eta} \sin \eta z \\ j \frac{(\sigma\beta)^2 + \eta^2}{\omega\mu_o\mu_e\eta} \sin \eta z & \cos \eta z + \frac{\sigma\beta}{\eta} \sin \eta z \end{bmatrix} \begin{bmatrix} V(z) \\ I(z) \end{bmatrix} \tag{3.7}$$

This experssion relates the impedance at one point in the transverse direction to a reference value of the impedance.

In the case of a dielectric material, the transfer matrix can be written as

$$\begin{bmatrix} V(o) \\ I(o) \end{bmatrix} = \begin{bmatrix} \cos \eta z & j \frac{\omega\mu_o}{\eta} \sin \eta z \\ j \frac{\eta}{\omega\mu_o} \sin \eta z & \cos \eta z \end{bmatrix} \begin{bmatrix} V(z) \\ I(z) \end{bmatrix} \tag{3.8}$$

This can be derived by letting $\sigma = 0$ and $\mu_e = 1$ in (3.7)
The transverse resonance equivalent network for the structure in Fig. 3.1 is given by removing the current source in Fig. 3.3. The current source appears when the equivalent transverse network concept is introduced in the analysis of the grating structure with metal strips. Such a process will be explained in the next section.

The eigenvalue equation $Y_U + Y_L = 0$ provides the propagation constant β. Note that we obtain two different values of β corresponding to waves propagating in the opposite directions.

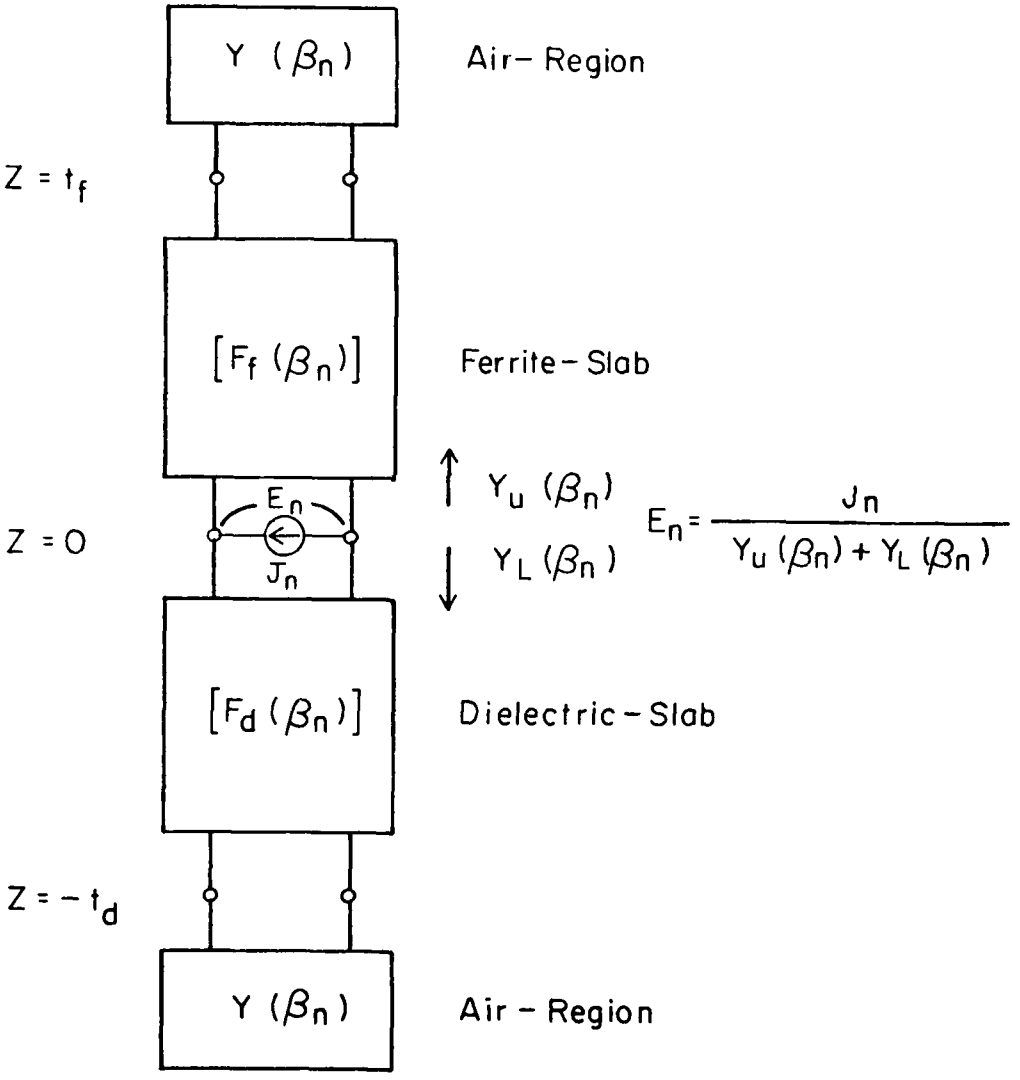

Fig. (3.3) Transverse equivalent network for the space harmonics.

3.2 Floquet's Theorem and the Space Harmonics

The basis for a study of periodic transmission systems is a theorem due to a French mathematician, Floquet. This theorem may be stated as follows: For a given mode of propagation at a given steady-state frequency, the fields at one cross section differ from those a period away only by a complex constant. The theorem is true whether or not the structure contains loss as long as it is periodic. The proof of the theorem lies in the fact that when the structure having infinite length is displaced along its axis by one period, it cannot be distinguished from its original structure. Hence, we write the electric or magnetic field as

$$\bar{E} = E(x, y, z)\ e^{-\gamma(x)}\ e^{j\omega t} \tag{3.9}$$

where $E(x, y, z)$ is periodic in x with period d.

The field $E(x, y, z)\ e^{-\gamma x}$ can be expanded in a Fourier series of the form

$$E(x, y, z)\ e^{-\gamma x} = \sum_{\text{all } n} E_n(y, z)\ e^{-j(2\pi n/d)x}\ e^{-\gamma x} \tag{3.10}$$

To find $E_n(y,z)$, multiply the above by $e^{j(2\pi m/d)x + \gamma x}$

$$E(x, y, z)\ e^{j(2\pi m/d)x} = \sum_{\text{all } n} E_n(y, z)\ e^{j(2\pi m/d)x - j(2\pi n/d)x} \tag{3.11}$$

Integrate both sides from x_1 to $x_1 + d$

$$\int_{x_1}^{x_1+d} E(x,y,z)\ e^{j(2\pi m/d)x}\ dx = \sum_{\text{all } n} \int_{x_1}^{x_1+d} E_n(y,z)\ e^{j(2\pi/d)(m-n)x}\ dx$$

$$= 0 \quad , \quad m \neq n$$

$$= E_n(y,z)d \quad , \quad m = n \tag{3.12}$$

Therefore,

$$E_n(y,z) = \frac{1}{d} \int_{x_1}^{x_1+d} [E(x,y,z)\ e^{-\gamma z}]\ e^{[\gamma + j\ (2\pi n/d)]x}\ dx \tag{3.13}$$

This expression is used later to calculate the amplitude of individual terms in the series.

The n-th term on the right of the series representation is called the n-th space harmonic. It has a propagation constant $\gamma + j\ \frac{2\pi n}{d}$. If there are no losses in the system, it turns out that γ is either purely real or purely imaginary. If imaginary, we write $\gamma = j\beta_o$ and define

$$\beta_n = \beta_o + \frac{2n\pi}{d} \tag{3.14}$$

where β_n is called the phase constant for the n-th space harmonic. A velocity $v_n = \omega/\beta_n$ is the phase velocity of the n-th space harmonic.

Applying Floquet's theorem to the structure containing periodic metal strips, we can write expressions for the electric field and the current on the strips as

$$E_y = \sum_{n=-\infty}^{\infty} E_n(z) \cdot e^{j\beta_n x} \tag{3.15}$$

$$J_y = \sum_{n=-\infty}^{\infty} J_n e^{j\beta_n x} \quad , \quad \beta_n = \beta + \frac{2n\pi}{d} \tag{3.16}$$

Since E_y and J_y are expressed in the same manner, we only need to relate E_n and J_n. Since E_n and J_n are no longer functions of x, we can use the spectral domain immittance method. For each space harmonic, each layer is replaced with a transfer matrix. From the transverse equivalent circuit (Fig. 3.3) the space harmonics of the E_y at z = 0 and of J are related by

$$E_n = \frac{1}{Y_U(\beta_n) + Y_L(\beta_n)} J_n = Z_n J_n \tag{3.17}$$

The quantities Y_U and Y_L are input admittances looking upward and downward at z = 0. They could easily be found by the use of the transfer matrix methods discussed in the previous section. In fact, it is only necessary to substitute β_n for β in the expressions derived in that section.

3.3 Variational Formulation and Galerkin's Approximation

The next step is to obtain the dispersion characteristics of the structure by using the relation of E_n and J_n. To this end, we apply a variational formulation of the structure. The variational formulation of the structure could be written as

$$I = \frac{1}{a} \int_{-d/2}^{d/2} E(x)\ J(x)\ dx \tag{3.18}$$

This integral could be written as

$$I = \sum_n E_n J_n = \sum_n J_n^2 Z_n \tag{3.19}$$

Since the electric field on the metal strips and the current in the spacing between metal strips is zero, a stationary solution must make I vanish. Hence, $\sum_n J_n^2 Z_n = 0$.

We now expand J_n in terms of known basis functions.

$$J_n = \sum_{j=1}^{N} a_j J_n^{(j)} \tag{3.20}$$

N being the number of basis functions and a_j the unknown coefficient of each function. Substituting into the variational equation we get

$$\sum_{j=1}^{N} K_{ij} a_j = 0 \quad , \quad i = 1, 2, \ldots N \tag{3.21}$$

This process is identified as Galerkin's procedure. The above equation has a unique solution only if

$$\det [K_{ij}] = 0 \tag{3.22}$$

From this equation, the dispersion characteristics can be obtained, and we can compute β for a given frequency.

CHAPTER 4

THE COMPUTER PROGRAM

A computer program has been written to analyze the ferrite-dielectric structure containing metal strips (Fig. 3.1). The program is based on the theory discussed in Chapter 3. The best way to explain how the theory has been implemented numerically by the program is to look at the flow chart of the program (Fig. 4.1) relating how the subroutines are linked. A print-out of the program is given in the Appendix.

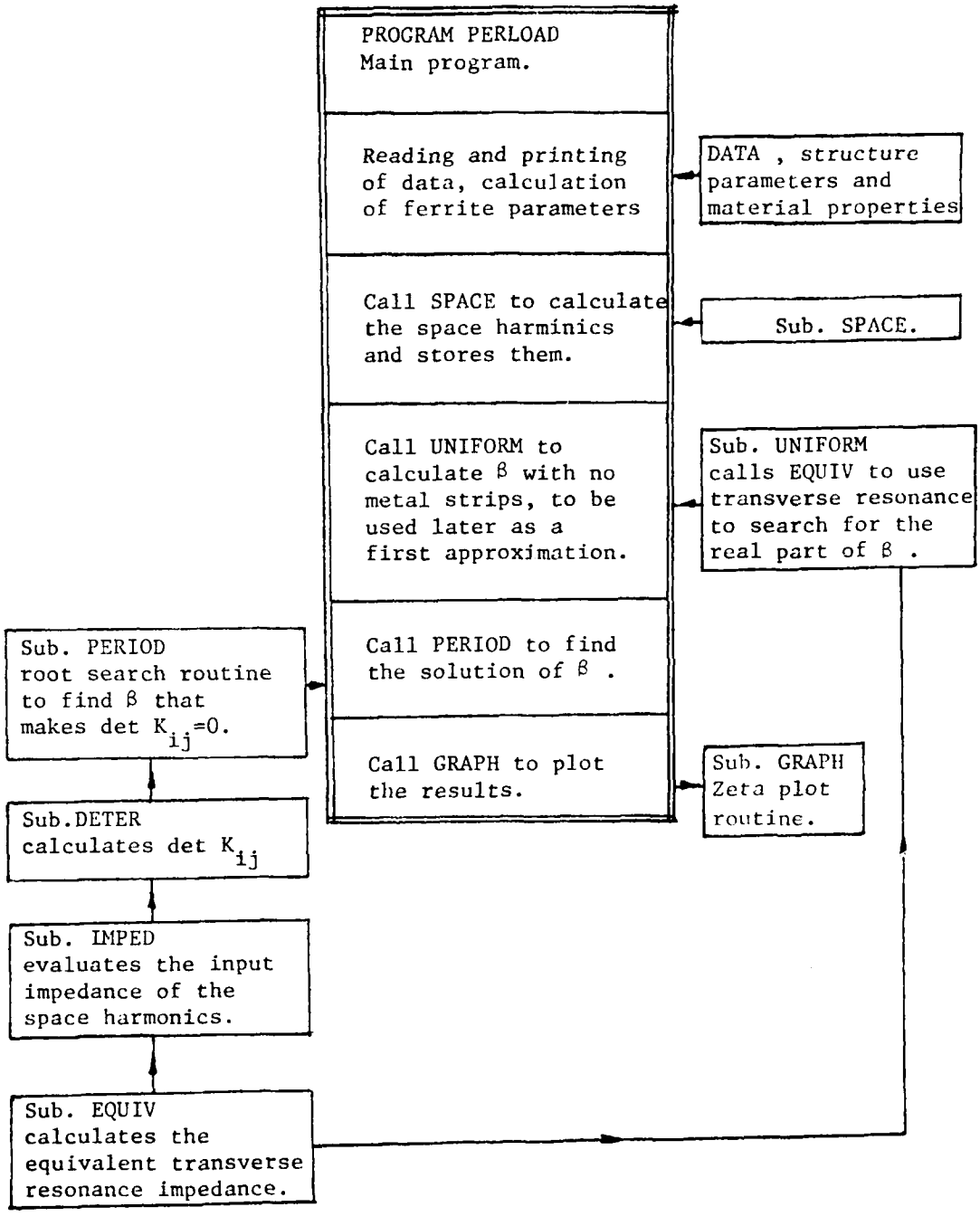
PROGRAM PERLOAD
Main program.
Reading and printing of data, calculation of ferrite parameters
DATA , structure parameters and material properties
Call SPACE to calculate the space harminics and stores them.
Sub. SPACE.
Call UNIFORM to calculate β with no metal strips, to be used later as a first approximation.
Sub. UNIFORM calls EQUIV to use transverse resonance to search for the real part of β .
Call PERIOD to find the solution of β .
Sub. PERIOD root search routine to find β that makes det K_{ij}=0.
Call GRAPH to plot the results.
Sub. GRAPH Zeta plot routine.
Sub.DETER calculates det K_{ij}
Sub. IMPED evaluates the input impedance of the space harmonics.
Sub. EQUIV calculates the equivalent transverse resonance impedance.

Fig. (4.1).

4.1 Program PERLOAD

This is the main program which controls all of the subroutines. First the data defining the structure dimensions and material properties are read and then printed. The space harmonics are then calculated and stored in an array by the subroutine SPACE.

Polders permeability tensor is then calculated, Green[10] and Sandy's formulas are used for the ferrite below saturation.

The program then calculates the propagation constant of the structure without periodic metal strips using Subroutine UNIFORM. This result is then used as a first approximation of β for the structure with the metal strips where the actual theory discussed in Chapter 3 is implemented.

Subroutine PERIOD is then called. This subroutine in turn calls the rest of the subroutines to implement the root search of the actual structure. This will be discussed in more detail in the next section. This subroutine will give the result of β for the respective frequencies desired. The program then calls subroutine GRAPH; this is a ZETA plot routine to plot the K-β diagram desired.

4.2 Subroutine SPACE

The function of this routine is to calculate the space harmonics of the basis functions used. In this particular program it has been determined that four basis functions would give enough accuracy. The basis used are truncated sines and cosines, best represented in Fig. 4.2.

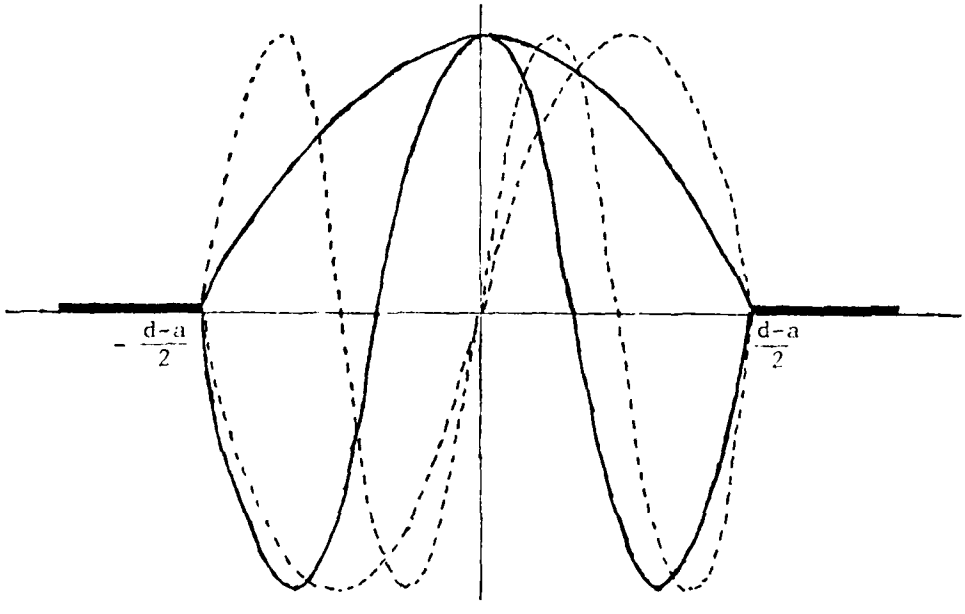

Fig. (4.2). Basis representing the field distribution between two periodic metal strips.

The normalized equations of the basis used to represent the electric field between two periodic metal strips are given by

$$\frac{\pi d}{2(d-a)} \; e^{j\beta_o x} \cos \frac{\pi x}{(d-a)} \qquad (4.1)$$

$$\frac{j\pi d}{(d-a)}\, e^{j\beta_o x} \sin\frac{2\pi x}{(d-a)}$$

$$\frac{-3\pi d}{2(d-a)}\, e^{j\beta_o x} \cos\frac{3\pi x}{(d-a)} \qquad (4.1)$$

$$\frac{2\pi d}{j(d-a)}\, e^{j\beta_o x} \sin\frac{4\pi x}{(d-a)}$$

As explained in Chapter 3 to calculate the space harmonics by Floquet's theorem, the following integral has to be performed.

$$\frac{1}{d}\int_{-\frac{d-a}{2}}^{\frac{d-a}{2}} [\text{BASIS}]\; e^{-j\beta_o x - j\frac{2\pi n x}{d}}\, dx \qquad (4.2)$$

The integrals for the four basis functions have been analytically calculated to give the following equations for the space harmonics which are programmed into subroutine SPACE.

$$C_1(N) = \frac{\cos X}{1-4Y}$$

$$C_2(N) = \frac{\sin X}{1-Y}$$

$$C_3(N) = \frac{\cos X}{1-\frac{4}{9}Y} \qquad (4.3)$$

$$C_4(N) = \frac{\sin X}{1-\frac{1}{4}Y}$$

$$\text{where } X = N\pi\left(1-\frac{a}{d}\right)$$

$$Y = \left(1-\frac{a}{d}\right)^2 N^2$$

4.3 Subroutine UNIFORM

This routine searches for a solution of β when the structure consists of just a dielectric-ferrite guide. Subroutine UNIFORM is called to give the impedance looking up and down transversely at the ferrite dielectric boundary. According to transverse resonance the solution of β occurs when the sum of the impedance looking up and looking down is zero.

This routine searches only for the real part of β. The way this is done is by fixing a lower and upper bound where β may exist and then scan this region by dividing it into 100 segments. The lower bound has been chosen to be the β of air only and the upper bound the β for ferrite only, since ferrite usually has the largest value of β. The only problem that may occur in this routine is when the effective permeability of the ferrite becomes negative. In this case either the value of β could be smaller than that of air or no solution would be found as has been frequently experienced.

4.4 Subroutine PERIOD

This routine is mainly a root search routine. The function is mainly to find β which makes the determinant zero. The determinant is calculated by subroutine DETER, so this routine gives the value of β, plugs it in DETER and then tries to find the value of β for zero determinant.

Muller's method is used to search for β. Muller's method is an improvement on Newton's method. For more detail one should refer to Peter Henrici, "Elements of Numerical Analysis," John Wiley & Sons, 1964, page 198.

This routine could be replaced by an IMSL routin such as ZANALY. ZANALY has been used and tested; it actually gives the same results as subroutine PERIOD. The only difference is that using IMSL is more expensive and one has less control of what goes on.

4.5 Subroutine DETER

The function of this routine is to calculate the determinant for a given input value of β. First, the matrix K_{ij} is formed by putting together the space harmonics of the basis functions. It has been found experimentally that taking ±40 space harmonics would give an accurate answer. In order to calculate the symmetric matrix K_{ij}, the routine calls subroutine IMPED which in turn calls subroutine EQUIV to get the necessary information on the impedance looking in the upper and lower regions, to be able to implement the formula

$$K_{ij} = \sum_{n=-\infty}^{\infty} J_n^{(i)} / \left[Y_U(\beta_n) + Y_L(\beta_n) \right] \qquad (4.4)$$

The determinant is then calculated using standard equations.

CHAPTER 5

THE EXPERIMENTAL INVESTIGATION

This chapter deals mainly with the experiments that have been carried out. Both theoretical and experimental results are included. The main purpose of this investigation is to try to see if the numerical results are reasonable. Another purpose is to investigate experimentally if this structure could be used as an isolator.

Extensive experiments have been performed to investigate the validity of the theory. Since the theory is based on the assumption that the structure is infinite in both X and Y directions, and practically no such device could be constructed, an experimental investigation has been carried out to see the effect of finiteness of the structure.

5.1 Evaluation of the Structure for Experimental Purposes

The structure analyzed in theory could be simulated by two kinds of guides, namely dielectric guides or image guides. Both systems have their advantages and disadvantages, but the fact that it is difficult to support dielectric guides makes the image guide more feasible to build an integrated system. Although experiments have been carried out using both systems, the image guide system has been finally adopted for these experiments. A brief description of the two systems used is given below.

(a) Dielectric Guide System

The structure used was made of Stycast Hi-K ($\varepsilon_r = 10$) as the dielectric and of Magnesium ferrite. The dielectric guide was fed from two identical horns. The horns have waveguide-to-coaxial adapters and the system was tested using a coaxial reflectometer. A schematic diagram of the entire system is given in Fig. 5.1. The setup was mechanically not very stable because the positioning of the dielectric between the horns was very sensitive to small movements. Another major problem with this system was that the reflection coefficient could not be well monitored since the coaxial-to-waveguide adapter produced significant reflections.

(b) Image Guide System

Two systems using image guides have been considered. One system used the coaxial reflectometer just like the dielectric guide

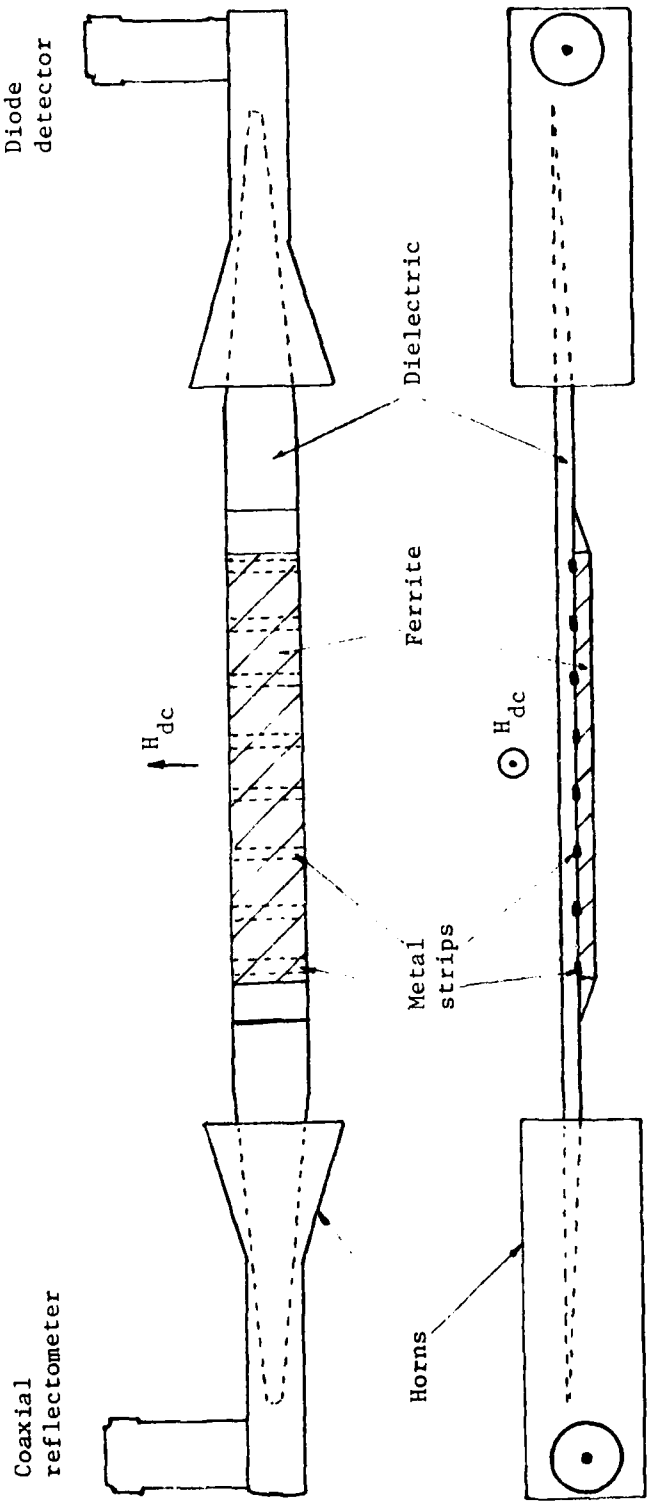

Fig. (5.1) Dielectric guide system used to simulate the theoretical structure.

system, and the other system was designed to work with a waveguide reflectometer. The use of the waveguide reflectometer was intended to eliminate the reflections caused by the waveguide to coaxial transition. A diagram explaining the image guide system is shown in Fig. 5.2. The waveguide reflectometer had a return loss of about -40 dB while the coaxial reflectometer with horn to horn position had a return loss of -15 dB.

A problem with the image guide system as compared to the dielectric guide system is whether or not the metal strips should contact the ground plane. This problem will be investigated in detail in a later section.

5.2 The Test Setup

The final choice of the setup was the image guide system using the waveguide reflectometer. Due to the X-band waveguides used, the frequency swept was from 7 GHz to 16 GHz. The measurements taken were mainly insertion loss and return loss using the H.P. scalar network analyzer. The magnet used was a water cooled Harvy Wells magnet which could go up to 8 KG with the supply available. A Gauss meter by F. W. Bell was used to monitor the magnetic field. A diagram of the whole setup is given in Fig. 5.3.

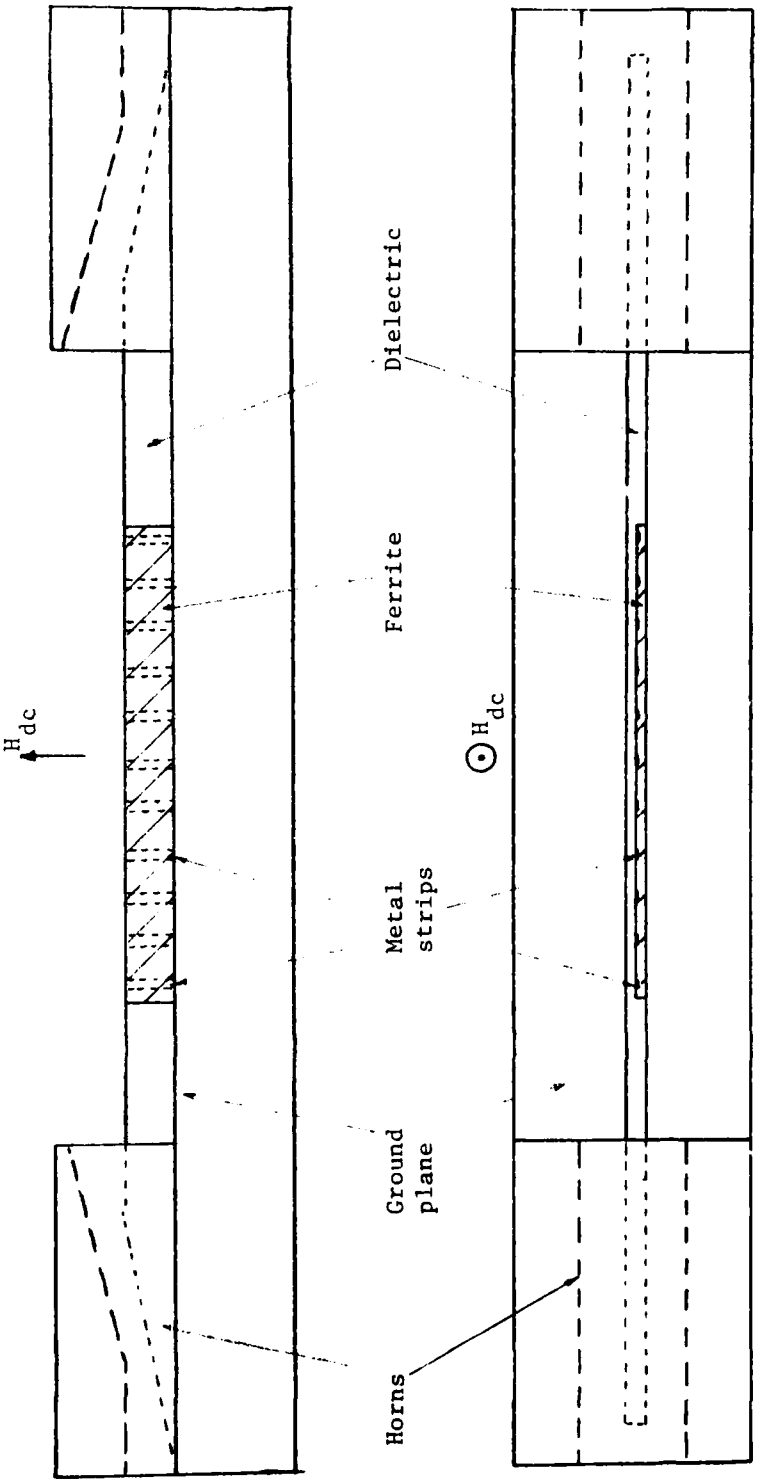

Fig. (5.2) Image guide system used to simulate the theoretical structure.

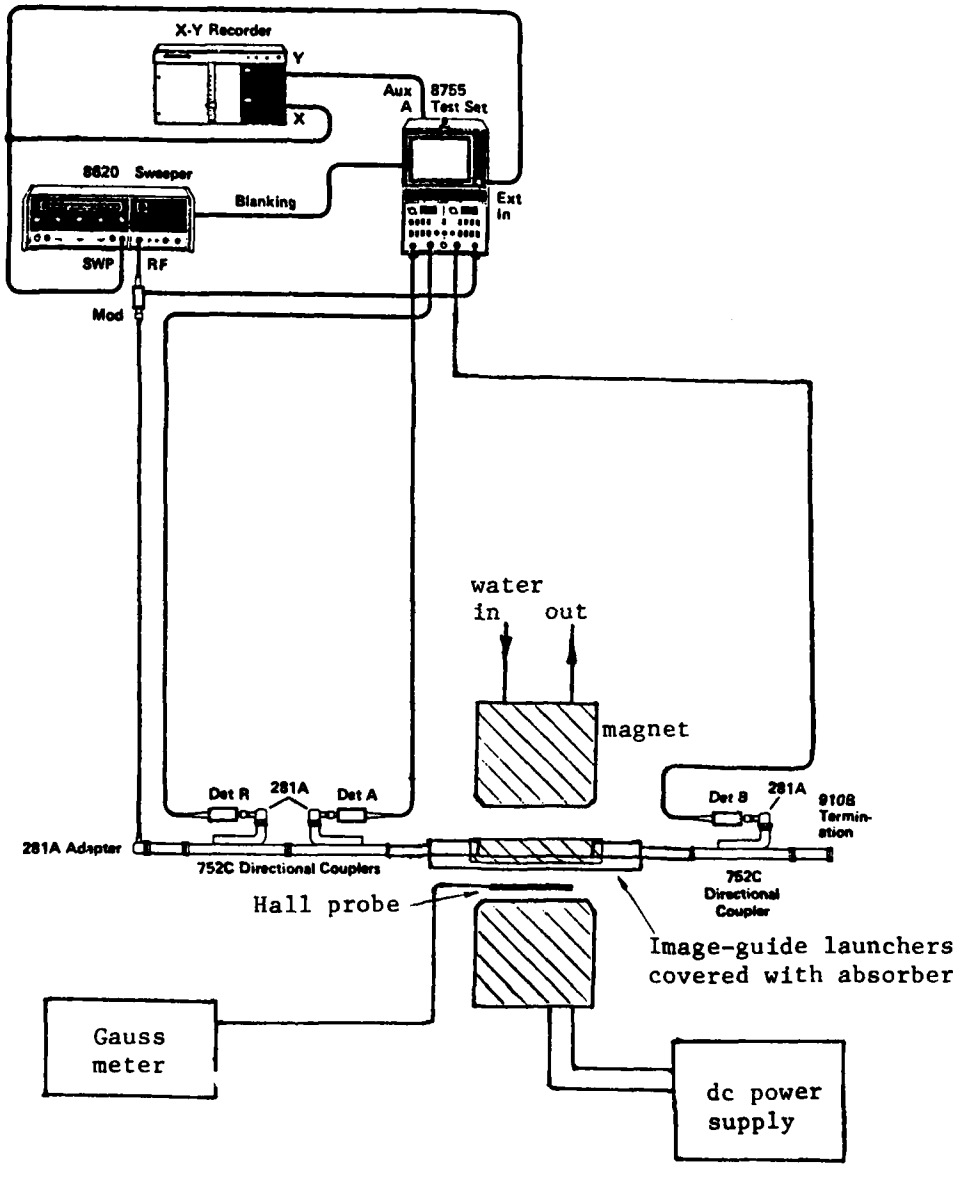

Fig. (5.3) The test setup used to measure the non-reciprocal effects of the proposed structure.

5.3 Preliminary Investigation, Non-reciprocal Effects on Applying an External Magnetic Field

This investigation has been made to answer some of the questions that could be put forth on the structure used. The dielectric used was Stycast HiK (ε = 10) and the ferrite was Magnesium type (TT-1-105). The ferrite and dielectric widths were 3 mm each and the height of the image guide was 5 mm. The period and strip width of the grating were 13 and 3 mm, respectively.

(a) No Metal Strips

This experiment has been carried out to verify that the waves behave in a reciprocal manner when the metal strips are not inserted. Another purpose of this experiment is to show at what frequency the ferrite resonates for a particular magnetization. From the results of the experiments shown in Fig. 5.4, one could easily see that in one direction the system goes in resonance at a lower frequency than the other direction. This behavior can not be explained as yet, but from what has been observed the difference in frequency is only 200 MHz at most. This system could be used for isolation purposes, but the bandwidth is very narrow.

(b) Metal Strips Touching Ground Plane

This experiment has been performed as part of the investigation to determine whether or not the metal strips should touch the ground plane. From the experimental results of Fig. 5.5, one

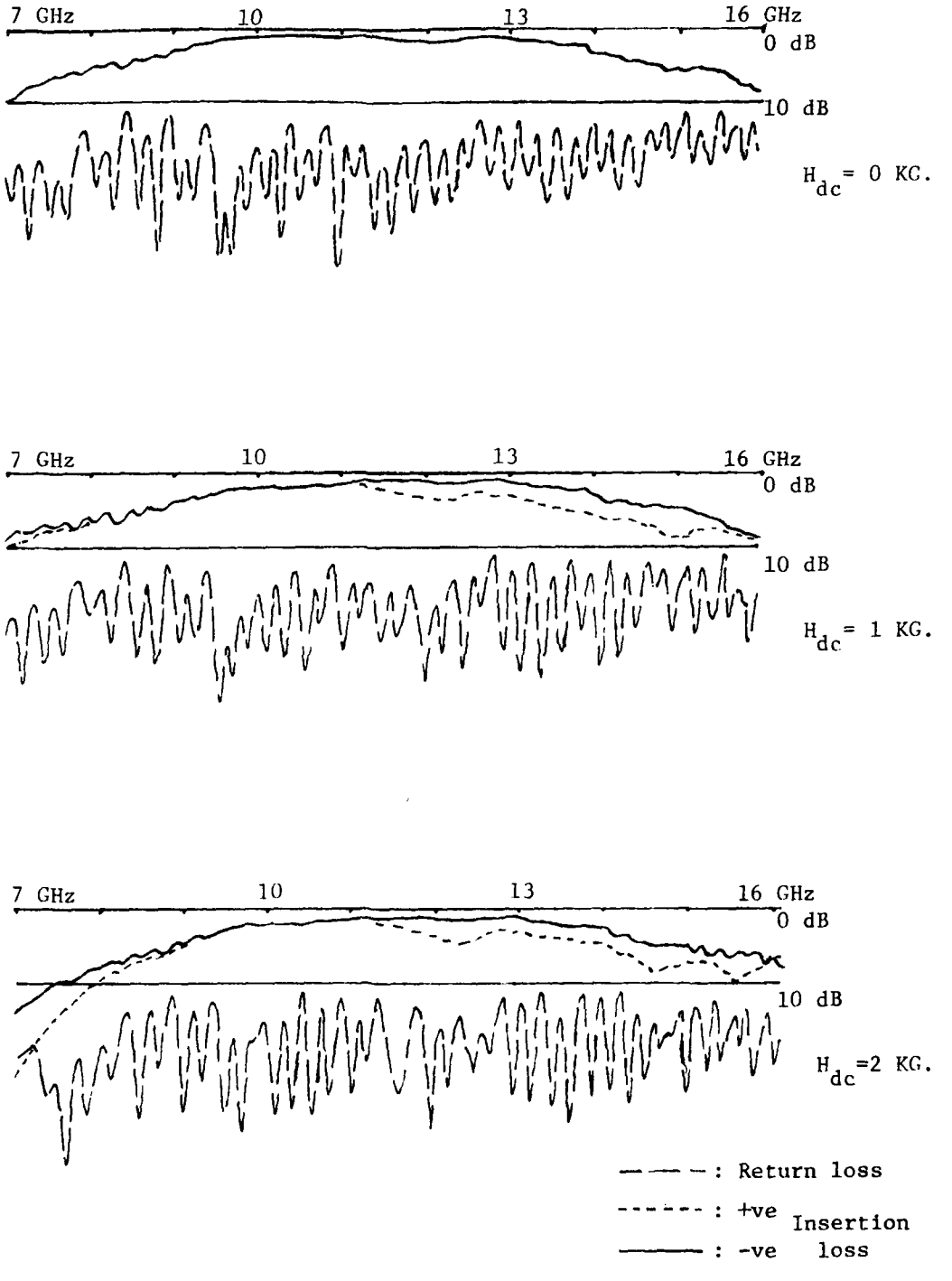

Fig. (5.4a) Guide with no metal strips.

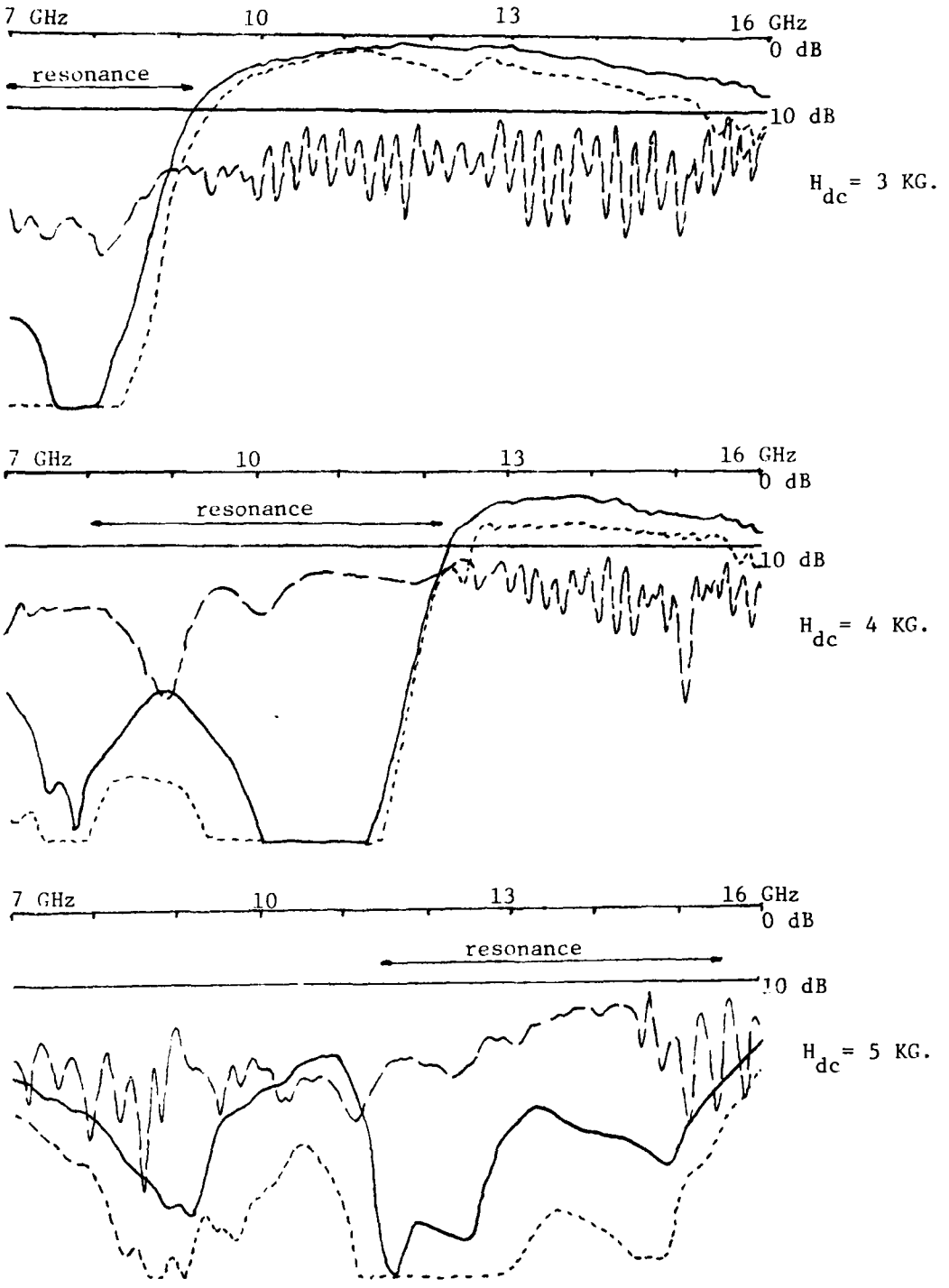

Fig. (5.4b) Guide with no metal strips.

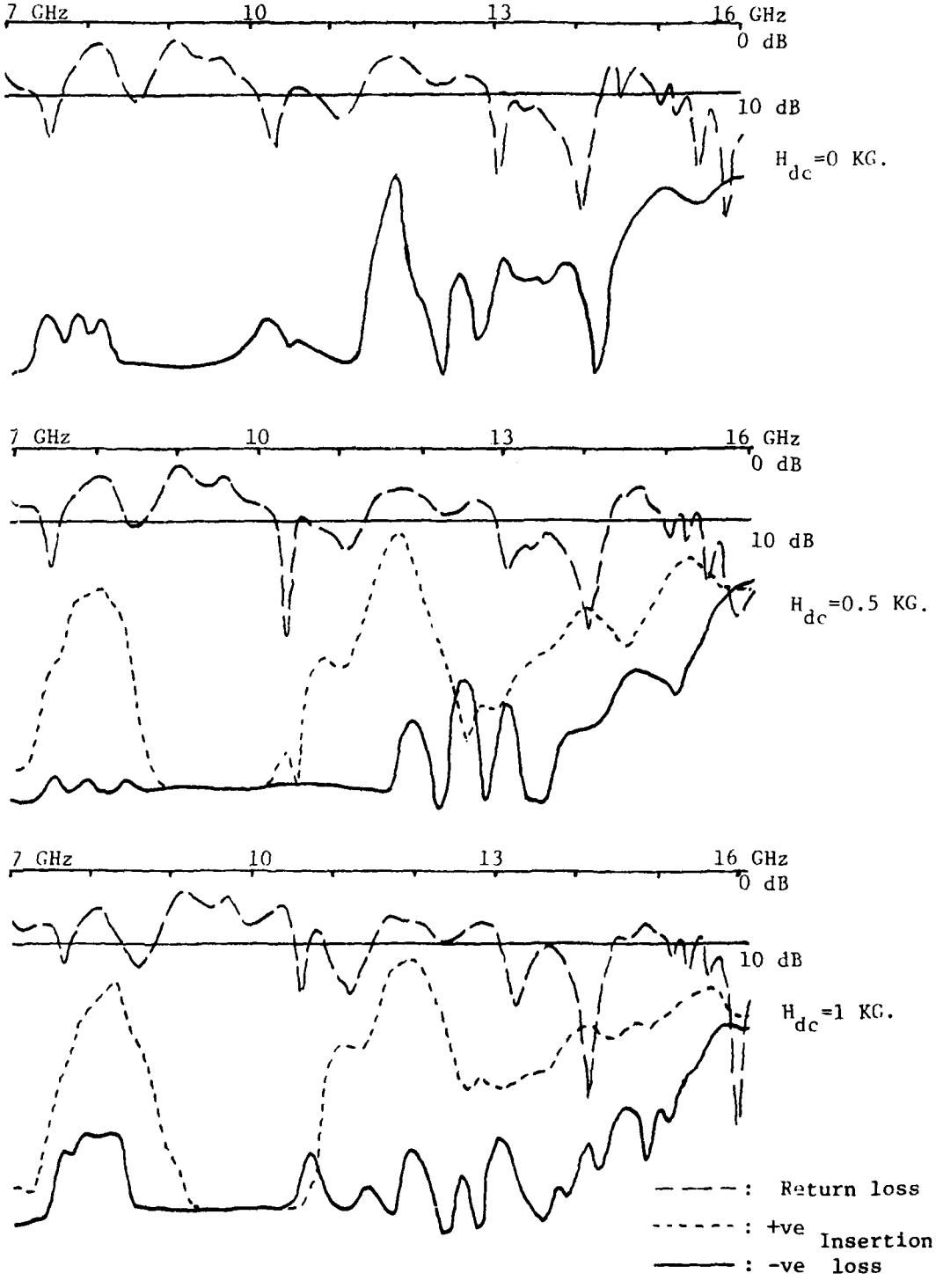

Fig.(5.5a) Metal strips touching ground plane.

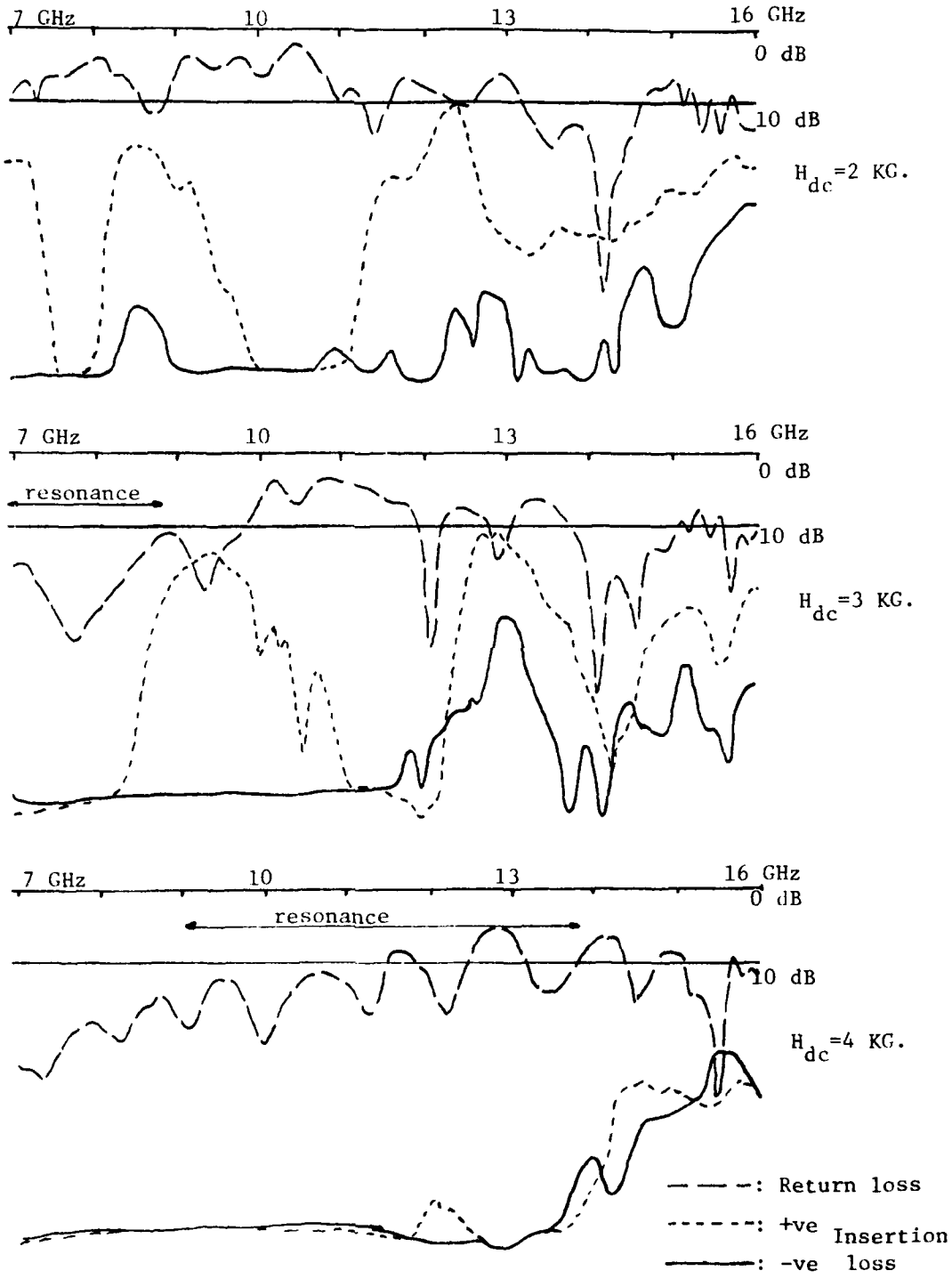

Fig.(5.5b) Metal strips touching ground plane.

could see that for no magnetization almost all the energy is scattered or attenuated. As the magnetic field is applied, large non-reciprocity is evident at two frequency ranges, namely from 8 to 9 GHz and 11.5 to 12.5 GHz. One notes that this occurs at a magnetization of only about .5 KG, indicating that the system is way below saturation and, of course, resonance.

This structure has not been considered further since at zero magnetization the theory does not predict that all the energy should be scattered. Although the insertion loss in the forward direction is about 10 dB, this structure may be useful if attenuation is reduced by optimization.

(c) Use of Low Dielectric Constant Slabs to Suspend the Guide Above the Ground Plane so that the Strips would not Touch

This experiment has also been part of the investigation to find out whether the strips should touch the ground plane or not. In the experimental results shown in Figs. 5.6 and 5.7, thin dielectric films of $\varepsilon = 2.3$ and 0.7 mm thickness have been inserted between the ferrite-dielectric rod and the ground plane. From the result, it is evident that a stopband and a leaky wave region could be seen at 8 and 9.5 GHz, respectively.

As compared to when the strips were touching the ground plane, the non-reciprocity at 12 GHz is still evident at low magnetization in the present case. The other phenomenon is that in

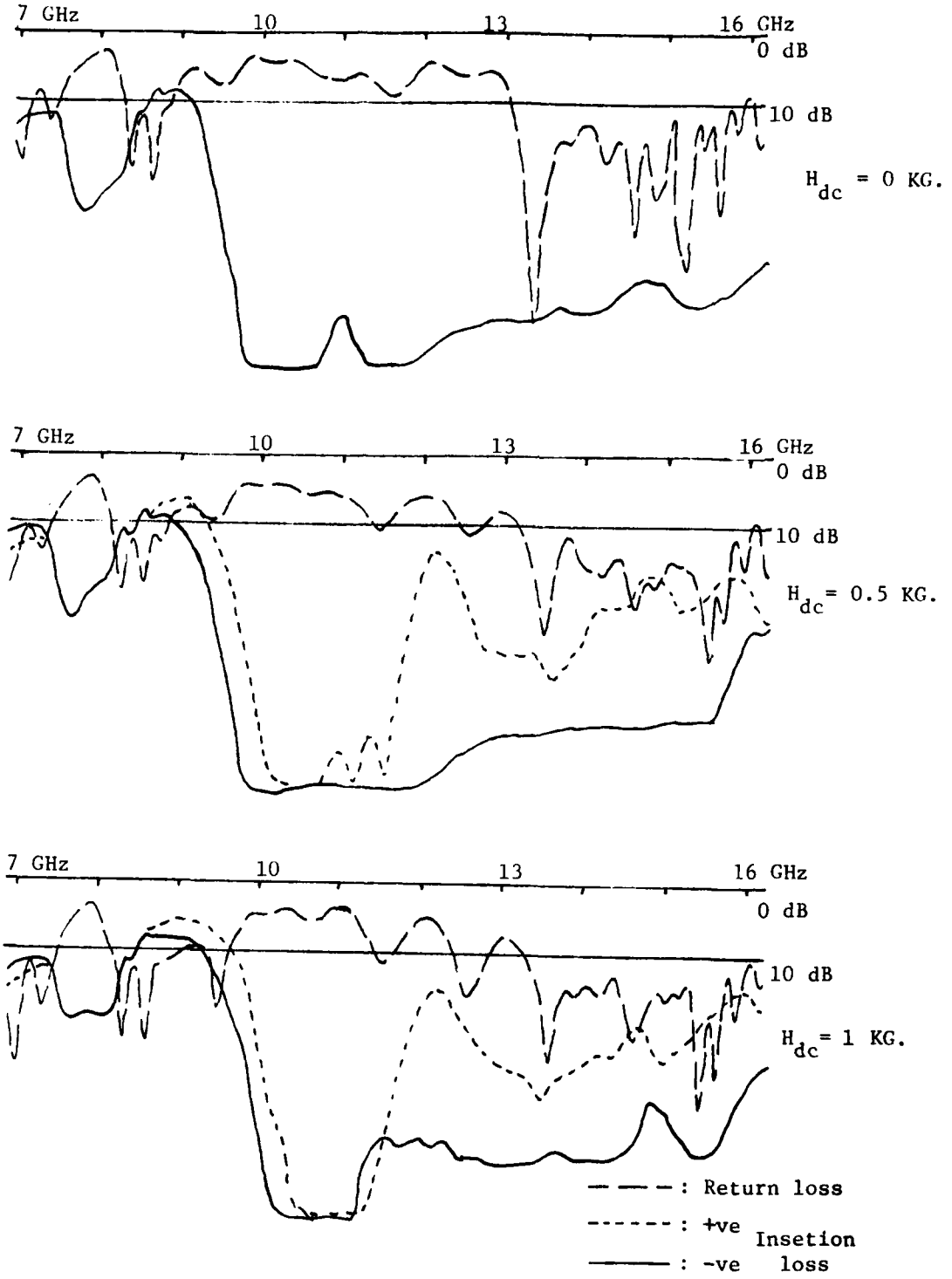

Fig. (5.6a) Guide suspended 0.7 mm above ground plane by means of dielectric

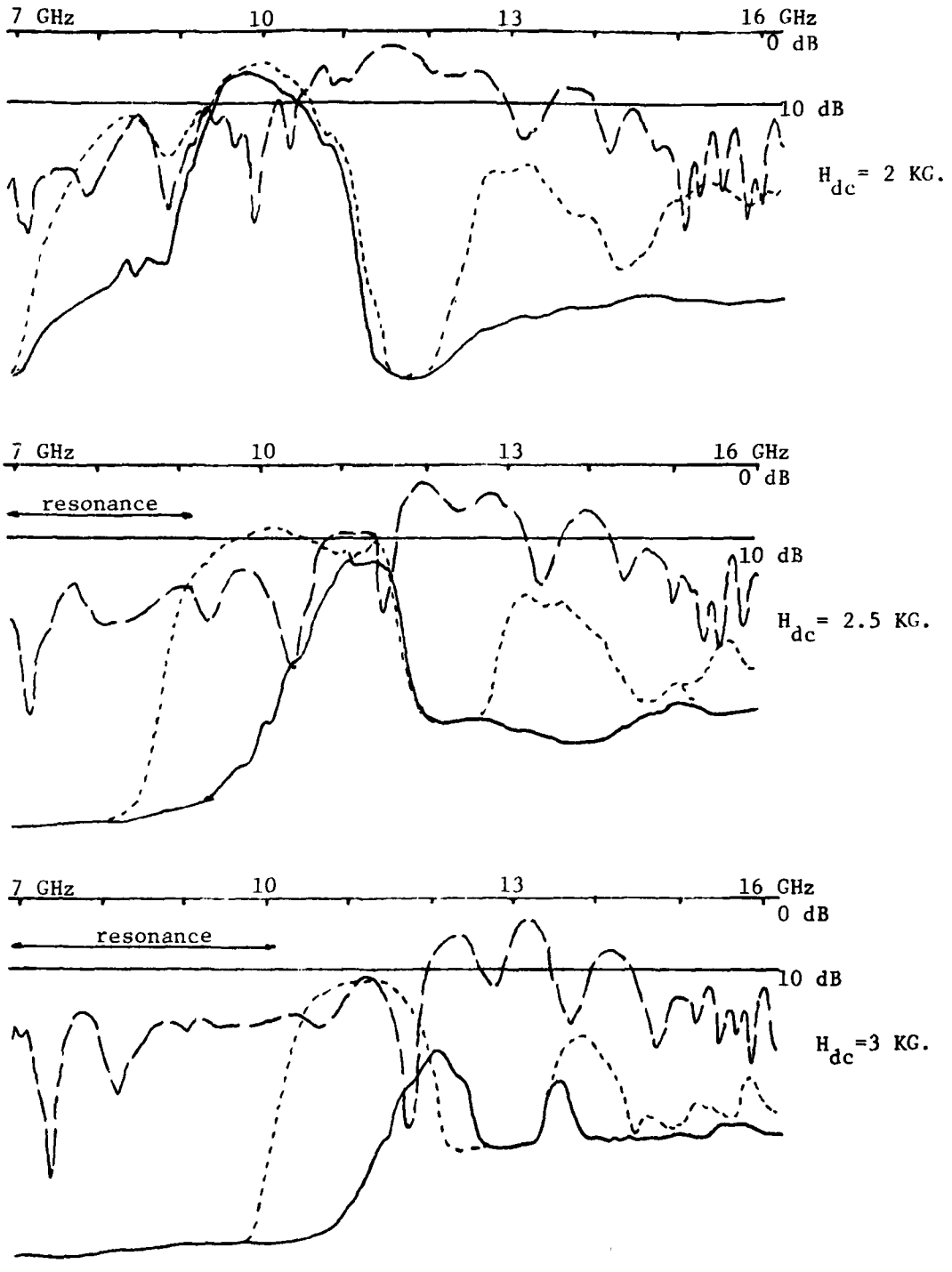

Fig. (5.6b) Guide suspended 0.7 mm above ground plane by means of dielectric

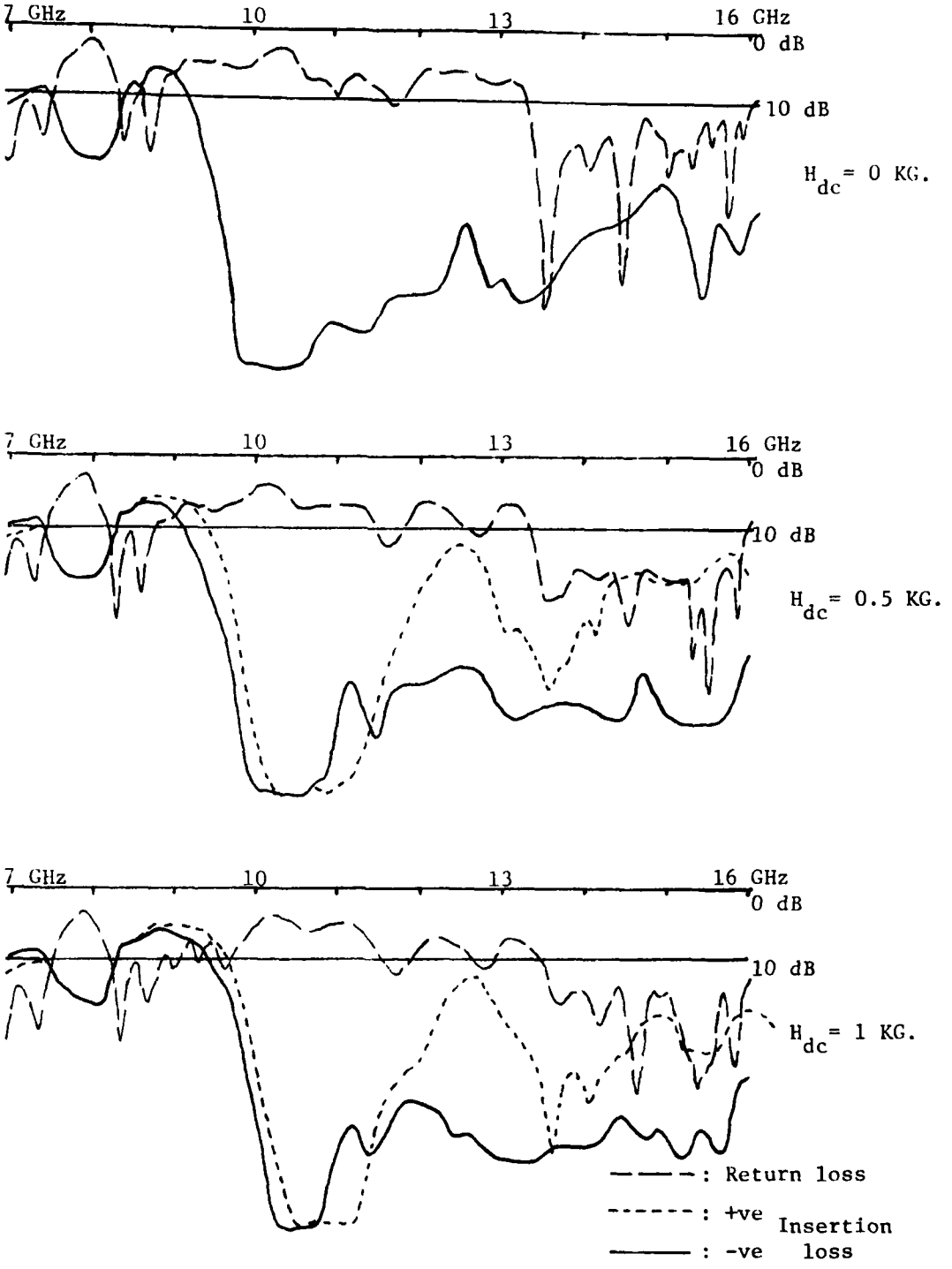

Fig. (5.7a) Guide suspended 1.4 mm above ground plane by means of dielectric

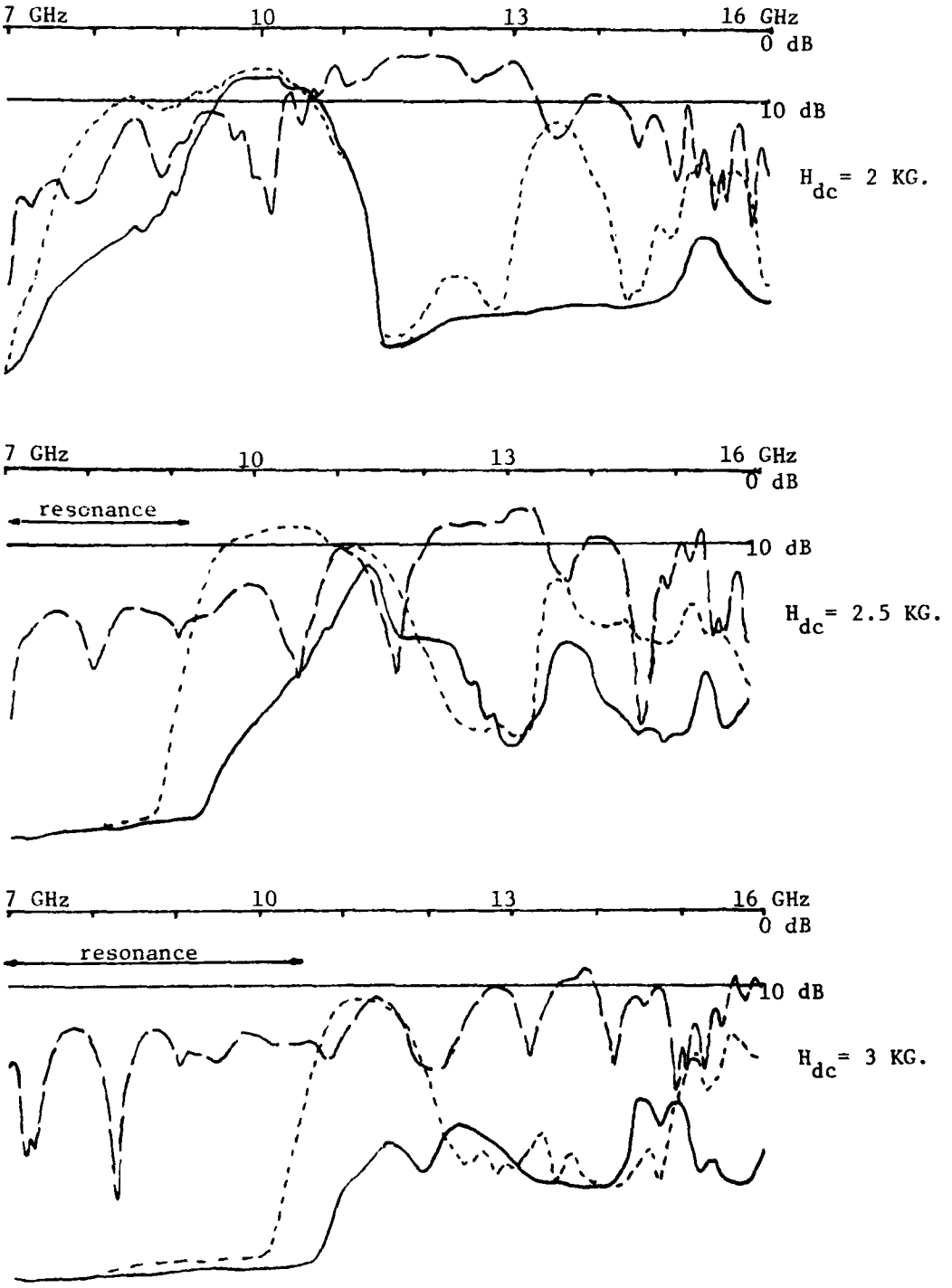

Fig. (5.7b) Guide suspended 1.4 mm above ground plane by means of dielectric

one direction the system goes in the leaky wave region at a different frequency than the other direction. This difference is only 100 MHz and could not be of much use. One also notices that in the negative permeability region non-reciprocity occurs. The bandwidth of the non-reciprocal effect is about 1.5 GHz. This effect is very visible especially near 3 KG.

To find out the effect of the thickness of the low dielectric constant layer, experiments have been performed for two different values of thickness. Fig. 5.6 is for one slab of .7 mm thickness while the data of Fig. 5.7 is for two slabs of .7 mm thickness each. A comparison of the results of Fig. 5.6 to those of 5.7, shows that the overall attenuation decreases with increase of the thickness of the low dielectric constant layer. On the other hand, the non-reciprocity and the stopband are larger for a thinner layer of low dielectric constant material.

(d) Use of Metal Strips which do not Touch Ground Plane: Strips are truncated at 1 mm Above Ground Plane

Another way of preventing the metal strips from touching the ground plane is to truncate the metal strips on the ground plane side. The results obtained with this structure are similar to the ones when the low dielectric slab was used. The only difference is that the overall attenuation is 2 dB less. This is mainly due to the use of shorter metal strips. The results of this investigation

are shown in Fig. 5.8. The stopband in this system is hardly visible at 8 GHz since the metal perturbation is small.

(e) The Effect of the Period and Strip Width

The change in period of the metal strips should only change the position of the stopband, although it may have an effect on the bandwidth of the non-reciprocal part of the result. Experimentally not much has been made in this respect. The only experiment performed is with the period and strip width 11 mm and 1.5 mm, respectively instead of 13 mm and 3 mm as in the previous case. The results of this experiment are shown in Fig. 5.9.

From the results, one could see that the overall attenuation is reduced compared to Fig. 5.8, while the non-reciprocal effects are still preserved. This observation makes sense since the narrower the metal strips, the less scatter and perturbation occurs.

5.4 Effect of having a Finite Grating Structure

In this section, we study the effect of finite length of the grating section. The analysis of a periodic structure applies to an infinitely long structure in the strict sense. It is expected that the characteristics of a grating of finite length will differ somewhat from those of an infinitely long one. We will study such difference.

The structure used for this investigation was made of Alumina ($\varepsilon \approx 10$), and no ferrite has been used. The structure was

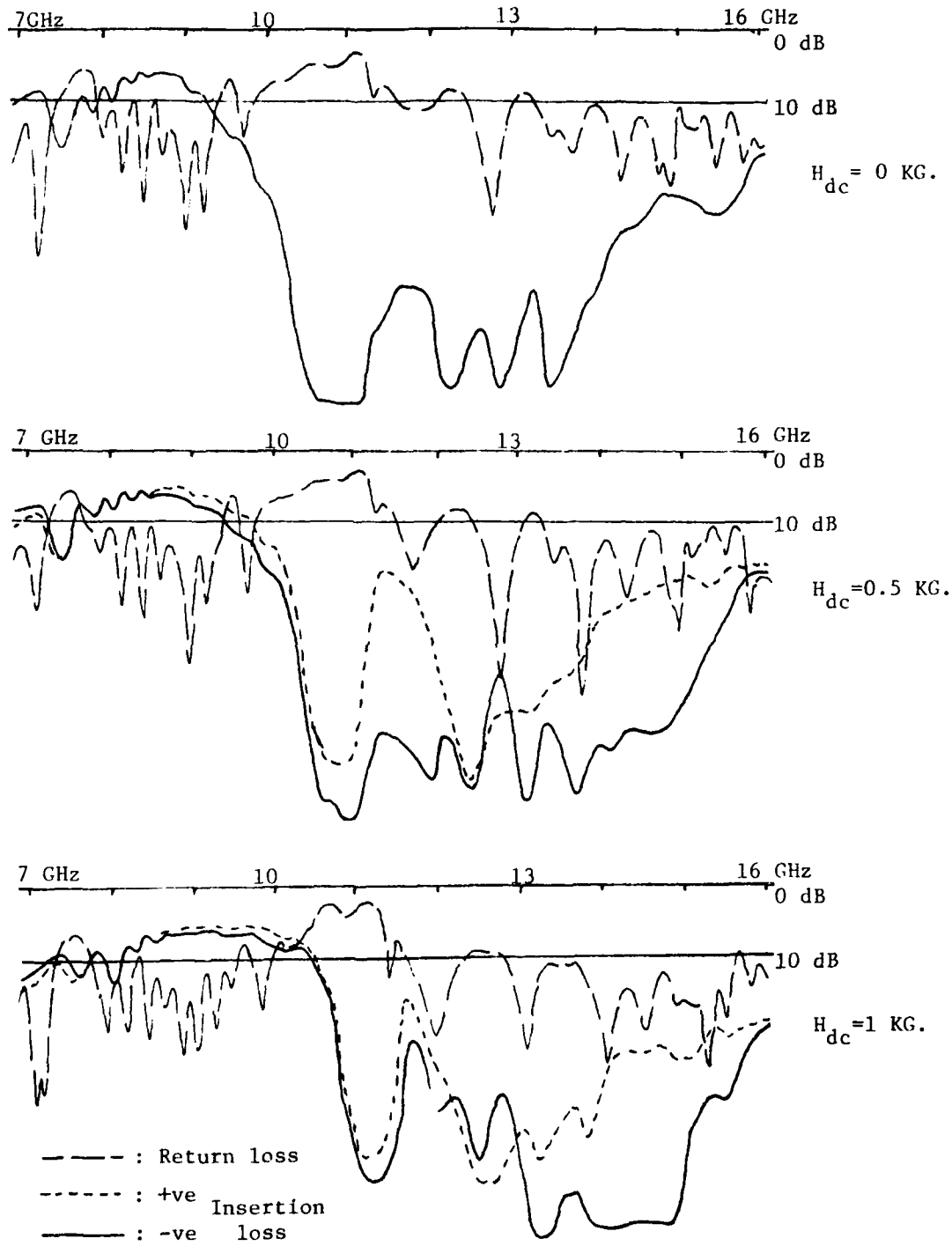

Fig. (5.8a) Guide with metal strips one mm above ground plane. d=13 mm, a=3 mm.

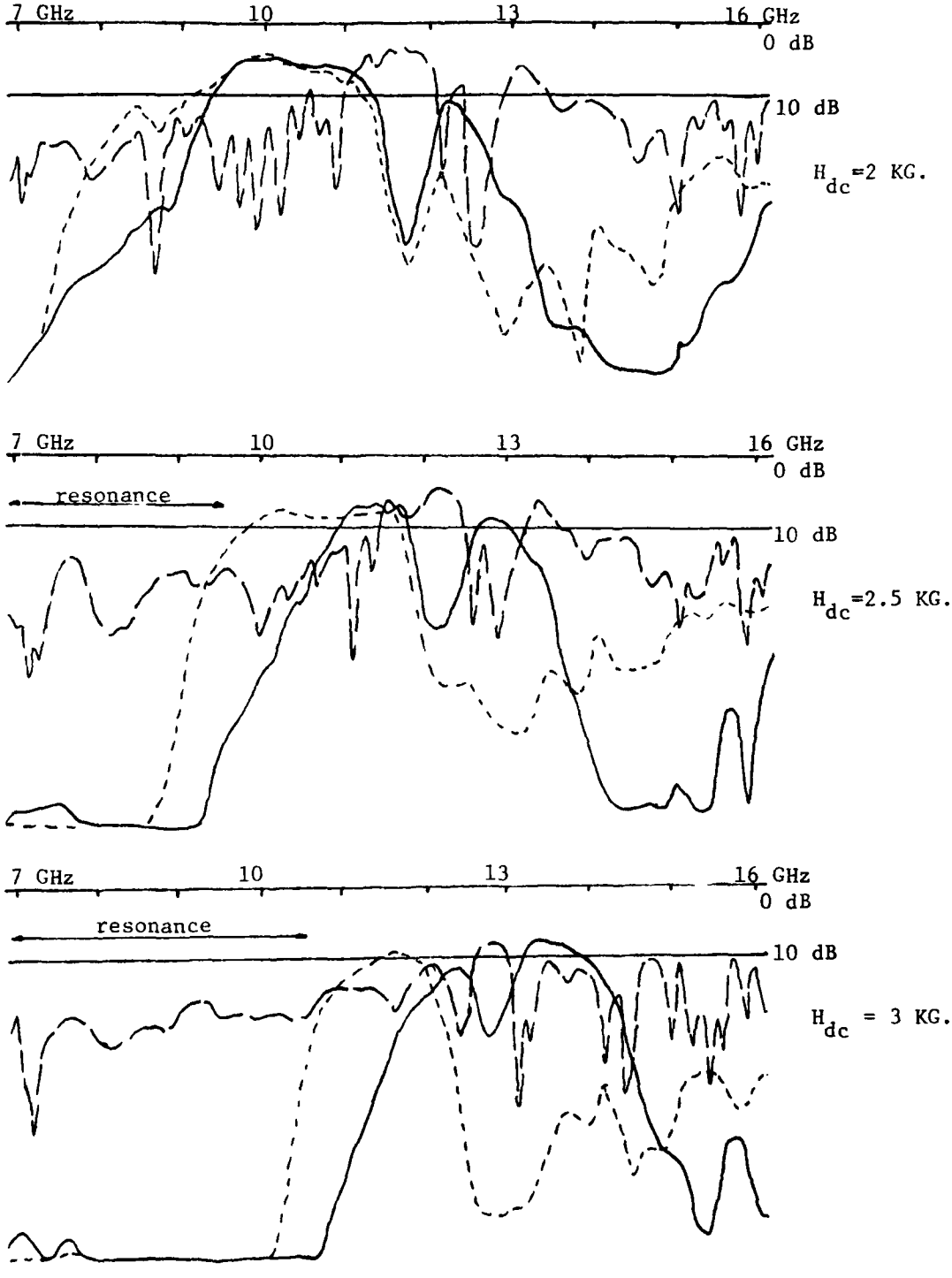

Fig. (5.8b) Guide with metal strips one mm above ground plane. d=13 mm, a= 3 mm.

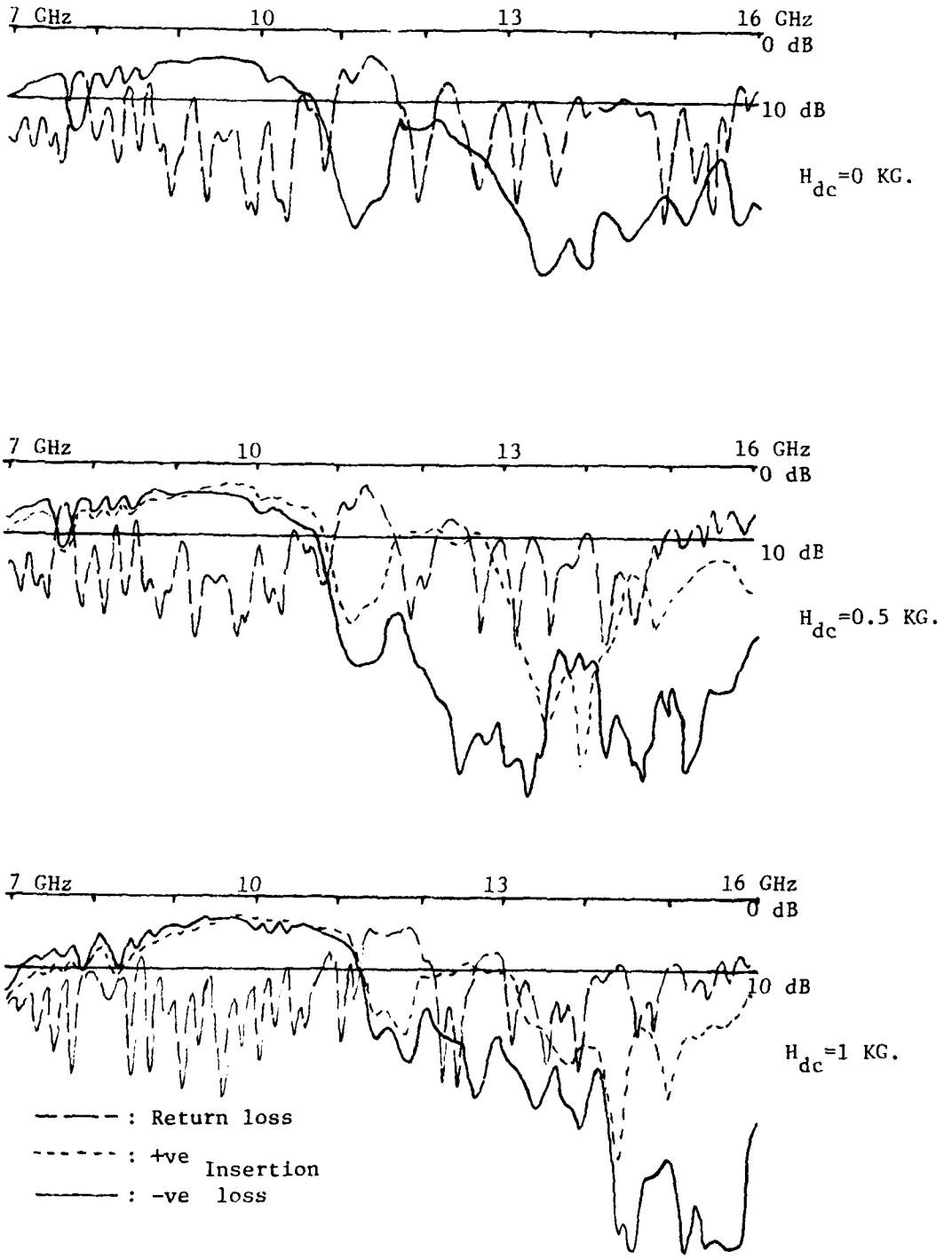

Fig. (5.9a) Guide with metal strips one mm above ground plane. d=11 mm , a=1.5 mm.

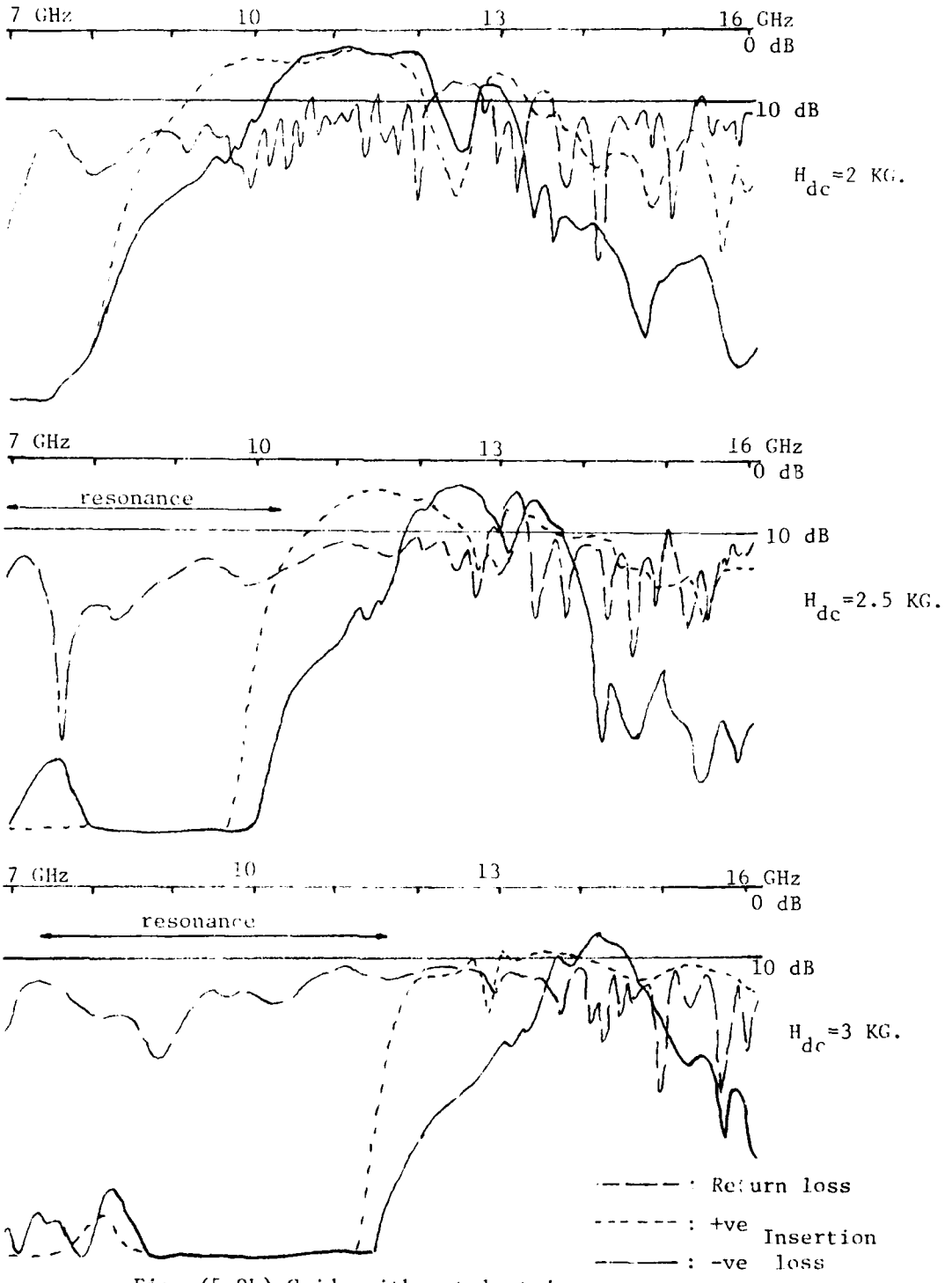

Fig. (5.9b) Guide with metal strips one mm above ground plane. d=11 mm, a=1.5 mm.

AD-A116 383 TEXAS UNIV AT AUSTIN DEPT OF ELECTRICAL ENGINEERING F/G 9/1
AN ISOLATOR IN IMAGE GUIDE.(U)
MAY 82 N CAMILLERI, T ITOH
UNCLASSIFIED UT-MW-N-82-1 N00014-79-C-0553 NL

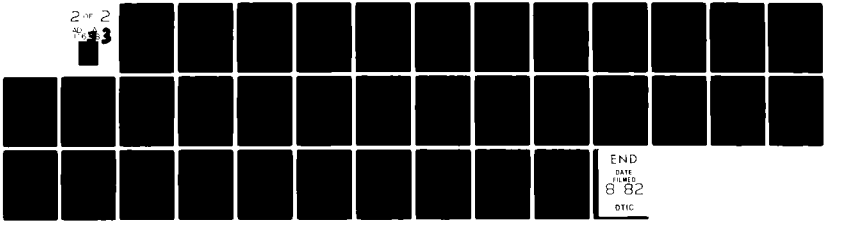

made with alumina on both sides of the metal strips. Two alumina slabs were glued together with the metal strips in the middle. The period and strip width was 10 mm and 2 mm, respectively. The thickness of the alumina slabs was 1.5 mm and the height 4 mm.

The experiment consisted of starting with 17 metal strips and then taking off four strips at a time to measure the system with 13, 9, 5, 3, 1 and finally no metal strips at all. In this experiment, the metal strips were isolated from the ground plane. Each of the seven structures described above were tested with five different types of isolation from the ground plane. In one of these five methods, the structure was isolated from the ground plane with a layer of 3M scotch tape. In the remaining four cases, four slabs of dielectric material ($\varepsilon = 2.3$) of .7 mm thickness each were placed under the alumina structure one by one to make different thicknesses of low dielectric constant material under the main guide. The experimental results of this investigation are shown in Fig. 5.10.

The computer program has been run for these particular cases to investigate if there is any correlation with the experimental results. The computer result is shown in Fig. 5.11, where the attenuation constant is given in Nepers per mm $\times$ $(\frac{\pi}{d})$.

The computer results show that the system should have a stopband between 10.5 GHz and 13 GHz. From the experimental result, the stopband is between 10 and 11.5 GHz, so there is a discrepancy of about 1 GHz in the bandwidth of the stopband. The overall shape

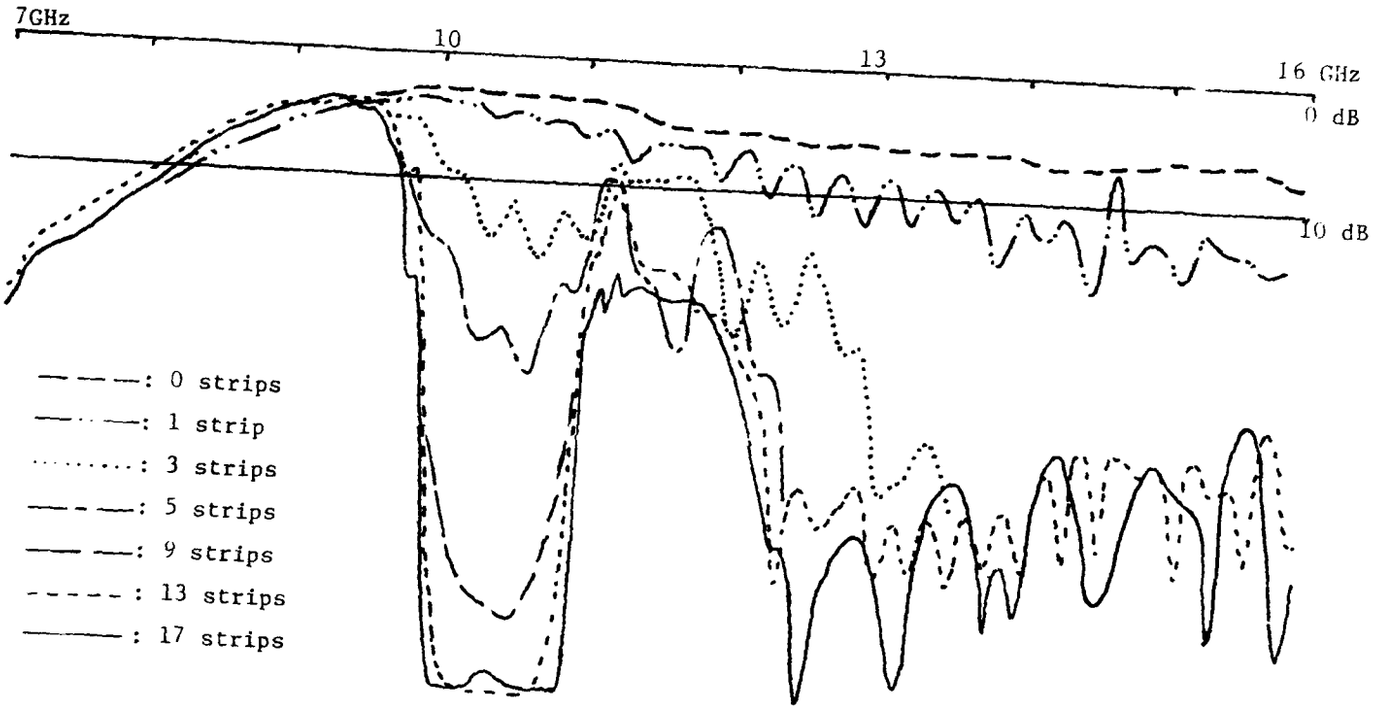

Fig.(5.10a) Graphs for a guide with alumina on both sides of the metal strips. This experiment shows what happens when the number of strips in the x -direction is finite. The strips are isolated from the ground plane by 3M scotch tape.

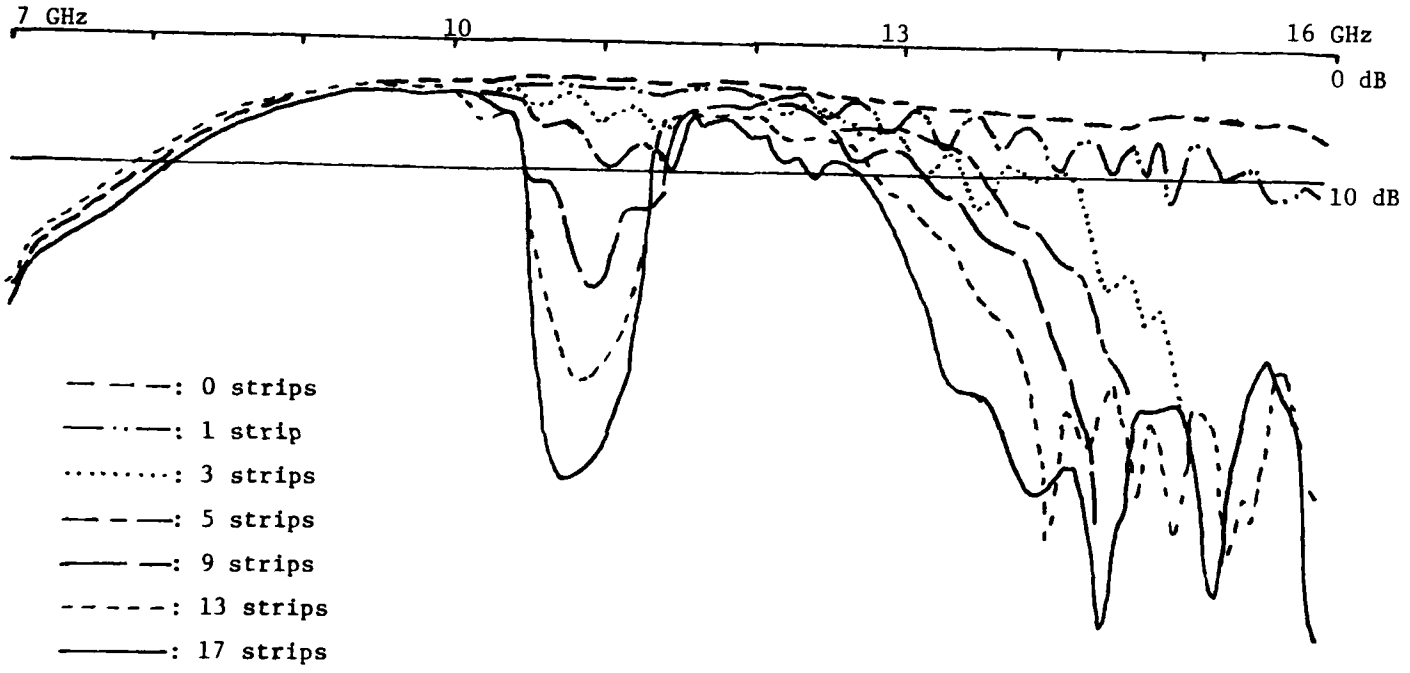

Fig. (5.10b) Graphs for a guide with alumina on both sides of the metal strips. The metal strips are isolated from the gr nd plane by 0.7 mm thickness of dielectric (ε=2.3).

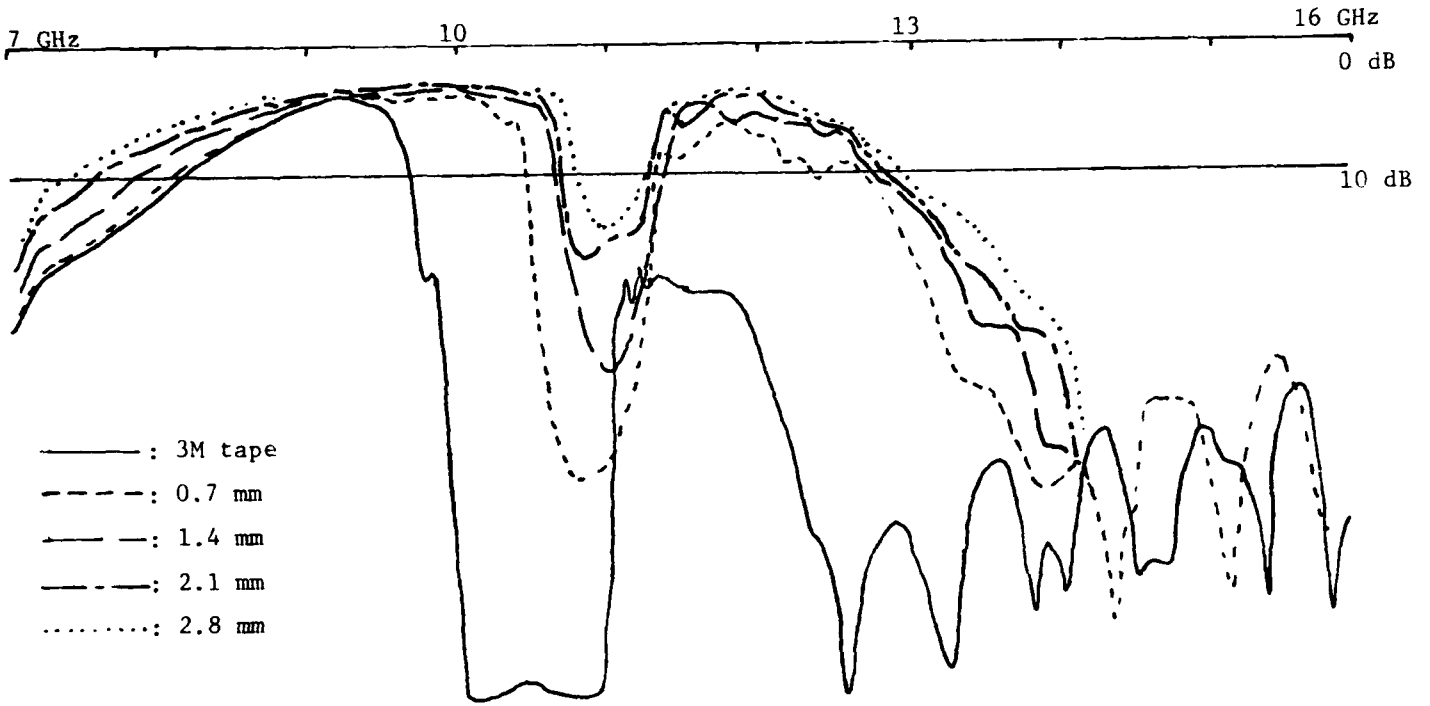

Fig. (5.10c) Graphs for a guide with alumina on both sides of seventeen metal strips. This experiment shows the effect of varying the thickness of a low dielectric constant material (ε=2.3) placed between the alumina and the ground plane to isolate the metal strips.

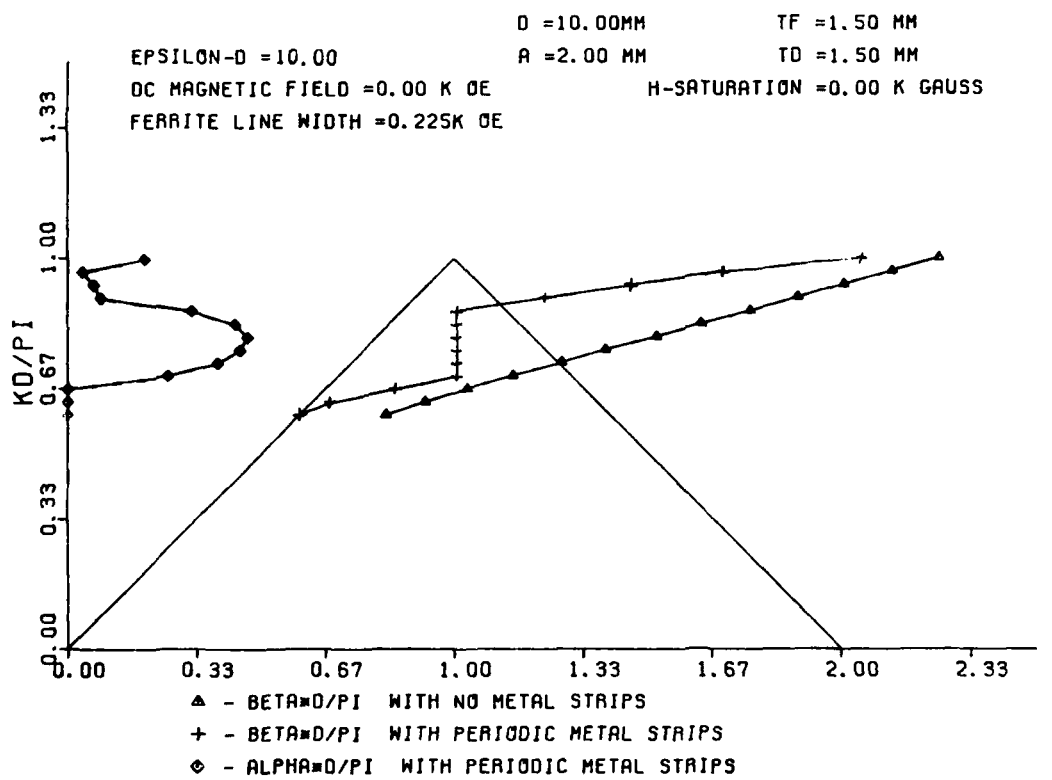
D =10.00MM
TF =1.50 MM
EPSILON-D =10.00
A =2.00 MM
TD =1.50 MM
DC MAGNETIC FIELD =0.00 K OE
H-SATURATION =0.00 K GAUSS
FERRITE LINE WIDTH =0.225K OE
KD/PI
0.00
0.33
0.67
1.00
1.33
1.67
2.00
2.33
△ - BETA=D/PI WITH NO METAL STRIPS
+ - BETA=D/PI WITH PERIODIC METAL STRIPS
◇ - ALPHA=D/PI WITH PERIODIC METAL STRIPS

Fig. (5.11)

of the theoretical and experimental results are very similar. It is evident theoretically that the attenuation at frequencies below the stopband is negligible. Experimentally, the insertion loss curves for the cases with and without metal strips differ very little for the region below the stopband. This confirms negligible loss predicted by theory. In the leaky region (which occurs at 14 GHz theoretically and at 12 GHz experimentally), the attenuation predicted is about 1 dB/cm. This ratio gives us about 10 dB of insertion loss for the particular length of device used in the experiment. The experimentally observed insertion loss is also about 10 dB. For this particular case, the computer program has been run using the effective dielectric constant[25] method to compensate for making the structure finite in the y direction.

The effective dielectric constant has been obtained in the following manner. The propagation constant of a dielectric guide with a height of 100 mm was first computed. We now assume that this guide has an infinite height and, hence, is a slab waveguide. Next, we adjust the value of the dielectric constant of a guide with a height of 4 mm in such a way that the propagation constant is identical to the one in the guide with an "infinite" height. Such a value of dielectric constant is taken as the effective dielectric constant of the 4 mm guide. Some standard software to calculate the propagation constant of an image guide has been used to calculate the effective dielectric constant. The

program has been run for each particular frequency since the effective dielectric constant is very dispersive, especially for a small guide like the one used here.

One should note that the effective dielectric constant method only takes care of a finite size dielectric, but does not take care of finite length of metal strips. On the other hand, it is very difficult to do the same effective dielectric constant method for the case where ferrite is involved since no extensive study is available to date to calculate the effective dielectric constant and the effective permeability of a ferrite guide.

5.5 Effect of Making the Structure Finite in the Y-Direction

It was pointed out in the previous section that the effective dielectric constant method cannot be applied to the structure containing ferrite. It is, therefore, necessary to experimentally study the effect of a finite size structure. It is inferred that the waveguide with a larger dimension exhibits better agreement with the theory based on the infinitely high structure.

To make this investigation, three different sizes of guides were produced. Each of the three guides had a different height. One was 5 mm in height and the others were in turn 10 mm and 15 mm. The period of the metal strips used was 10 mm and the strip width was 2 mm. On the basis of the previous investigation (see 5.4), the number of strips used was 11. The thickness of ferrite was 1.5 mm and the thickness of dielectric also 1.5 mm.

The dielectric was Stycast HiK (ε_r = 10) and the ferrite material had a dielectric constant of 12 and a saturation magnetization of 1.75 KG. Each of the three structures was run in the magnet with and without metal strips. One run was made with just one layer of 3M scotch tape and one with one slab of dielectric of .7 mm thickness and 2.3 dielectric constant. Experiments have also been made with a dielectric material only on both sides of the metal strips.

The experimental results of this investigation are shown in Fig. 5.12. Figs. 5.13 and 5.14 are tables listing the observations worth noticing from these experimental results. The most important observation from those results is that non-reciprocity occurs in the negative permeability region. The best example of this is shown at a magnetization of 3 K Gauss. In the experimental results, the non-reciprocity is seen clearly for 10 mm and 15 mm thickness. The region of non-reciprocity occurs from 11 GHz to 12 GHz. This frequency range corresponds directly with the negative permeability region. Although the negative permeability region is from 10.6 GHz to 13.3 GHz, the permeability is mostly a large negative number between 11 GHz and 12 GHz. Fig. 5.15 shows how theoretically the negative permeability region occurs.

The computer program has been used to investigate if this non-reciprocal effect could be predicted theoretically. Unfortunately, for the structure with no metal strips in the positive direction, no solution was found for the negative permeability

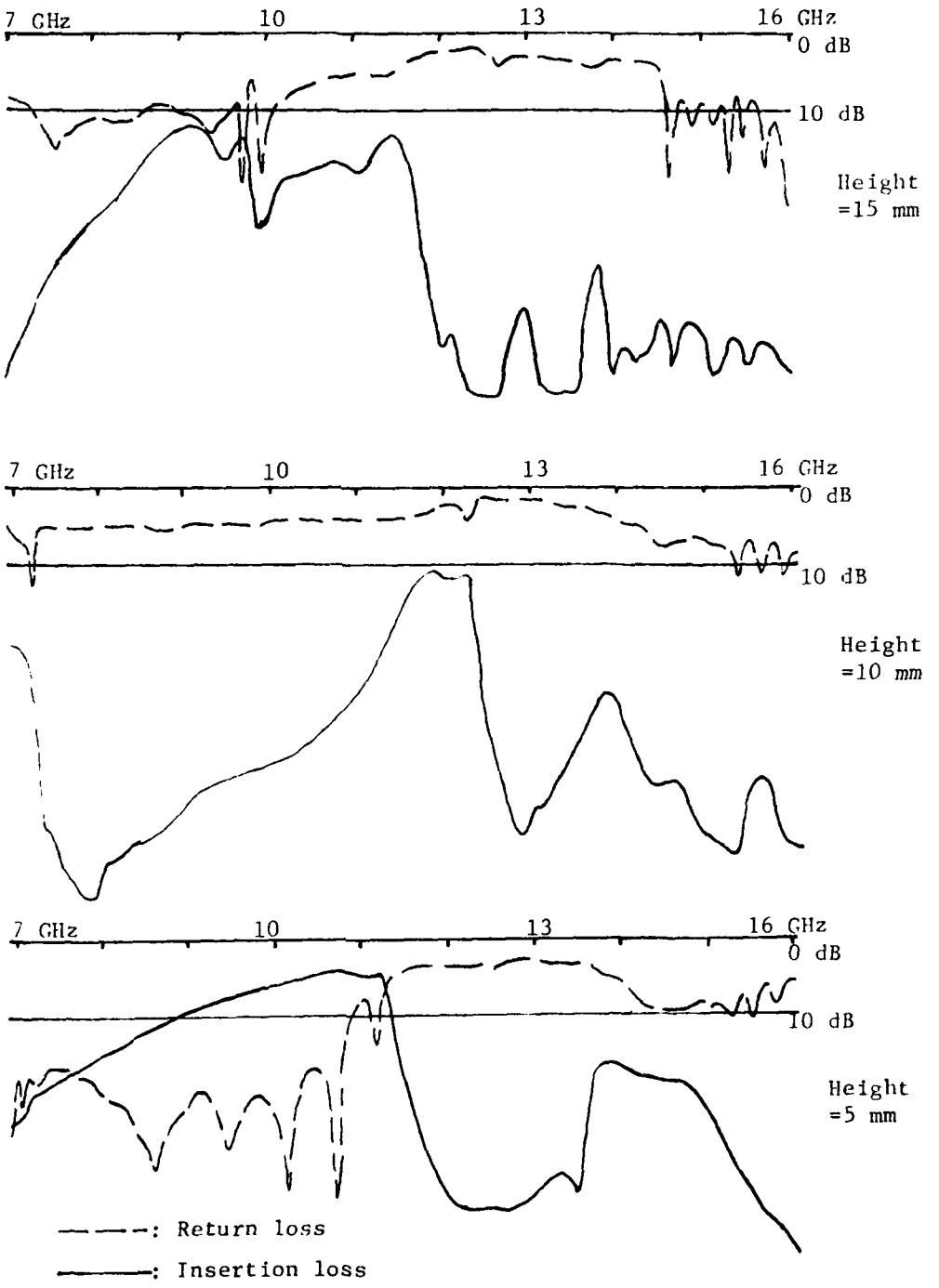

Fig. (5.12a) Dielectric is used on both sides of the eleven metal strips.

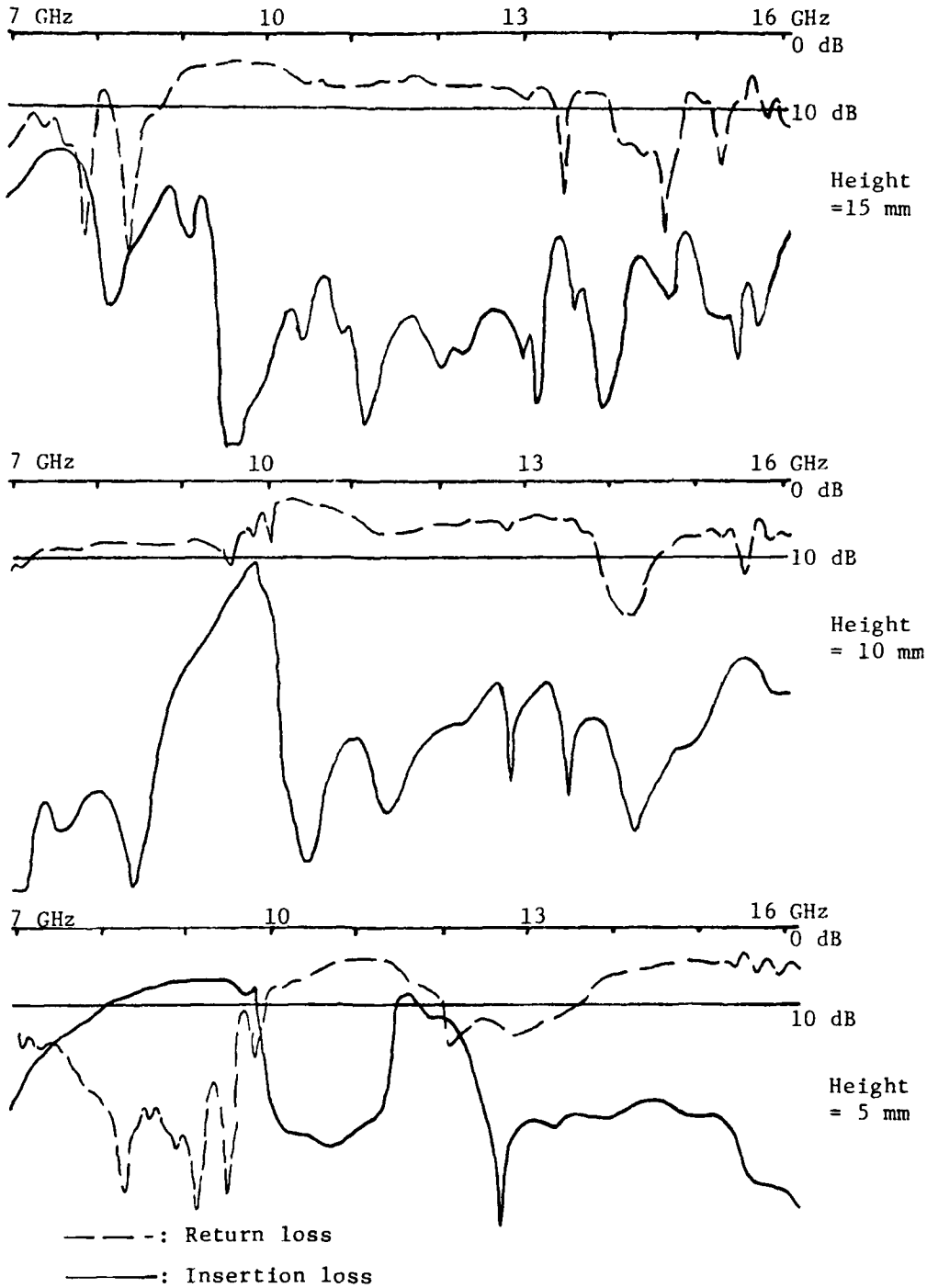

Fig.(5.12b) Dielectric - metal strips - ferrite structure with H_{dc}=0 KG.

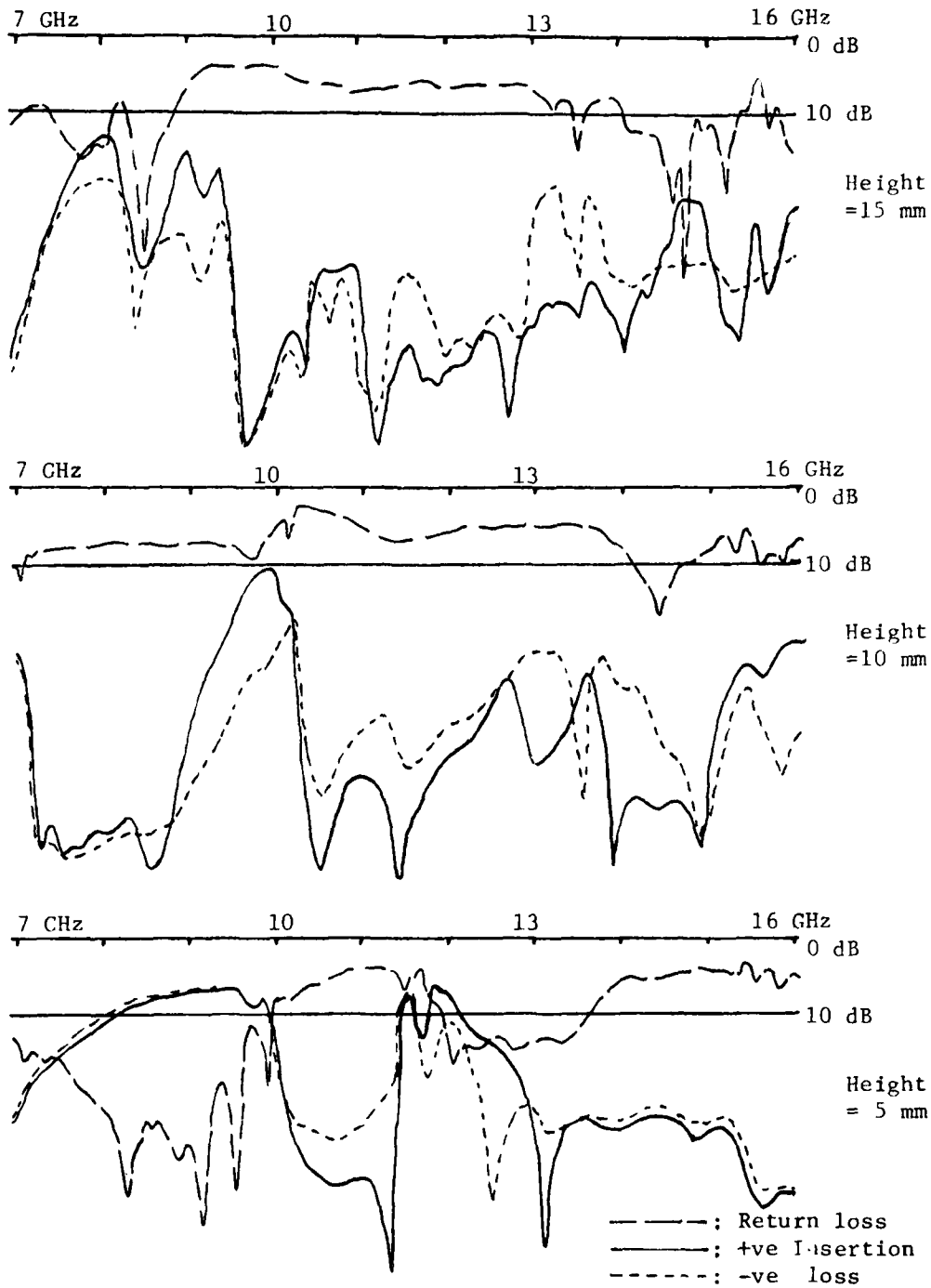

Fig.(5.12c) Dielectric - metal strips - ferrite structure with H_{dc}=1 KG.

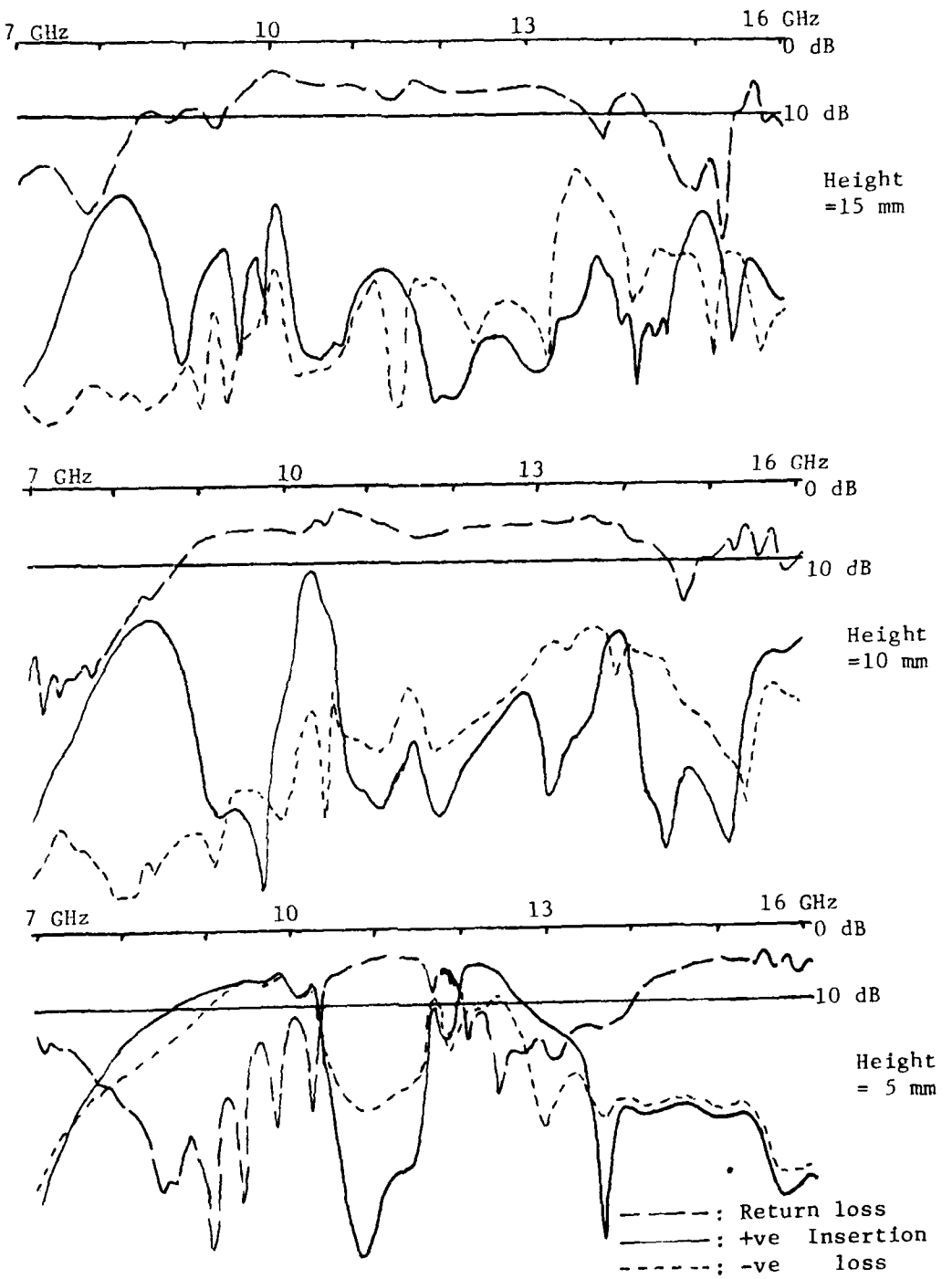

Fig.(5.12d) Dielectric - metal strips - ferrite structure with H_{dc}= 2 KG.

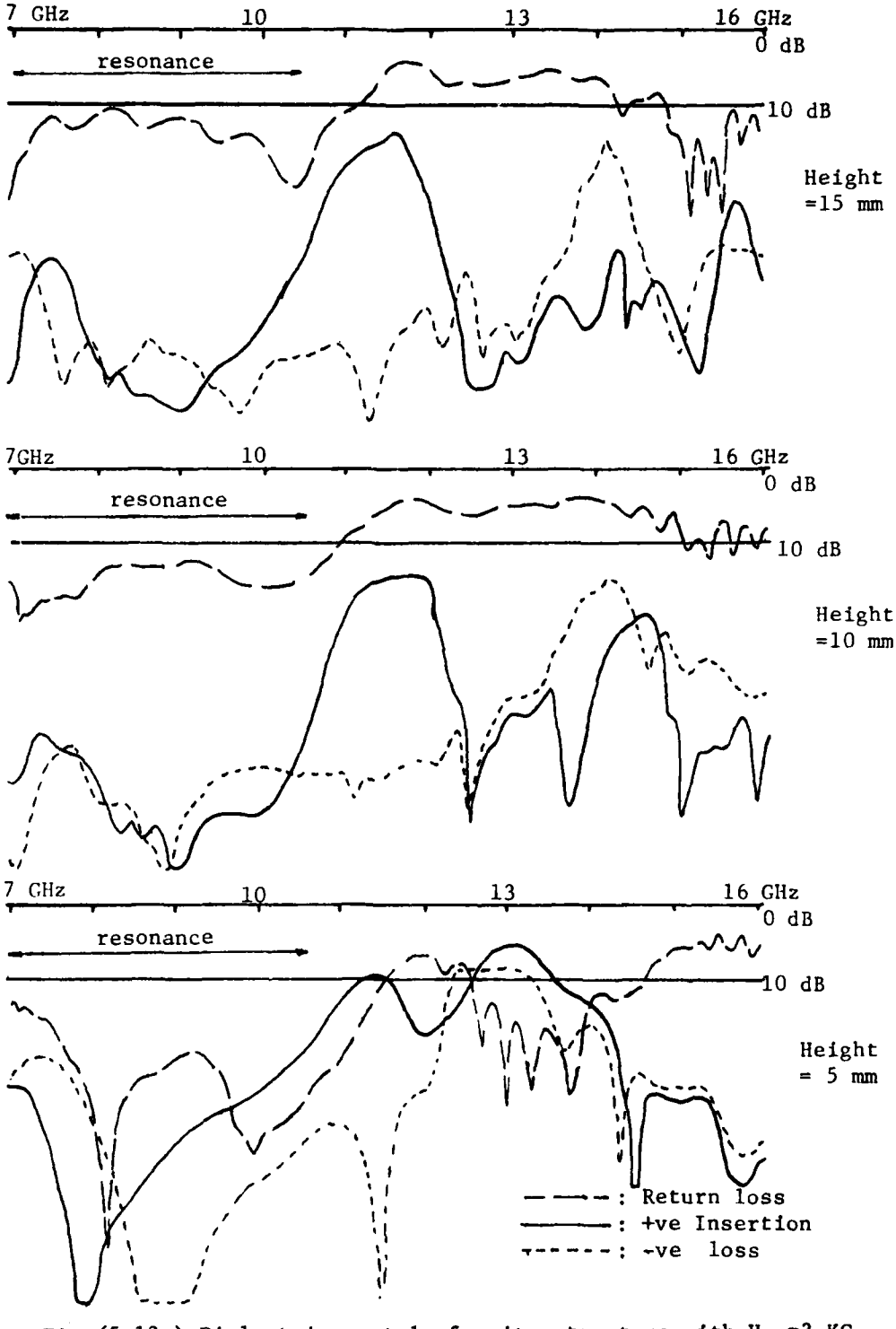

Fig.(5.12e) Dielectric -metal- ferrite structure with H_{dc}=3 KG.

Height of structure	Structure with no metal strips	structure with metal strips
5 mm.	+ve direction goes into resonance at a frequency 200 MHz higher than the -ve direction.	-ve direction goes into resonance at a frequency 1 GHz higher than the +ve direction. So the non-reciprocity occures just below resonance, that is in the negative permeability region.
10 mm.	+ve direction goes into resonance at a frequency 100 MHz higher than the -ve direction.	The -ve direction goes into resonance at a frequency 1.5 GHz higher than the +ve direction. The over all insertion loss is higher than the case when the height was 5 mm.
15 mm.	+ve direction goes into resonance at a frequency 70 MGz higher than the -ve direction.	The same as for the 10 mm heihgt, the only difference is that there is more insertion loss over the whole band.

Fig. (5.13) Comparison between the structure with and without metal strips.

	Height = 5 mm.	Height = 10 mm.	Height = 15 mm.
H_{dc}=0 KG.	Stop band is visible in a way similar to what the theory predicts.	Stop band is not visible, only the starting edge is visible. This may be due to the large attenuation present in the stop band.	Stop band not visible, this may be due to the large attenuation present in the stop band.
H_{dc}=1 KG.	No non-reciprocity	Some non-reciprocity occures	No non-reciprocity
H_{dc}=2 KG.	Non-reciprocity evident only in stop band.	Non-reciprocity occures just before resonance, that is in the -ve permeability region.	Same as for the 10mm height, only the over all insertion loss is larger.
H_{dc}=3 KG.	Non-reciprocity is evident in the -ve permeability region although band width is narrower than the case where 10 and 15 mm heights were used.	Well defined non-reciprocal effect occures in the -ve permeability region.	Same as for the 10mm height, only the over all insertion loss is larger.

Fig.(5.14) Comparison of the results when using various guide heights, for the structure with metal strips.

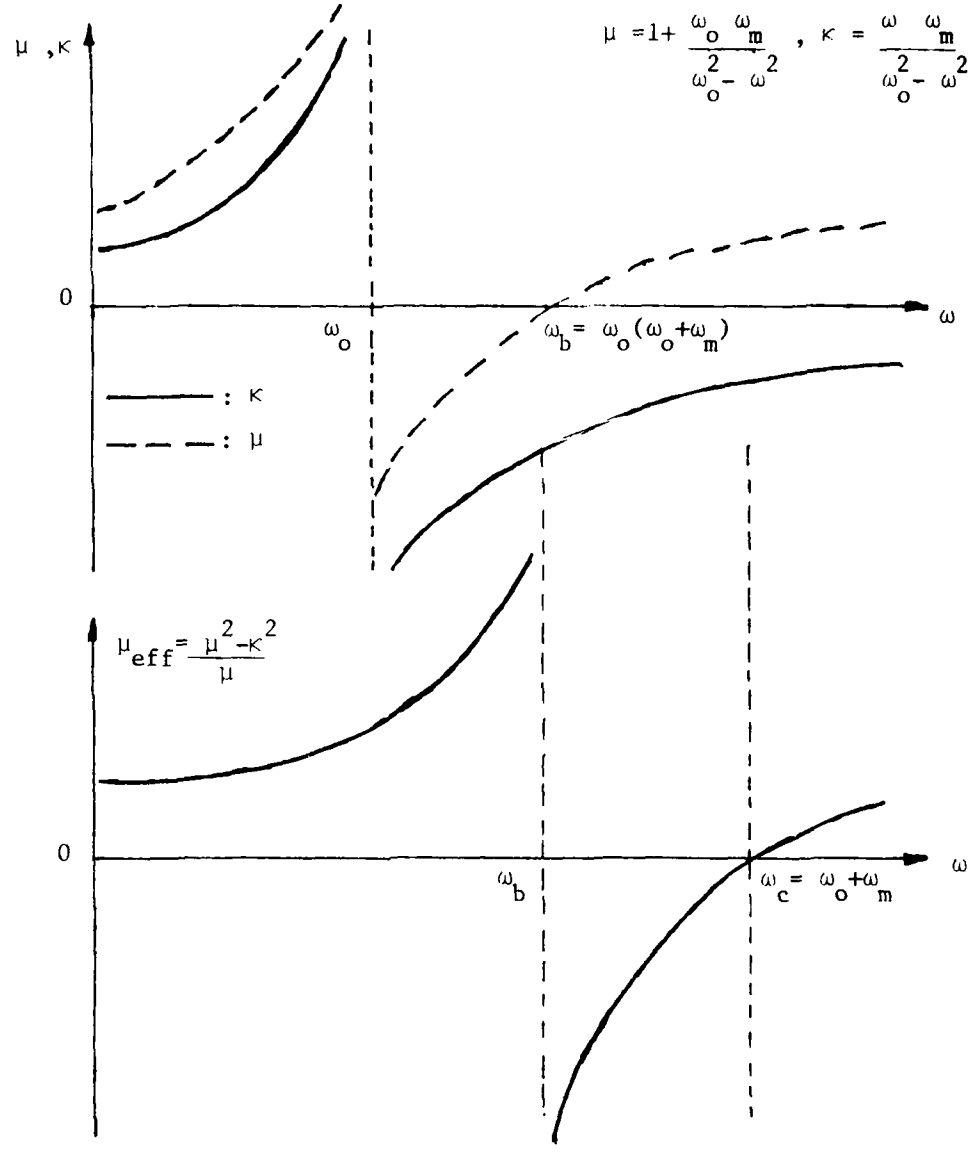

Fig. (5.15) Graphs showing how the negative permeability region is related to the resonance frequency and the components of the permeability tensor.

region between 11 and 12 GHz. Therefore, no initial guess was available to determine how the structure behaves with metal strips.

From the theoretical results, it is evident that more than one mode exists in the system. From the computer results at 3 KG (Fig. 5.16), it could be easily seen that two modes exist for the system both with and without metal strips. These two modes may be identified as the magnetostatic mode and the dynamic mode.

Most probably the non-reciprocity occurring in the negative permeability region is due to the dynamic mode, since according to the work done by Bolle,[7] this mode is the most dominant in this region.

So, since no initial guess was available, variuos arbitrary initial guesses were run through the computer program for the determination of the propagation constant. Fig. 5.17 and Fig. 5.18 show the results obtained in the frequency range from 10 to 13 GHz with different values of initial guess. It is evident that when a small initial guess was chosen, there was no non-reciprocity in the attenuation coefficient. On the other hand, when a large initial guess was used, non-reciprocity is evident in the 11 to 12 GHz frequency range. From the computer result, the forward loss should be about 30 dB while the backward loss should be about 60 dB. Experimentally, with a structure of 10 mm height, the forward loss is about 15 dB while the backward loss is about 38 dB. Although these results do not correlate exactly, one could infer what takes place since the

greater the height of the structure, the closer the correlation with the theory.

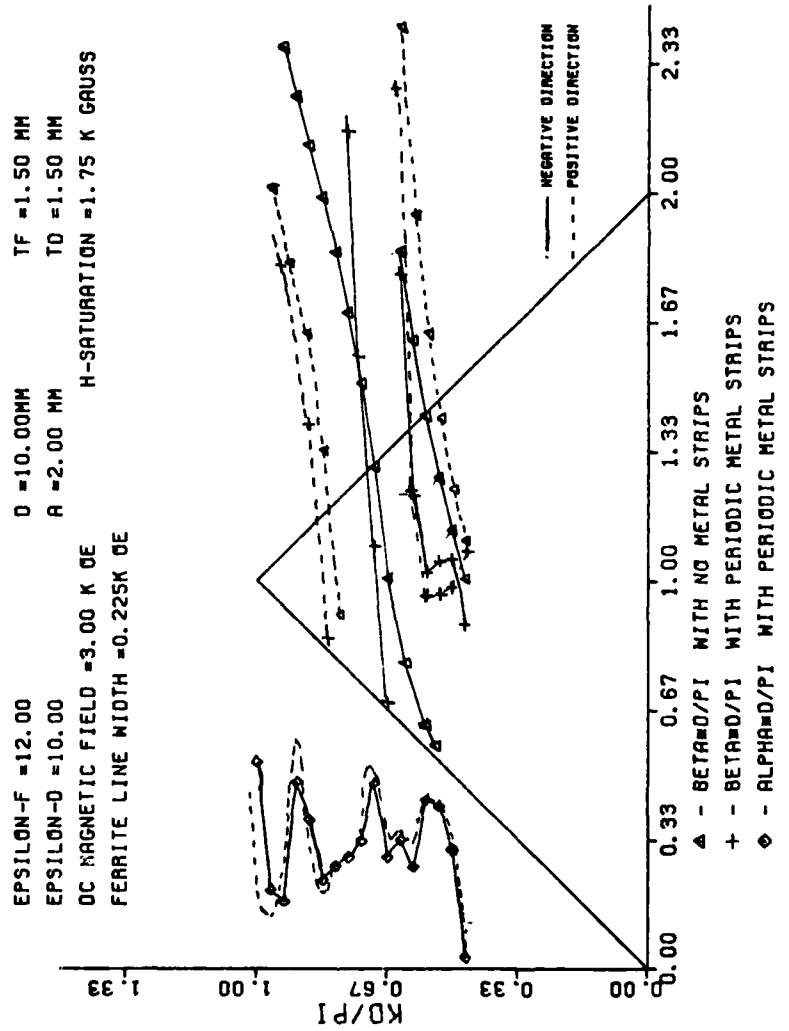
EPSILON-F =12.00
EPSILON-D =10.00
DC MAGNETIC FIELD =3.00 K ØE
FERRITE LINE WIDTH =0.225K ØE
D =10.00MM
A =2.00 MM
H-SATURATION =1.75 K GAUSS
TF =1.50 MM
TD =1.50 MM
KD/PI
0.00
0.33
0.67
1.00
1.33
1.67
2.00
2.33
NEGATIVE DIRECTION
POSITIVE DIRECTION
▲ - BETA=D/PI WITH NO METAL STRIPS
+ - BETA=D/PI WITH PERIODIC METAL STRIPS
◆ - ALPHA=D/PI WITH PERIODIC METAL STRIPS

Fig. (5.16)

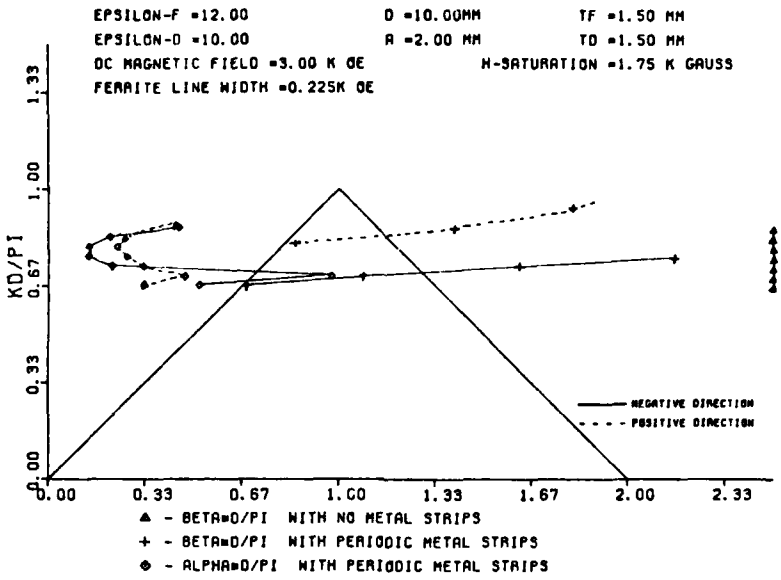

Fig. (5.17)

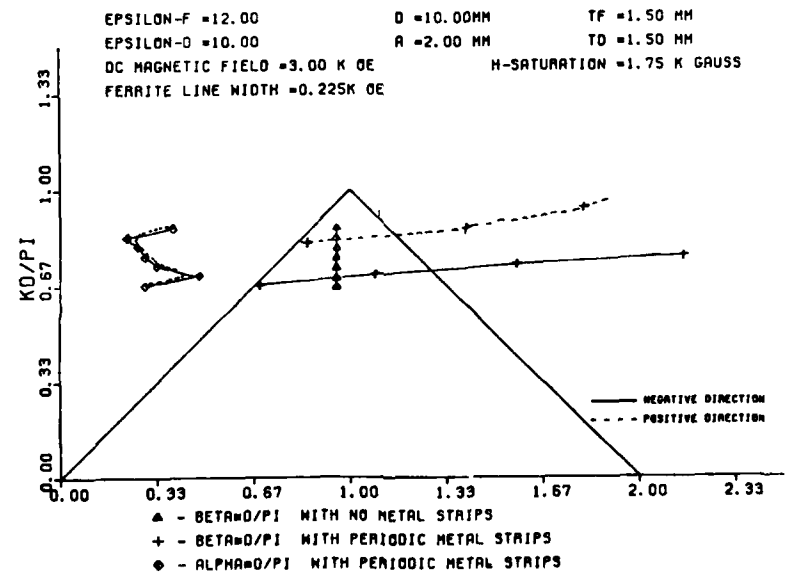

Fig. (5.18)

CHAPTER 6

CONCLUSIONS

6.1 The Theoretical Formulation

The theory used in this article assumed that the structure is infinite in the x and y directions. Having the structure finite in the x-direction may not be very far from being infinite since all the parameters derived from the program are per unit length in the x direction. When the number of strips is finite, one must then consider the edge effects due to the first and last strips. For an appreciable length of the periodic structure, the edge effect may, however, be neglected.

The main deficiency of the theory is the assumption that the structure is infinite in the y-direction. Development of the theory for a finite y-dimension is very difficult, since one has also to take into consideration that the metal strips are finite. The use of the effective dielectric constant method is not sufficient since it only considers the propagation constant of the structure without metal strips. From the experiments performed to investigate the effect of varying the y-dimensions, it seems difficult to correlate the results for the same structures having different y-dimensions. This suggests that there exists large difference between structures finite and infinite in the y-direction.

6.2 The Experimental Investigation

The apparatus used for the first investigation was quite adequate. The waveguide reflectometer system was very effective and the overall characteristics of the system are quite stable. A piece of apparatus that could have really helped the measurements is a sweeper that could go from 7 to 16 GHz in one sweep, instead of having to use several narrower-band sweeps to cover the entire spectrum. Such a sweeper would have reduced the experimental time by almost one-half.

The experimental measurements made in such a system were a function of three variables, namely, frequency, attenuation or reflection and magnetization. A three dimensional plot would be quite convenient for these measurements. Such plots would make the experimental results much more presentable and easily interpreted. Three dimensional plots could be produced if computer graphics had been available. In such a case the experimental data of, say, one magnetization would be directly stored in memory on a fast sweep rate and then sweep the magnetization at a slower rate than the frequency sweep, and putting information in the computer of the value of the magnetic field by using the external output of a Gauss meter.

If such a system were used it would take only a few minutes to obtain detailed experimental results, since the magnetic field could be varied in smaller discrete steps. As it was, with the apparatus used to take the data for the structures presented in this

article, about three hours were required to plot the characteristics of one structure.

6.3 Possible Improvements and Uses of Proposed Structure

From the experimental results obtained, it is evident that non-reciprocity exists. The only problem that detracts from the utility of the device is that up to now the forward loss is about 10 dB. This forward loss can be reduced by a number of techniques such as adjusting the period and strip width and the dimensions of the guides.

In the future, an investigation of the effects of period and strip width on the non-reciprocity could be made in much more detail. One might also consider using tapered metal strips to reduce the reflections due to the strips in the edge of the device.

As long as the non-reciprocity occurs in the negative permeability region, the only control on the bandwidth of the isolator is obtained by using ferrite materials with different saturation magnetizations. This is somewhat limited since the highest saturation magnetization available is in the 5 K Gauss region, which would produce a bandwidth of about 3 to 4 GHz.

In the design of an operational device one must also take into consideration the sizes of the dielectric and the ferrite slabs. In this investigation most of the work has been made with the same thickness of ferrite and dielectric, and the dielectric used had a relatively high dielectric constant.

Finally, one item of great interest is the experiment made with the metal strips touching the ground plane. In this case, it has been observed that non-reciprocity occurs at 12 GHz with the applied magnetic field in the 500 Gauss region or less, which means that we have non-reciprocity at a very low biasing magnetic field, so that the ferrite is not even saturated. Such a device has not been extensively investigated in this article. This should be considered in the future.

Devices based on the present structures are believed useful. They are compatible with image guide systems and could be easily used at millimeter-wave frequencies. Another possible use of such a device is in the design of masers since the structure consists of a slow wave structure and it is non-reciprocal.

APPENDIX

```
      PROGRAM PERLOAD (INPUT,OUTPUT,PLOTR)
C   FERRITE WAVEGUIDE WITH PERIODIC METAL LOADING IS ANALYZED
C   BY USING THE SPECTRAL DOMAIN APPROACH.
C   SUBROUTINE(SPACE) CALCULATES ALL SPACE HARMONICS
C   OF THE BASIS FUNCTIONS.
C   SUBROUTINE(UNIFORM) SOLVES UNIFORM FERRITE-DIELECTRIC
C   WAVEGUIDE WITHOUT METAL STRIPS, AND ITS ROOT IS USED
C   AS AN INITIAL GUESS FOR THE PERIODIC STRUCTURE.
C   SUBROUTINE(PERIOD) SOLVES PERIODIC FERRITE-DIELECTRIC
C   WAVEGUIDE WITH METAL STRIPS, BY MEANS OF MULLER METHOD.
C   SUBROUTINE(DETER) CALCULATES THE MATRIX ELEMENTS OF
C   CHARACTERISTIC EQUATION BY SUMMATION AND THEN
C   CALCULATES ITS DETERMINANT.
C   SUBROUTINE(IMPED) FORMALLY CALCULATES INPUT IMPEDANCES/
C   ADMITTANCES OF THE +- N-TH ORDER SPACE HARMONICS.
C   SUBROUTINE(EQUIV) ACTUALLY CALCULATES EQUIVALENT
C   TRANSVERSE  CIRCUIT, THAT IS, F-MATRICES
C   FOR BOTH FERRITE AND DIELECTRIC SLABS AND THE
C   CHARACTERISTIC ADMITTANCE FOR AIR REGION FOR ANY BETA,
C   AND THEN OBTAINS INPUT IMPEDANCE FOR METAL SURFACE.
C   SUBROUTINE (GRAPH) PLOTS THE VALUES OF KD/PAI
C   VS. BD/PAI AND AD/PAI
C
      DIMENSION C1(50),C2(50),C3(50),C4(50)
      DIMENSION AA(50),BB(2,50),CC(2,50),DD(2,50),EE(6,50)
      COMPLEX BETA,ERROR,BP,BK,HILW,HI2,AM,AK,EM,SI
      PAI=3.1415926
C   WAVEGUIDE STRUCTURE IS GIVEN HERE.
C   NOTE STRUCTURE IS INFINITE IN THE Y-DIRECTION
C   EF = DIELECTRIC CONSTANT OF FERRITE LAYER
C   HI = DC MAGNETIC FIELD APPLIED IN Y-DIRECTION (K OERSTEDS)
C   SM = SATURATION MAGNETISATION OF FERRITE (K GAUSS)
C   TF = THICKNESS OF FERRITE LAYER (MM)
C   ED = DIELECTRIC CONSTANT OF DIELECTRIC LAYER
C   TD = THICKNESS OF DIELECTRIC LAYER (MM)
C   D  = PERIOD OF METAL STRIPS (MM)
C   A  = WIDTH OF METAL STRIPS (MM)
C   WL = LINE WIDTH OF FERRITE LAYER (K OERSTEDS)
      READ 100,EF,HI,SM,TF,ED,TD,D,A,WL
  100 FORMAT(9F8)
C   PRINTING OF ALL THE DATA
      PRINT 150
  150 FORMAT(1H1,'FERRITE -'/4X,'PERMITIVITY',4X,
     1'INT. MAG. FIELD (KOE)'
     1,4X,'SATURATION (KGAUSS)',4X,'THICKNESS (MM)',
     15X,'LINE WIDTH (KOE)')
      PRINT 200,EF,HI,SM,TF,WL
  200 FORMAT(1H ,4X,F7.3,13X,F7.3,17X,F7.3,13X,F7.3,13X,F7.3)
      PRINT 250
  250 FORMAT(1H0,'DIELECTRIC -'/4X,'PERMITIVITY',4X,
     1'THICKNESS (MM)')
      PRINT 275,ED,TD
  275 FORMAT(1H ,5X,F7.3,8X,F7.3)
      PRINT 800
  800 FORMAT(1H0,'METAL STRIPS -'/4X,'PERIOD (MM)',
     14X,'WIDTH (MM)')
      PRINT 850,D,A
  850 FORMAT(1H ,4X,F7.3,8X,F7.3)
      DA=D/A
C   NO. OF SPACE HARMONICS
```

```
C    NO. OF SPACE HARMONICS
C    NMAX MUST BE LESS THAN OR EQUAL TO 50.
       NMAX=40
C    FOURIER TRANSFORM OF BASIS CURRENT DISTRIBUTIONS
C    WILL BE CALCULATED.
C    BASIS FUNCTIONS ARE INDEPENDENT OF FREQUENCY AND WAVEGUIDE
C    STRUCTURES AND DETERMINED BY ONLY PERIOD AND STRIP WIDTH.
       CALL SPACE(DA,C1,C2,C3,C4,NMAX)
C    NO. OF BASIS FUNCTIONS
C    N MUST BE LESS THAN OR EQUAL TO 4.
       N=4
C    CONVERGENCE CRITERIA
       EPS=1.E-9
       PRINT 400,N,EPS
  400 FORMAT(1H ,'NO. OF BASIS FUNCTIONS =',I2/X,
     *'CONVERGENCE CRITERIA =',E13.5//)
C    2.8 IS GYROMAGNETIC RATIO. (UNIVERSAL CONSTANT)
       WL=WL/2.
       HILW=CMPLX(HI,WL)*2.8
       SM=SM*2.8
       HI2=HILW*HILW
C    LOOPING ON THE +VE AND -VE DIRECTIONS OF THE MAGNETIC FIELD
       DO 10 I=1,2
C    THE DIRECTION OF MAGNETIZATION IS SPECIFIED.
       HI=-HI
       HILW=-HILW
       SM=-SM
       IF(1.EQ.1) GO TO 1
       PRINT 110
  110 FORMAT(1H0,'POSITIVE DIRECTION')
       GO TO 2
    1  PRINT 120
  120 FORMAT(1H0,'NEGATIVE DIRECTION')
    2  CONTINUE
C    FREQUENCY WILL BE SWEPT.
       DO 20 J=6,18
       K=J-5
       F=FLOAT(J)
       F2=F*F
C    TENSOR PERMEABILITY OF MAGNETIZED FERRITE IS GOVERNED
C    BY POLDER'S FORMULA, AS SHOWN BELOW.
C    AM IS DIAGONAL ELEMENT (MYU) .
C    AK IS OFF-DIAG. ELEMENT (KAPA) .
       AM=1.+HILW*SM/(HI2-F2)
       AK=SM*F/(HI2-F2)
C    PERMIABILITY TENSOR BELOW SATURATION
C    EQUATIONS DUE TO GREEN AND SANDY
       SMX=SM+.75/2.8
       IF(ABS(HI).GE.ABS(SM)) GOTO 111
       IF(ABS(HI).GT.ABS(SMX)) GOTO 111
       PRINT 999 ,F
  999 FORMAT (1H ,F15.7)
       UM0=2./3.*SQRT(1.-(SM/F)**2)+1./3.
       AM=UM0+(1.-UM0)*SQRT((HI*2.8/SM)**3)
       AK=-HI*2.8/F
  111 CONTINUE
C    EM IS EFFECTIVE PERMEABILITY
C    SI=KAPA/MYU
C    WN IS WAVENUMBER IN FREE SPACE.
       EM=(AM*AM-AK*AK)/AM
       SI=AK/AM
       WN=F*2.*PAI/300.
       PRINT 300 ,F,EM,SI
  300 FORMAT(1H ,'F=',F7.3,'(GHZ)',2X, EM=',E13.5,2X,E13.5,2X,
     1'SI=',E13.5,2X,E13.5)
       PRINT 350,HILW,SM,AM,AK
```

```
      PRINT 350,HILW,SM,AM,AK
  350 FORMAT(1H ,'HILW=',F7.3,2X,F7.3,2X,'SM=',F7.3,/
     1,1X,'AM=',F7.3,2X,F7.3,2X,'AK=',F7.3,2X,F7.3)
      WD=WN*D/PAI
      PRINT 351,WD
  351 FORMAT(1H ,'KD/PAI=',E13.5)
C     AT FIRST, UNIFORM WAVEGUIDE IS ANALYZED.
      CALL UNIFORM(EF,EM,SI,TF,ED,TD,WN,D,B0)
C     B0 IS USED FOR INITIAL GUESS FOR PERIODIC STRUCTURE.
      B0K=B0/WN
      PRINT 355,B0K
  355 FORMAT(1H ,'B0/WN=',E13.5)
C     PERIODIC WAVEGUIDE WILL BE SOLVED.
      CALL PERIOD(WN,EF,EM,SI,TF,ED,TD,D,N,C1,C2,C3,C4,
     *NMAX,B0,BETA,MI,EPS,ERROR)
C     BETA IS PROPAGATION CONSTANT OF PERIODIC WAVE.
C     REAL PART IS PHASE CONSTANT
C     IMAG. PART IS ATTENUATION CONSTANT DUE
C     TO REFLECTION OR LEAKAGE.
C     MI IS NO. OF ITERATION IN MULLER METHOD.
C     ERROR IS DEFINED BY FUNCTION(BETA).
      PRINT 360,BETA,MI,ERROR
  360 FORMAT(1H ,'BETA=',E13.5,2X,E13.5,5X,'MI=',I3,
     *2X,'ERROR=',E13.5,2X,E13.5)
      BK=BETA/WN
      PRINT 370,BK
  370 FORMAT(1H ,'BETA/WN=',E13.5,2X,E13.5)
      BP=BK*WD
  380 FORMAT(1H ,'BD/PAI=',E13.5,2X,E13.5/)
      PRINT 380,BP
C     FORMATION OF ARRAYS TO MAKE PLOTING EASYER
      BD1=B0*D/PAI
      BD2=REAL(BP)
      BD3=ABS(AIMAG(BP))
C     LOGIC TO AVOID GOING OUT OF RANGE ON THE PAPER WHEN PLOTING
      IF (WD.LT.0.0) WD=0.0
      IF (WD.GT.1.5) WD=1.5
      IF (BD1.LT.0.0) BD1=0.0
      IF (BD1.GT.2.5) BD1=2.5
      IF (BD2.LT.0.0) BD2=0.0
      IF (BD2.GT.2.5) BD2=2.5
      IF (BD3.LT.0.0) BD3=0.0
      IF (BD3.GT.2.5) BD3=2.5
      AA(K)=WD
      BB(I,K)=BD1
      CC(I,K)=BD2
      DD(I,K)=BD3
   20 CONTINUE
   10 CONTINUE
      DO 15 I=1,2
      DO 25 K=1,13
      EE(I,K)=BB(I,K)
      EE(I+2,K)=CC(I,K)
      EE(I+4,K)=DD(I,K)
   25 CONTINUE
   15 CONTINUE
      WL=WL*2.
      SM=SM/2.8
      CALL GRAPH (EE,AA,EF,HI,SM,TF,ED,TD,D,A,WL)
      STOP
      END
C
C
C
C
C
```

```
190 ... C
191 ...       SUBROUTINE SPACE(PD,C1,C2,C3,C4,NMAX)
192 ...       DIMENSION C1(50),C2(50),C3(50),C4(50)
193 ... C   SPACE HARMONICS OF FIELD DISTRIBUTIONS ON THE APERTURE.
194 ...       PAI=3.1415926
195 ...       X=PAI*(1.-1./PD)
196 ... C   EDGE CONDITION IS NOT CONSIDERED.
197 ... C   THE BASIS FUNCTIONS USED ARE
198 ... C   E1 = PAI*D/2/(D-A)*EXP(J*B0*X)*COS(PAI*X/(D-A))
199 ... C   E2 = J*PAI*D/(D-A)*EXP(J*B0*X)*SIN(2*PAI*X/(D-A))
200 ... C   E3 = -3*PAI*D/2/(D-A)*EXP(J*B0*X)*COS(3*PAI*X/(D-A))
201 ... C   E4 = 2*PAI*D*J/(D-A)*EXP(J*B0*X)*SIN(4*PAI*X/(D-A))
202 ... C
203 ... C   THE SPACE HARMONICS OF THE BASIS FUNCTIONS HAVE BEEN
204 ... C   CALCULATED ANALYITICALLY AND ARE GIVEN BY C1(N),C2(N),
205 ... C   C3(N),C4(N) RESPECTIVLY
206 ...       DO 10 N=1,NMAX
207 ...       XN=X*FLOAT(N)
208 ...       XN2=XN*XN
209 ...       E=XN2*4./PAI/PAI
210 ...       A=1.-E
211 ...       B=1.-E/4.
212 ...       C=1.-E/9.
213 ...       D=1.-E/16.
214 ...       SN=SIN(XN)
215 ...       CN=COS(XN)
216 ...       C1(N)=CN/A
217 ...       C2(N)=SN/B
218 ...       C3(N)=CN/C
219 ...       C4(N)=SN/D
220 ...    10 CONTINUE
221 ...       PRINT 100,NMAX
222 ...   100 FORMAT(1H ,'NO. OF SPACE HARMONICS /X,'NMAX= ,I2)
223 ...       RETURN
224 ...       END
225 ... C
226 ... C
227 ... C
228 ... C
229 ... C
230 ...       SUBROUTINE PERIOD(WN,EF,EM,SI,TF,ED,TD,E,N,C1,C2,C3,C4,
231 ...      *NMAX,B0,BETA,MI,EPT,ERROR)
232 ...       COMPLEX BETA,B(3),F(3),ERROR,F32,F21,F321,LAMDA,
233 ...      *DET,RDET,TF,TN,H,BN,EM,SI
234 ...       DIMENSION C1(50),C2(50),C3(50),C4(50)
235 ... C   PERIODIC STRUCTURE IS SOLVED.
236 ...       EPS=EPT
237 ...       P=E
238 ...       MC=1
239 ... C   INITIAL GUESS OF BETA
240 ...       B(1)=B0
241 ...       B(2)=B(1)*0.95
242 ...       B(3)=B(1)*0.9
243 ... C   PROPAGATION CONSTANT OF EIGEN MODE WILL BE SOLVED
244 ... C   BY MEANS OF MULLER METHOD.
245 ... C   MULLER'S METHOD IS A GOOD METHOD TO FIND THE ROOTS OF
246 ... C   A COMPLEX FUNCTION IF THE DERIVATIVE OF THE FUNCTION
247 ... C   IS NOT KNOWN. FOR MORE DETAIL ABOUT MULLER'S METHOD
248 ... C   SEE 'ELEMENTS OF NUMERICAL ANALYSIS' BY PETER HENRICI,
249 ... C   JOHN WILEY & SONS. 1964. CHAPTER 10 ,PAGE 198.
250 ... C   OBJECTIVE FUNCTION IS APPROXIMATED BY POLYNOMINAL
251 ... C   OF SECOND DEGREE.
252 ...       DO 10 I=1,3
253 ... C   (DETER) IS A SUBROUTINE WHERE YOU FEED IN BETA AND IT
254 ... C   WILL GIVE YOU BACK THE DETERMINANT F,WHICH  WE NEED TO
255 ... C   MINIMIZE TO ZERO IF POSSIBLE.
```

```
255 ... C    MINIMIZE TO ZERO IF POSSIBLE.
256 ... C    CALLING OF DETER FOR THE FIRST THREE INITIAL POINTS
257 ... C    OF MULLER'S METHOD
258 ...        CALL DETER(B(I),F(I),EF,EM,SI,TF,ED,TD,WN,P,N,
259 ...       1C1,C2,C3,C4,NMAX)
260 ...     10 CONTINUE
261 ...     30 IF(CABS(B(3)-B(2)).LE.EPS) GO TO 24
262 ...        F32=(F(3)-F(2))/(B(3)-B(2))
263 ...        IF(CABS(B(2)-B(1)).LE.EPS) GO TO 24
264 ...        F21=(F(2)-F(1))/(B(2)-B(1))
265 ...        IF(CABS(B(3)-B(1)).LE.EPS) GO TO 24
266 ...        F321=(F32-F21)/(B(3)-B(1))
267 ...        LAMDA=(B(3)-B(2))*F321+F32
268 ...        IF(CABS(LAMDA).GE.1.E37) GO TO 27
269 ...        DET=LAMDA**2-4.*F(3)*F321
270 ...        RDET=CSQRT(DET)
271 ...        TP=LAMDA+RDET
272 ...        TN=LAMDA-RDET
273 ...        IF(CABS(TP).GE.CABS(TN)) GO TO 22
274 ...        H=-2.*F(3)/TN
275 ...        GO TO 23
276 ...     22 CONTINUE
277 ...        H=-2.*F(3)/TP
278 ...     23 BN=B(3)+H
279 ... C    NEW APPROXIMATE ROOT
280 ...        B(1)=B(2)
281 ...        B(2)=B(3)
282 ...        B(3)=BN
283 ...        F(1)=F(2)
284 ...        F(2)=F(3)
285 ...        IF(CABS(H/B(3)).LE.EPS) GO TO 40
286 ...        IF(MC.GE.50) GO TO 24
287 ...        MC=MC+1
288 ... C    LOOPING ON DETER TO OPTIMIZE THE SOLUTION OF HAVEING F=0
289 ...        CALL DETER(B(3),F(3),EF,EM,SI,TF,ED,TD,WN,P,N,
290 ...       1C1,C2,C3,C4,NMAX)
291 ...        GO TO 30
292 ...     24 MI=MC+50
293 ...        GO TO 50
294 ...     40 MI=MC
295 ...     50 BETA=B(3)
296 ... C    FINAL CALL OF DETER TO PRINT RESULT
297 ...        CALL DETER(B(3),F(3),EF,EM,SI,TF,ED,TD,WN,P,N,
298 ...       1C1,C2,C3,C4,NMAX)
299 ...        ERROR=F(3)
300 ...        RETURN
301 ...     27 MI=999
302 ...        ERROR=1.E49
303 ...        RETURN
304 ...        END
305 ... C
306 ... C
307 ... C
308 ... C
309 ... C
310 ...        SUBROUTINE DETER(B,F,EF,EM,SI,TF,ED,TD,WN,R,M,
311 ...       1C1,C2,C3,C4,NMAX)
312 ... C    CALCULATION OF DETERMINANT OF CHARACTERISTIC EQUATION
313 ...        DIMENSION C1(50),C2(50),C3(50),C4(50)
314 ...        COMPLEX B,F,P11,P12,P13,P14,P22,P23,P33,P24,P34,P44
315 ...       *,D(4),Z,ZP,ZN,ZA,ZS,U,EM,SI
316 ... C    CALCULATION OF MATRIX ELEMENTS
317 ...        Q=R
318 ... C    (IMPED) GIVES THE VALUES OF THE ADMITANCES AT THE POINTS
319 ... C    WHERE THE METAL STRIPS ARE SITUATED THAT IS YU+YL .
320 ... C    NOW ZP AND ZN ARE THE ADMITANCES OF THE +VE AND -VE
```

```
320 ... C    NOW ZP AND ZN ARE THE ADMITANCES OF THE +VE AND -VE
321 ... C    DIRECTIONS RESPECTIVLY.
322 ... C    SO FINALLY WE WILL END UP WITH 2*NMAX+1 SPACE HARMONICS.
323 ... C    NOTE THAT THE MATRIX IS FORMED BY THE PRODUCT OF
324 ... C    EN*EN*YN AND NOT BY JN*JN*ZN.
325 ... C
326 ... C    THE ZEROTH SPACE HARMINIC IS CALLED HERE
327 ...        CALL IMPED(ZP,ZN,B,0,EF,EM,SI,TF,ED,TD,WN,Q)
328 ...        Z=ZP
329 ...        P11=Z
330 ...        P12=(0.0,0.0)
331 ...        P13=Z
332 ...        P14=(0.0,0.0)
333 ...        P22=(0.0,0.0)
334 ...        P23=(0.0,0.0)
335 ...        P24=(0.0,0.0)
336 ...        P33=Z
337 ...        P34=(0.0,0.0)
338 ...        P44=(0.0,0.0)
339 ...        DO 10 N=1,NMAX
340 ... C    LOOPING ON THE REST OF THE SPACE HARMONICS
341 ... C    TO FORM THE MATRIX.
342 ...        CALL IMPED(ZP,ZN,B,N,EF,EM,SI,TF,ED,TD,WN,Q)
343 ...        ZA=ZP+ZN
344 ...        ZS=ZP-ZN
345 ...        D1=C1(N)
346 ...        D2=C2(N)
347 ...        D3=C3(N)
348 ...        D4=C4(N)
349 ...        P11=P11+ZA*D1*D1
350 ...        P12=P12+ZS*D1*D2
351 ...        P13=P13+ZA*D1*D3
352 ...        P14=P14+ZS*D1*D4
353 ...        P22=P22+ZA*D2*D2
354 ...        P23=P23+ZS*D2*D3
355 ...        P24=P24+ZA*D2*D4
356 ...        P33=P33+ZA*D3*D3
357 ...        P34=P34+ZS*D3*D4
358 ...        P44=P44+ZA*D4*D4
359 ...     10 CONTINUE
360 ... C    CALCULATION OF DETERMINANT
361 ...        D(1)=P11
362 ...        D(2)=P11*P22-P12*P12
363 ...        D(3)=P11*P22*P33+2.*P12*P23*P13-P13*P13*P22-P23*
364 ...       1P23*P11-P12*P12*P33
365 ...        D(4)=P11*(P22*(P33*P44-P34*P34)-P23*(P23*P44-P34*
366 ...       1P24)+P24*(P23*P34-P33*P24))-P12*(P12*(P33*P44-P34*
367 ...       2P34)-P23*(P13*P44-P34*P14)+P24*(P13*P34-P33*P14))+
368 ...       3P13*(P12*(P23*P44-P34*P24)-P22*(P13*P44-P34*P14)
369 ...       4+P24*(P13*P24-P23*P14))-P14*(P12*(P23*P34-P33*P24)-
370 ...       5P22*(P13*P34-P33*P14)+P23*(P13*P24-P23*P14))
371 ...        F=D(M)
372 ...        RETURN
373 ...        END
374 ... C
375 ... C
376 ... C
377 ... C
378 ... C
379 ...        SUBROUTINE IMPED(ZP,ZN,B,N,EF,EM,SI,TF,ED,TD,WN,P)
380 ... C    EVALUATION OF INPUT IMPEDANCE OF SPACE HARMONICS BY USING
381 ... C    EQUIVALENT TRANSMISSION LINE.
382 ...        COMPLEX B,BNP,BNN,ZP,ZN,Z,EM,SI
383 ...        PAI=3.1415926
384 ...        BNP=B+2.*PAI/P*FLOAT(N)
385 ...        BNN=B-2.*PAI/P*FLOAT(N)
```

```
385 ...         BNN=B-2.*PAI/P*FLOAT(N)
386 ... C     INPUT IMMITANCE FOR +N-TH ORDER HARMONICS.
387 ...         CALL EQUIV(BNP,EF,EM,SI,TF,ED,TD,WN,Z)
388 ...         ZP=Z
389 ... C     INPUT IMMITANCE FOR -N-TH ORDER HARMONICS.
390 ...         CALL EQUIV(BNN,EF,EM,SI,TF,ED,TD,WN,Z)
391 ...         ZN=Z
392 ...         RETURN
393 ...         END
394 ... C
395 ... C
396 ... C
397 ... C
398 ... C
399 ...         SUBROUTINE EQUIV(B,EF,EM,SI,TF,ED,TD,WM  ,Z)
400 ... C     INPUT IMMITANCE OF SPACE HARMONICS IS CALCULATED.
401 ... C     AIR-FERRITE - METAL DIELECTRIC -AIR STRUCTURE
402 ...         COMPLEX B,B2,PF,PA,PD,SF,SG,AF,BF,CF,DF,AD,BD,CD,DD,
403 ...        1YL,Y,YF,YD,Z,U,SD,YU,AW,BW,CW,DW,EM,SI
404 ...         U=(0.,1.)
405 ...         B2=B*B
406 ...         WN=WM
407 ...         WN2=WN*WN
408 ... C     SELECTION OF BRANCH
409 ...         PA=CSQRT(B2-WN2)/U
410 ...         PF=CSQRT(WN2*EF*EM-B2)
411 ...         PD=CSQRT(WN2*ED-B2)
412 ...         SF=PF*TF
413 ...         SD=PD*TD
414 ...         SG=SI*B/PF
415 ...         YF=PF/WN/EM
416 ...         YD=PD/WN
417 ... C     F-MATRIX OF FERRITE SLAB
418 ...         AF=CCOS(SF)-SG*CSIN(SF)
419 ...         DF=CCOS(SF)+SG*CSIN(SF)
420 ...         BF=U*CSIN(SF)/YF
421 ...         CF=U*CSIN(SF)*YF*(1.+SG*SG)
422 ... C     F-MATRIX OF DIELECTRIC SLAB
423 ...         AD=CCOS(SD)
424 ...         DD=AD
425 ...         BD=U*CSIN(SD)/YD
426 ...         CD=U*CSIN(SD)*YD
427 ... C     CHARACTERISTIC ADMITTANCE OF AIR REGION
428 ...         Y=PA/WN
429 ... C     INPUT ADMITTANCE OF LOWER REGION
430 ...         YL=(CD+DD*Y)/(AD+BD*Y)
431 ... C     INPUT ADMITTANCE OF UPPER REGION
432 ...         YU=(CF+AF*Y)/(DF+BF*Y)
433 ... C     INPUT IMPEDANCE
434 ...         Z=YU+YL
435 ...         RETURN
436 ...         END
437 ... C
438 ... C
439 ... C
440 ... C
441 ... C
442 ...         SUBROUTINE UNIFORM(EF,EM,SI,TF,ED,TD,WN,D,BO)
443 ... C     DISPERSION RELATION OF UNIFORM FERRITE-DIELECTRIC
444 ... C     WAVEGUIDE WITHOUT METAL.
445 ...         COMPLEX B,Z,Y,EM,SI
446 ...         PAI=3.1415926
447 ... C     DETERMINATION OF THE REGION FOR THE SEARCH
448 ... C     OF A SOLUTION FOR BETA.
449 ...         BM=EF*REAL(EM)
450 ...         BN=ED*3.
```

```
      BN=ED*3.
      IF(BM.LT.BN) BM=BN
      BM=SQRT(BM)*0.99999*3.
      DB=(BM-1.00001)/100.
      ZI=0.0
      BD=0.0
      DO 30 K=1,101
      B=(1.+DB*FLOAT(K-1))*WN/3.0
      CALL EQUIV(B,EF,EM,SI,TF,ED,TD,WN,Y)
      Z=Y
      IF(K.EQ.1) GO TO 1
    4 ZJ=AIMAG(Z)
      BP=REAL(B)
      S=ZI*ZJ
      IF(S.LT.0.0) GO TO 3
      ZI=ZJ
      BR=BP
      GO TO 2
    1 ZI=AIMAG(Z)
      BR=REAL(B)
      GO TO 4
    3 IF(ABS(ZI).GT.1.) GO TO 6
C   INTERPOLATING FOR A BETTER VALUE OF BETA
C   ONCE THE SOLUTION CHANGES FROM +VE TO-VE
      BD=(ZI*BP-ZJ*BR)*D/(ZI-ZJ)/PAI
      PRINT 300,BD
  300 FORMAT(1H ,'BD/PAI= ',E13.5)
    6 ZI=ZJ
      BR=BP
    2 CONTINUE
   30 CONTINUE
      B0=BD*PAI/D
      PRINT 200,B0
  200 FORMAT(1H ,'B0=',E13.5/X,'UNIFORM END')
      RETURN
      END
C
C
C
C
C
      SUBROUTINE GRAPH (EE,AA,EF,HI,SM,TF,ED,TD,D,A,WL)
C   (GRAPH) PLOTS THE VALUES OF KD/PAI VS. BD/PAI AND AD/PAI
C   THAT IS THE REAL AND IMAGINARY PARTS OF BETA
C   FOR THE FERRITE-METAL STRIPS-DIELECTRIC STRUCTURE.
C   IT ALSO PLOTS THE SOLUTION OF BETA FOR JUST THE FERRITE-
C   DIELECTRIC STRUCTURE THAT IS WITH NO METAL STRIPS.
      DIMENSION EE(6,50),AA(50),EE1(50)
      CALL PLOTS (0,0,5LPLOTR)
C   PRINTING OF THE DATA
      CALL SYMBOL (2.0,.6,.1,2,0.,-1)
      CALL SYMBOL(2.2,.55,.1,
     *33H- BETA*D/PI  WITH NO METAL STRIPS,.0,33)
      CALL SYMBOL (2.,.35,.1,3.0,-1)
      CALL SYMBOL (2.2,.3,.1,
     *39H- BETA*D/PI  WITH PERIODIC METAL STRIPS,0.,39)
      CALL SYMBOL (2.,.1,.1,5,0.,-1)
      CALL SYMBOL (2.2,.05,.1,
     *40H- ALPHA*D/PI  WITH PERIODIC METAL STRIPS,0.,40)
      CALL SYMBOL (1.5,5.75,.1,11HEPSILON-F =,0.,11)
      CALL NUMBER (2.6,5.75,.1,EF,0.,2)
      CALL SYMBOL (4.5,5.75,.1,10HD =     MM,0.,10)
      CALL NUMBER (4.8,5.75,.1,D,0.,2)
      CALL SYMBOL (6.5,5.75,.1,11HTF =     MM,0.,11)
      CALL NUMBER (6.9,5.75,.1,TF,0.,2)
      CALL SYMBOL (1.5,5.5,.1,11HEPSILON-D =,0.,11)
```

```
515 ...        CALL SYMBOL (1.5,5.5,.1,11HEPSILON-D =,0.,11)
516 ...        CALL NUMBER (2.6,5.5,.1,ED,0.,2)
517 ...        CALL SYMBOL (4.5,5.5,.1,10HA =      MM,0.,10)
518 ...        CALL NUMBER (4.8,5.5,.1,A,0.,2)
519 ...        CALL SYMBOL (6.5,5.5,.1,11HTD =      MM,0.,11)
520 ...        CALL NUMBER (6.9,5.5,.1,TD,0..2)
521 ...        CALL SYMBOL (1.5,5.25,.1,
522 ...       *28HDC MAGNETIC FIELD =      K OE,0..28)
523 ...        CALL NUMBER (3.4,5.25..1,HI,0.,2)
524 ...        CALL SYMBOL (5.5,5.25,.1,
525 ...       *26HH-SATURATION =      K GAUSS,0.,26)
526 ...        CALL NUMBER (6.9,5.25,.1,SM,0.,2)
527 ...        CALL SYMBOL (1.5,5.0,.1,
528 ...       *29HFERRITE LINE WIDTH =      K OE,0.,29)
529 ...        CALL NUMBER (3.5,5.0,.1,WL,0.,3)
530 ...        CALL SYMBOL (6.5,1.75,.07,
531 ...       *26H------- NEGATIVE DIRECTION,0.,26)
532 ...        CALL SYMBOL (6.5,1.55..07,
533 ...      . *26H- - - - POSITIVE DIRECTION,0.,26)
534 ...        CALL AXIS (1.0,1.0,17HBD/PI  AND  AD/PI,-0,7.5,
535 ...       *0.0,0.0,0.3333333)
536 ...        CALL AXIS (1.0,1.0,5HKD/PI,5,4.5,90.0,0.0,0.3333333)
537 ...        CALL PLOT (1.0,1.0,3)
538 ...        CALL PLOT (4.0,4.0,2)
539 ...        CALL PLOT (7.0,1.0,2)
540 ... C    SETTING OF THE ORIGIN
541 ...        CALL ORIGIN (1.0,1.0,0)
542 ...        DO 11 N=1,6
543 ...        DO 9 K=1,13
544 ...        EE1(K)=EE(N,K)
545 ...       9 CONTINUE
546 ... C    SCALING OF THE AXIS THAT IS UNITS PER INCH OF PLOT
547 ...        AA(14)=0.0
548 ...        EE1(14)=0.0
549 ...        AA(15)=0.33333333
550 ...        EE1(15)=0.33333333
551 ... C    LOGIC TO DETERMINE THE APPROPRIATE SHADES AND
552 ... C    SYMBOLS OF GRAPHS.
553 ...        IF (N.EQ.1) M=1
554 ...        IF (N.EQ.3) M=1
555 ...        IF (N.EQ.5) M=1
556 ...        IF (N.EQ.2) M=0
557 ...        IF (N.EQ.4) M=0
558 ...        IF (N.EQ.6) M=0
559 ...        IF (N.EQ.1) I=2
560 ...        IF (N.EQ.3) I=3
561 ...        IF (N.EQ.5) I=5
562 ...        IF (N.EQ.2) I=5
563 ...        IF (N.EQ.4) I=5
564 ...        IF (N.EQ.6) I=5
565 ...        IF (N.EQ.3) CALL NEWPEN (2)
566 ...        IF (N.EQ.5) CALL NEWPEN (4)
567 ... C    PLOTTING OF THE SIX GRAPHS
568 ...        CALL LINE (EE1,AA,13,1,M,I)
569 ...       11 CONTINUE
570 ...        CALL PLOT (6.5,0.0,999)
571 ...        RETURN
572 ...        END
```

BIBLIOGRAPHY

[1] Araki, K., Song, B. S., and Itoh, T., "Nonreciprocal effects in an open dielectric waveguide with grating structures," IEEE Int. Microwave Symp., Washington, D.C., May 1980, pp. 319-321.

[2] Araki, K. and Itoh, T., "Analysis of periodic ferrite slab waveguides by means of improved perturbation methods," IEEE Trans. MTT, September 1981, pp. 911-916

[3] Araki, K. and Naito, Y., "Canonical representation and figure of merit of circulator," IECE of Japan Trans., Vol. E64, No. 9, September 1981, pp. 583-590.

[4] Araki, K., Koyama, T., and Naito, Y., "Reflection problems in a ferrite stripline," IEEE Trans. MTT, August 1976, pp. 491-498.

[5] Artman, J. O. and Tannenwald, P. E., "Measurement of susceptibility tensor in ferrites," J. Appl. Phys., Vol. 26, No. 9, September 1955, pp. 1124-1132.

[6] Awai, I. and Itoh, T., "Multilayered open dielectric waveguide with a gyrotropic layer," Int. Journal of Infrared and Millimeter waves, Vol. 2, No. 1, 1981, pp. 1-14.

[7] Bolle, D. M. and Talisa, S. H., "The edge-guided mode nonreciprocal phase shifter," IEEE Trans. MTT, November 1979, pp. 878-882.

[8] Bolle, D. M. and Talisa, S. H., "On the modeling of the edge-guided mode stripline isolators," IEEE Trans. MTT, June 1979, pp. 584-591

[9] Dydyk, M., "Edge guide: one path to wideband isolator design," Microwaves, January 1977, pp. 54-56

[10] Green, J. J. and Sandy, F., "Microwave characterization of partially magnetized ferrite," IEEE Trans. MTT, June 1974, pp. 641-651.

[11] Hines, M. E., "Reciprocal and nonreciprocal modes of propagation in ferrite stripline and microstrip devices," IEEE Trans. MTT., May 1971, pp. 442-451.

Bibliography (Cont'd)

[12] Itoh, T., "Spectral domain immittance approach for dispersion characteristics of shielded microstrips with tuning septums," 9th European Microwave Conf., Brighton, England, September 1979, pp. 435-439.

[13] Kittel, C., "Solid state physics," 5th Edition, John Wiley & Sons Inc., 1976, pp. 438-491.

[14] Knerr, R. H., "An annotated bibliography of microwave circulators and isolators: 1968-1975," IEEE Trans. MTT, October 1975, pp. 818-825.

[15] Kravitz, L. C. and Helber, G. S., "Resonance isolator at 70 KMC," Proc. IRE, February 1959, pp. 331.

[16] Lax, B. and Botton, K. J., "Microwave ferrites and ferrimagnetics," McGraw-Hill, 1962.

[17] Landau, L. and Lifshitz, E., "On the theory of the dispersion of magnetic permeability in ferromagnetic bodies," Physik Z. Sovjetunion, Vol. 8, pp. 153, 1953 (in English).

[18] Muraguchi, M. and Naito, Y., "Nonreciprocal devices in open-boundary structures for millimeter-wave integrated circuits," Journal IECE of Japan, July 1971, Vol. J64-B, No. 7, pp. 604-611.

[19] Marcuvitz, N., "Waveguide handbook," Dover Publications, Inc., New York, 1951, Chapter 8.

[20] Nanda, V. P., "A new form of ferrite device for millimeter-wave integrated circuits," IEEE Trans. MTT, November 1976, pp. 876-879.

[21] Polder, D., "On the theory of ferromagnetic resonance," Phil. Mag., 40, 1949, pp. 99-115.

[22] Roberts, J., "High frequency applications of ferrites," The English University Press, Ltd., 1960.

[23] Soohoo, R. F., "Theory and application of ferrites," Prentice-Hall, Inc., New Jersey, 1960.

[24] Sucher, M. and Fox, J., "Handbook of microwave measurements," John Wiley and Sons, Inc., 1963, Chapter XV.

Bibliography (Cont'd)

[25] Toulios, P. P, and Knox, R. M., "Rectangular dielectric image lines for millimeter integrated circuits," Wescon Conf., Los Angeles, CA, August 1970.

[26] Trans-Tech, Inc., 12 Meem Avenue, Gaithersburg, MD, 20760. Data Sheets.

[27] Thaxter, J. B. and Heller, G. S., "Circulators at 70 and 140 KMC," Proc. IRE, January 1960.

[28] Von Aulock, W. H. and Fay, C. E., "Linear ferrite devices for microwave applications," Advances in Electronic and Electron Physics, Supplement 5, Academic Press, 1968.

[29] Weiss, P. and Beck, P. N., "Chaleur specifique et champ moleculaire des substances ferromagnetiques," J. Phys., Ser. 4, Vol. 7, pp. 249, 1908.

[30] Weiss, M. T. and Dunn, F. A., "A 5-mm resonance isolator," IRE Trans., MTT, July 1958, pp. 331.